

**Mathematical modelling of  
the dynamics and morphology of  
aeolian dunes and dune fields**

Hiroshi Momiji

University College London

Thesis submitted to the University of London  
for the Degree of Doctor of Philosophy

ProQuest Number: U641913

All rights reserved

INFORMATION TO ALL USERS

The quality of this reproduction is dependent upon the quality of the copy submitted.

In the unlikely event that the author did not send a complete manuscript and there are missing pages, these will be noted. Also, if material had to be removed, a note will indicate the deletion.



ProQuest U641913

Published by ProQuest LLC(2015). Copyright of the Dissertation is held by the Author.

All rights reserved.

This work is protected against unauthorized copying under Title 17, United States Code.  
Microform Edition © ProQuest LLC.

ProQuest LLC  
789 East Eisenhower Parkway  
P.O. Box 1346  
Ann Arbor, MI 48106-1346

# Abstract

The aim of this thesis is to model the dynamics of free sand dunes.

In the first part, a new theoretical scheme is presented to model the shape and migration speed of a sand dune at equilibrium. Unlike earlier models it does not require iterative calculations of the interaction between the wind flow and the topography. As the first step, a self-consistent model which describes two-dimensional dune migration is introduced, which is comprised of a grain-scale model of sand deposition in the lee of dune and the assumption of equilibrium. The model gives quantitative relations between sand grain diameter, wind velocity on level ground and dune height. By further incorporating theory based on aerodynamics, the wind-directional profile of barchan dunes can be estimated.

The thesis goes on to develop a computer simulation model that describes the three-dimensional morphology and dynamics of an aeolian dune field. Following recent advances, the proposed model is based on an approach using discrete lattice dynamics. In the model, dunes are treated as accumulations of ‘sand slabs’ on a two-dimensional lattice, whose motion is the result of wind-directional sand transport and avalanching. By incorporating new features, which reflect physically observed mechanisms, the model can simulate dunes whose individual shape and collective patterns are similar to those observed in nature. The model can also quantitatively simulate dune growth and dune migration. Some dune patterns can be explained by the model in terms of seasonally changing wind direction and sand availability (initial sand depth).

These two approaches are complimentary. Some results in this thesis may be applicable to the morphology and dynamics observed in subaqueous and other terrestrial bedforms.

# Acknowledgement

First of all, I would like to thank my supervisors, Professors Andrew Warren and Steven R. Bishop for their continuous supervision and encouragement. Very frequent and intense discussion with them made it all possible. The author knows well that this is not always the case amongst PhD students.

Discussion also with two of my collaborators: Dr Ricardo Carretero-González and Professor Hiraku Nishimori has been a vital part of this study throughout these three years.

This work has greatly been improved with comments to my manuscripts, which were submitted to journals or are in preparation, from both anonymous and unanonymous reviewers: Professors Gary Kocurek, Jim L. Best, Julian C.R. Hunt, Nicholas Lancaster, John H. van Boxel, and Dr Giles F.S. Wiggs.

I owe a lot to Professor Yasuji Sawada, Dr Masaaki Futamoto, Mr Kazumi Kawamoto and the International Office, UCL, who assisted with my original application to UCL.

During the preparation of this thesis, the computer environment has greatly been improved with support by Dr Julian R. Thompson.

Life in London has been fruitful with my friends, in particular: Miss Tomoko Yoshitani, Mr Taro Niikura, Mr and Mrs Kumagai, and Mr and Mrs Okumura.

Finally, many thanks to my parents and brother for their continuous support and encouragement throughout this study.

This study was partly supported in finance by UCL Open Scholarship. Support from British Petroleum is also acknowledged.

# Contents

Abstract . . . . .	2
Acknowledgements . . . . .	3
List of figures . . . . .	8
List of tables . . . . .	12
List of symbols . . . . .	13
<b>1 Aims of the study</b>	<b>18</b>
1.1 Motivation and aims . . . . .	18
1.2 Modelling philosophy . . . . .	21
1.3 Scope . . . . .	27
<b>2 Introduction to desert dune geomorphology and aeolian processes</b>	<b>28</b>
2.1 Hierarchies in aeolian geomorphology . . . . .	28
2.2 Classification of simple (elementary) dunes . . . . .	29
2.3 Formative environment of each type of dune . . . . .	32
2.4 Dune dynamics and sand transport induced by wind and by gravity	33
2.4.1 Sediment continuity equation . . . . .	33
2.4.2 Sand motion induced by wind . . . . .	34
2.4.3 Sand transport formulae . . . . .	35
2.4.4 Wind flow over a dune . . . . .	37
2.4.5 Avalanche and sand deposition on the lee face . . . . .	39
2.4.6 Dune migration . . . . .	40
2.5 The structure and evolution of a dune field . . . . .	41
2.6 Analytical studies of emergence and shape of dunes . . . . .	43
2.6.1 Linear instability analysis . . . . .	43

2.6.2	Kinematic analysis . . . . .	44
2.6.3	Difficulties in analytical studies . . . . .	46
2.7	Computer modelling of dunes and dune fields . . . . .	46
2.7.1	Models dealing with an isolated dune on a flat surface . . . . .	47
2.7.2	Models dealing with dune field dynamics . . . . .	51
<b>3</b>	<b>Modelling a transverse and a barchan dune</b>	<b>56</b>
3.1	Introduction: shape and migration speed . . . . .	56
3.2	Migration speed of transverse dunes and sand trapping efficiency . . . . .	61
3.2.1	Migration speed of transverse dunes at equilibrium . . . . .	61
3.2.2	Sand trapping efficiency . . . . .	65
3.3	Windward slope profile of a barchan dune . . . . .	70
3.3.1	Windward slope profile of barchan dunes in the field . . . . .	72
3.3.2	Wind-flow modelling with the Jackson-Hunt theory . . . . .	74
3.4	Conclusions in this chapter . . . . .	81
<b>4</b>	<b>Model results and comparison to nature</b>	<b>83</b>
4.1	Migration speed . . . . .	83
4.1.1	Numerical calculations and comparison to nature . . . . .	83
4.1.2	Model applicability to subaqueous and terrestrial aeolian dunes (section 2.6.2) . . . . .	92
4.1.3	Model limitations and future work . . . . .	94
4.2	Windward surface morphology . . . . .	95
4.2.1	General characteristics . . . . .	97
4.2.2	Calculations for dunes in southern Peru . . . . .	101
4.2.3	Calculations for dunes in California . . . . .	106
4.2.4	Towards a model of a three-dimensional dune . . . . .	107
4.3	Shape and migration speed of proto-dunes . . . . .	110
4.4	Conclusions in this chapter . . . . .	114
<b>5</b>	<b>Developing dune field model with discrete dynamics</b>	<b>117</b>
5.1	Introduction: modelling concepts for dune field dynamics . . . . .	117
5.2	Werner's model and algorithm . . . . .	118

5.3	Simulated dune shape and dynamics with Werner's model . . . . .	122
5.4	No erosion in shadow zones . . . . .	125
5.5	Introducing wind speedup . . . . .	126
5.5.1	Linear wind speedup: Kinematic formulation . . . . .	127
5.5.2	Non-linear wind speedup . . . . .	129
5.6	Sand availability and reference number of slabs correction . . . . .	129
5.7	Introducing wind directional change . . . . .	130
5.8	Conclusions in this chapter . . . . .	132
<b>6</b>	<b>Comparisons with field studies</b>	<b>133</b>
6.1	No erosion in shadow zones . . . . .	133
6.2	The effects of wind speedup over a dune . . . . .	135
6.2.1	The effects of linear wind speedup . . . . .	136
6.2.2	The effects of non-linear wind speedup and equilibrium dune field . . . . .	138
6.3	The effects of sand availability and wind variability . . . . .	143
6.3.1	Dune types in a uni-directional wind regime: pattern and sand availability . . . . .	143
6.3.2	Spatial and temporal scales in the model: quantitative com- parison to nature . . . . .	146
6.3.3	Dune types in a bi-directional wind regime . . . . .	149
6.4	Conclusions in this chapter . . . . .	151
<b>7</b>	<b>Conclusions</b>	<b>153</b>
7.1	General conclusions . . . . .	153
7.2	Assessment of models and methodology . . . . .	155
7.2.1	Reductionism/universalism . . . . .	156
7.2.2	Four criteria for a good model (Kirkby, 1996) . . . . .	157
7.2.3	Engineering aspects . . . . .	160
7.2.4	Contributions to geomorphology in general and to other disciplines . . . . .	161
7.3	Future work . . . . .	162
7.3.1	Single dune model . . . . .	162

7.3.2	Dune field model . . . . .	163
7.3.3	Collaboration . . . . .	165

<b>References</b>		<b>167</b>
-------------------	--	------------



# List of figures

2.1	Schematic views of typical dunes: (a) dome dune, (b) barchan dune, (c) transverse dune, (d) linear dune, (e) star dune and (f) network dune.	31
2.2	Dune type diagram with regard to sand availability and wind-direction variability. . . . .	33
2.3	Flow chart for dune modelling in the conventional method. . . . .	48
3.1	Schematic views of a barchan dune (a) from top and (b) from side. .	57
3.2	Flow chart for dune modelling in the conventional method. . . . .	58
3.3	Cross-sectional geometry of a migrating shape-invariant transverse dune: (a) global view (b) magnified view of windward surface (c) sand flux ( $q(x)$ ) over a dune. . . . .	63
3.4	Model and co-ordinate system used in calculation of sand trapping efficiency ( $T_E$ ). . . . .	66
3.5	Flow chart for dune modelling in the new approach examined in this thesis. . . . .	71
3.6	Measured data of dune height ( $H$ ) and the average angle of windward slope ( $\theta_{\text{avg}}$ ) taken from Finkel (1959), Long and Sharp (1964), Hastenrath (1967) and Sauermann <i>et al.</i> (2000). . . . .	73
3.7	The normalised surface profiles ( $f(\xi)$ ) of (a) a cosine hill and (b) a Gaussian hill, and examples of normalised surface shear stress profiles ( $\tau(\xi)/\tau_0$ ) over them. . . . .	78
4.1	Relations between sand trapping efficiency ( $T_E$ ) and dune height ( $H$ ) calculated for various shear velocities at the dune crest ( $u_*(0)$ ). . . .	85
4.2	Relations between sand trapping efficiency ( $T_E$ ) and shear velocity on a level surface ( $u_*(-\infty)$ ) for various dune heights ( $H$ ). . . . .	87

4.3	Relations between dune migration speed ( $c_d$ ) and shear velocity on a level surface ( $u_*(-\infty)$ ), for various dune heights ( $H$ ). . . . .	87
4.4	Relations between dune migration speed ( $c_d$ ) and wind velocity at 10 m height on a level surface ( $u_{10m}(-\infty)$ ) for various dune heights ( $H$ ). . . . .	88
4.5	Relations between shear velocity at the dune crest ( $u_*(0)$ ) and dune height ( $H$ ). . . . .	88
4.6	Relations between dune migration speed ( $c_d$ ) and dune height ( $H$ ), for various shear velocities on a level surface ( $u_*(-\infty)$ ). . . . .	90
4.7	An example relation between dune migration speed ( $c_d$ ) and the inverse dune height ( $1/H$ ). Data collected by Hastenrath (1967) are analysed. . . . .	92
4.8	Bedforms formed in the wind tunnel that simulated Venusian atmosphere. . . . .	93
4.9	The calculated relation between the normalised increase in the shear stress at the dune crest ( $\frac{\tau(0)-\tau_0}{\tau_0}$ ) and dune height ( $H$ ) for various shear velocities on the level surface ( $u_*(-\infty)$ ). . . . .	97
4.10	The calculated relation between the average windward slope angle ( $\theta_{w_{avg}}$ ) and dune height ( $H$ ) for various shear velocities on the level surface ( $u_*(-\infty)$ ). The sand grain diameter ( $D_g$ ) is taken as 0.15 mm. Field data collected by Hastenrath (1967) are also plotted. . . . .	102
4.11	The relation between the maximum windward slope angle ( $\theta_{w_{max}}$ ) and dune height ( $H$ ) for various shear velocities on the level surface ( $u_*(-\infty)$ ). . . . .	104
4.12	The relation between dune migration speed ( $c_d$ ) and dune height ( $H$ ) for some shear velocities on a level surface ( $u_*(-\infty)$ ). Sand grain diameter ( $D_g$ ) is assumed to be 0.15 mm. Field data collected by Hastenrath (1967) are also plotted. . . . .	104
4.13	Schematic explanation of the origin of (a) barchan and (b) parabolic shapes. . . . .	105

4.14	The relation between windward slope angle ( $\theta_{\text{wavg}}$ ) and dune height ( $H$ ) for various shear velocities on a level surface ( $u_*(-\infty)$ ). Sand grain diameter ( $D_g$ ) is 0.250 mm. Field data collected by Long and Sharp (1964) are also plotted. . . . .	107
4.15	The relation between dune migration speed ( $c_d$ ) and dune height ( $H$ ) for data by Long and Sharp (1964) and for calculations with sand grain diameter ( $D_g$ ) of 0.250 mm. . . . .	108
4.16	Schematic plan view of the transverse dune system comprised of barchanoid and linguoid parts. . . . .	109
4.17	The calculated relation between the windward slope length ( $L_w$ ) and dune height ( $H$ ) for various shear velocities on the level surface ( $u_*(-\infty)$ ). The sand grain diameter ( $D_g$ ) is taken as 0.25 mm. . . . .	113
4.18	The calculated relation between dune migration speed ( $c_d$ ) and dune height ( $H$ ) for some shear velocities on a level surface ( $u_*(-\infty)$ ). Sand grain diameter ( $D_g$ ) is assumed to be 0.25 mm. . . . .	115
5.1	Lattice model configuration and algorithms: a) wind-directional sand transport, b) shadow zone and c) avalanching. . . . .	120
5.2	Transverse dunes (a) in $(i, j)$ space simulated with Werner's original model, from a random initial morphology, and (b) in nature (Wahiba Sands, Oman). . . . .	123
5.3	Evolution of an initially introduced, isolated transverse dune, simulated with Werner's original model. . . . .	124
5.4	Calculated relation between saltation length ( $\lambda$ ) and shear velocity ( $u_*$ ).130	
5.5	Modelling scheme for a dune field where the wind changes direction. The lattice is rotated in response to the wind directional change. . . .	131
6.1	Evolution of an initially introduced, isolated transverse dune simulated without erosion in shadow zones. . . . .	135
6.2	Transverse dunes simulated from an initially random morphology. No erosion occurs in shadow zones. . . . .	136
6.3	Evolution of an initially introduced, isolated transverse dune simulated with various shear-velocity-increase coefficients ( $C_1$ ). . . . .	137

6.4	Asymmetric transverse dunes formed from a random initial morphology by introducing wind speedup. . . . .	137
6.5	Time evolution of a 1-dimensional dune field, from a random initial morphology. . . . .	139
6.6	Time evolution of transverse dunes simulated on the 1-dimensional lattice with non-linear increase of the transport length, from a random initial morphology. . . . .	139
6.7	Relations between maximum dune height and simulation time ( $t$ ). The relations with and without the non-linear increase of the transport length are averaged from 13 and 15 runs on the 1-dimensional lattice, respectively. . . . .	141
6.8	Transverse dunes simulated with non-linear increase of the transport length, on the 2-dimensional lattice, from a random initial morphology.	142
6.9	Different types of dune simulated with various sand availabilities ( $h_{avg}$ ); (a) 2, (b) 7 and (c) 20. . . . .	144
6.10	Downwind migration of barchan dunes in two simulations. . . . .	148
6.11	Dune types and wind directional change. Sand availability and angle between two directions of wind ( $h_{avg}, \theta$ ) are a) (100, 60°), b) (100, 120°), c) (2, 60°) and d) (2, 120°). . . . .	150
6.12	Dune type diagram with regard to sand availability and wind direction variability. The summary of simulations is inside. . . . .	152
7.1	Various types of dune in the Great Western Sand Sea in Algeria. . . .	164
7.2	Current ripples development observed in a flume. . . . .	165

# List of tables

4.1	Values and constants used for numerical calculation. . . . .	84
4.2	Some published dune migration data and model results. . . . .	91
4.3	Example results with a cosine hill and a Gaussian hill. . . . .	98
4.4	Some published field data of the flow over a low hill. . . . .	102
6.1	Simulation parameters. . . . .	134
6.2	Maximum dune height when sand availabilities are below and above the threshold. . . . .	145
6.3	Conservation of the initial dune pattern below the threshold in sand availability. . . . .	146
6.4	Dune pattern and the slab transport length ( $L_0$ ) at the reference height.	149

# List of symbols

$a$	coefficient in Anderson's set of equations about saltation length coefficient in a Fourier transform formula
$a_{c_d}$	coefficient in the proposed formulae for dune migration speed against dune height
$a_L$	coefficient in the logarithmic relation between dune migration speed and dune height
$\alpha$	windward slope angle
$\alpha_i$	sand grain incident angle ( $10^\circ$ )
$B$	barchan dunes
$B$	barchanoid part
$b$	coefficient in Anderson's set of equations about saltation length
$b_{c_d}$	coefficient in the proposed formulae for dune migration speed against dune height
$b_L$	coefficient in the logarithmic relation between dune migration speed and dune height
$\beta$	temporal variable for calculation of $x_{0c}$
$C_B$	coefficient in Bagnold's sand transport formula
$c$	coefficient in Anderson's set of equations about saltation length
$C_{LL}$	coefficient in Lettau and Lettau's sand transport formula
$c_{c_d}$	coefficient in the proposed formula for dune migration speed against dune height
$c_d$	dune migration speed (celerity)
$C_1$	linear wind speedup coefficient of slab transport length
$C_2$	non-linear wind speedup coefficient of slab transport length

D	dune pattern
$d$	coefficient in Anderson's set of equations about saltation length
$D_g$	sand grain diameter
$D_r$	reference sand grain diameter (0.25 mm)
$\varepsilon$	perturbation variable in the Jackson-Hunt theory (1975)
$f$	surface undulation function surface profile
$\hat{f}$	Fourier transform of surface profile ( $f$ )
$f_\eta$	function which relates $\eta(x)$ and $(u_*(-\infty), H, D_g)$
$f_0$	function which relates $u_*(-\infty)$ and $(u_*(0), H, D_g)$
$f_{-\infty}$	function which relates $u_*(0)$ and $(u_*(-\infty), H, D_g)$
$G_1$	coefficient in a gamma function formula
$G_2$	coefficient in a gamma function formula
$g$	gravitational acceleration ( $9.8 \text{ m s}^{-2}$ )
$\Gamma$	gamma function
$\gamma$	sand bulk density temporal variable for calculation of $x_{0c}$
$H$	dune height
$h$	number of sand slabs
$\hat{h}$	Fourier transform of number of sand slabs ( $h$ )
$h_{\text{avg}}$	average number of slabs
$H_{\text{max}}$	the largest dune height in a dune field
$h_{\text{max}}$	maximum number of slabs
$H_{\text{min}}$	the smallest dune height in a dune field
$h_{\text{min}}$	minimum number of slabs
$h_{\text{ref}}$	reference number of slabs
$\eta$	(dune) surface height
$\eta'$	modified dune surface
$\eta_{\text{avg}}$	average (dune) surface height
$\eta_\Lambda$	maximum height of undulation ( $f$ )
I	isolated dunes
$i$	lattice suffix in wind direction

$i$	unit of imaginary numbers ( $\sqrt{-1}$ )
$i_{\text{new}}$	lattice suffix in wind direction after lattice rotation
$j$	lattice suffix in transverse direction to the wind
$j_{\text{new}}$	lattice suffix in transverse direction to the wind after lattice rotation
$k$	temporal parameter for counting $i$ Fourier wave number
$\kappa$	von Kármán's constant
L	linear dunes
$L$	linguoid part horizontal characteristic length of a dune sand slab transport length
$l$	inner-layer thickness
$L_0$	sand slab transport length at sites where $h = h_{\text{ref}}$
$L_{\text{PD}}$	proto-dune length in the wind direction
$L_s$	lattice size
$L_w$	windward slope length of a dune
$\Lambda$	wavelength of undulation
$\lambda$	saltation distance of a sand grain
N	no pattern
$N_{x_0}$	number of sand grains arriving at $x_0$
$N_0$	number of sand grains departing at $x'$
$P$	probability function of saltation distance
$P_{\text{ns}}$	slab deposition probability at sites without sand slab (0.4)
$P_s$	slab deposition probability at sites with at least one slab (0.6)
$\phi$	phase constant in the expression of $\hat{\tau}_d$ ( $+\pi/4$ or $-\pi/4$ )
$q$	sand flux
$R^2$	R-squared value, correlation measure of linear regression analysis
$\rho_a$	air density ( $1.2 \text{ kg m}^{-3}$ )
$\rho_s$	quartz-sand grain density ( $2,650 \text{ kg m}^{-3}$ )
T	transverse dunes
$t$	actual or simulation time
$T_E$	sand trapping efficiency



$T_{E_0}$	function which relates $T_E$ and $(u_*(0), H, D_g)$
$T_{E-\infty}$	function which relates $T_E$ and $(u_*(-\infty), H, D_g)$
$\theta$	slip face angle angle of lattice rotation
$\theta_{\text{avg}}$	average windward slope angle
$\theta_c$	angle of repose
$\theta_{\text{wmax}}$	maximum windward slope angle
$\theta_{\text{ph}}$	phase difference between topography and surface shear stress
$\theta_{\text{sz}}$	angle of shadow zone ( $15^\circ$ )
$\tau$	surface shear stress
$\tau_0$	surface shear stress on the flat surface
$\tau_d$	spatial variation in the surface shear stress
$\hat{\tau}_d$	Fourier transform of $\tau_d$
$u$	wind speed
$u_{10\text{m}}$	wind speed at the height of 10 m
$u_z$	wind speed at the height of measurement ( $z$ )
$u_*$	wind shear velocity
$u_{*t}$	threshold wind shear velocity
$v_0$	sand grain incident velocity
$v_*$	incident velocity of sand ejected at the dune crest
$vl_0$	mean grain lift-off velocity
$wl_0$	mean vertical grain lift-off velocity
$x$	horizontal distance in wind direction
$x'$	horizontal position of saltation entrainment
$x_0$	horizontal position on $z = 0$ plane corresponding to $x_p$
$x_{0c}$	horizontal position on $z = 0$ plane corresponding to $x_{pc}$
$x_p$	horizontal position on the slip face in wind direction
$x_{pc}$	horizontal position of the bottom end of slip face in wind direction
$\xi$	normalised horizontal distance ( $x/L$ )
$y$	horizontal distance
$z$	vertical distance temporal variable for calculation of $\hat{\tau}_d$

$z_p$  vertical position on the slip face  
 $z_0$  roughness length

# CHAPTER 1

## Aims of the study

### 1.1 Motivation and aims

This study aims to mathematically model the morphology and dynamics of desert dunes and dune fields. The ultimate goal is to provide geomorphology and other disciplines with novel concepts and methodologies, as well as to give new interpretations to long-debated issues in geomorphology.

At the start of the thesis, it is worth reviewing past studies of modelling in geomorphology as a whole and in aeolian geomorphology in particular, in order to assess the current state of the art, *i.e.*, what has been understood, in which directions the study is going and what is still needed. In the rest of this chapter, only a conceptual discussion, as regards the choice of method, is given. The detailed review of models in aeolian geomorphology is given in chapter 2.

Recently, especially in the last ten years, geomorphologists have been seriously concerned with the philosophy of their subject. A series of heated debates was triggered by Richards' question: what is 'real' geomorphology? (Richards, 1990, 1994; Bassett, 1994; Rhoads, 1994; Werner, 1995, 1999; Rhoads and Thorn, 1996). These debates lead to a symposium on 'The Scientific Nature of Geomorphology' (Rhoads and Thorn, 1996). Although not every part of these discussions is rele-

vant here, some of it is directly related to the choice of the appropriate method for the present study.

Geomorphology has followed a path of change in its methodology from extensive and empirical studies, which rely on the statistical consideration of data from large samples, to intensive and in-depth studies of small numbers of cases, as seen in the investigations of river meandering (Richards, 1996). Other in-depth studies have considered micro-scale aeolian sand transport, where precise experiments using the state-of-the-art technologies have predominated (Mitha *et al.*, 1986; Willetts and Rice, 1989; Butterfield, 1991; Rice *et al.*, 1995, 1996). The inclusion of mathematical modelling in these in-depth studies (Richards, 1996) has greatly deepened our knowledge about micro-scale phenomena.

The study of desert dunes and related aeolian features has a history of more than a hundred years, in which changes in methodology from extensive to intensive can be seen at different timings for different scales of interests. Field studies of desert dunes began in late 19th century, and the major desert dune areas were all explored by 1980, as summarised in Goudie (1999, table 1.1). Empirical field studies have contributed basic knowledge, for example about dune shape and mobility (see for example Cooke *et al.*, 1993; Lancaster, 1995; Goudie *et al.*, 1999).

In the meantime, attempts to understand the underlying physics had also begun. Cornish discussed ripples and dunes in terms of waves (Goudie, 1999), which is however a rather descriptive approach. In the 1930s, Bagnold conducted experiments using a wind tunnel to study sand transport by wind. He introduced the newly developed fluid-dynamic theory into the study, and succeeded in explaining the relationship between sand flux and wind velocity (Bagnold, 1941). Since this seminal work, mathematically formulated discussions and experiments both in the field and in laboratories have continued. Bagnold also studied dunes, in which he mathematically discussed the relation between dune and sand flux profiles which are parallel to the wind direction, and gave qualitative discussion of

dune form and alignment to wind-flow pattern.

Extensive and empirical study has continued nonetheless, not only at a dune-field scale but at the global scale. A comprehensive description of worldwide dune fields enabled Wilson (1972) to develop the idea of bedform hierarchy and the role of sand grain size. With the aid of satellite images, more detailed descriptions of dune fields have been made available (McKee, 1979a). Based on the accumulation of such knowledge, together with meteorological considerations, attempts to classify and understand dune forms in relation to its controls have been made (*e.g.* Wasson and Hyde, 1983). At the dune-scale, intensive morphometric investigations have revealed dune-form sensitivities to dune size and wind, which has become one of major interests in aeolian geomorphology (*e.g.* Hesp and Hastings, 1998).

There are three possible approaches to in-depth studies; field observations and experiments, laboratory experiments and theoretical analysis. When attempting to understand such large-scale and dynamic geomorphology as in dune fields, however, laboratory experiments are not appropriate, because it is extremely difficult to scale dunes and their environments consistently to laboratory dimensions. Although the wind flow over a dune has been studied by using a scaled model placed in a wind tunnel (Howard *et al.*, 1978; Wiggs *et al.*, 1996), the dynamic nature such as downwind migration has not been modelled experimentally. Bougan and Greeley's (1985) wind tunnel experiment is an exception, which however simulated aeolian dunes on Venus. Consequently, in the study of dune orientation in relation to wind directional variability, results of flume experiments (Rubin and Ikeda, 1990) were considered, with the expectation that aeolian and subaqueous dune dynamics shared the same mechanism (theoretical work (Rubin and Hunter, 1987) and examination of field data (Lancaster, 1991) also played significant roles). Speaking of geomorphology more generally, it is difficult to introduce the same boundary conditions in a laboratory as in the field. In the study of debris flow, for example, Hungr (2000) insisted that the longitudinal variation in material characteristics was important so that the excessive reliance

on laboratory experiments was not advisable.

It is because of this that the field study of dunes has been the primary means of study. For example, extensive field observations made it possible to compile a diagram of the relation between dune form and its controls: wind variability and sand availability (Wasson and Hyde, 1983). In addition, a field experiment that monitored the decay of an artificially constructed barchan dune successfully highlighted the importance of incoming sand flux for a dune to maintain its shape (Cooke *et al.*, 1993, p322). However, “Field studies of dune dynamics are time consuming, expensive to carry out, and sample short time periods on the scale of minutes. Models of the behaviour of dunes under varied air flow and transport conditions are necessary therefore to be able to predict the long term evolution of dunes.” (McKenna Neuman *et al.*, 1997, p1112). Despite the firm recognition of its necessity as shown in this quotation, theoretical analysis still lags far behind empirical studies (Nickling and McKenna Neuman, 1999), if only in the volume of published material.

## 1.2 Modelling philosophy

“Models ideally provide both an insight into the functioning of the natural environment, and a means of forecasting the range of likely outcomes, either in a forecasting sense or to assess the impact of alternative policies” (Kirkby, 1996). There are two distinct types of models; qualitative and conceptual models, and quantitative and analytical models. Qualitative models are effective in some dune studies, as when interpreting the stratigraphy embedded in a dune or a dune field (for example, Kocurek and Lancaster, 1999). Quantitative models are required particularly for civil and petroleum engineering, as well as for the understanding of natural phenomena. Predicting dune types and migration speeds is essential for designing roads and oil pipelines in dune environments. In this study, dunes and a dune field are modelled mathematically, and the results are mainly discussed

quantitatively but some qualitative comparisons are made.

There is no definitive method for quantitative modelling, though Kirkby (1996) listed the following criteria for a good model. 1) physical basis: if the model has a strong physical basis, 2) simplicity: if the model avoids an excess of complexity, 3) generality and richness: if the model can be applied to other fields of study (generality) and how much the model can explain in the field of interest (richness), and 4) potential for scaling up and down: if the model can apply to problems whose scale is larger or smaller than that of interest. Analytical (pen-and-paper) study, if possible, is thought to be better than computational modelling, since analytical models identify the physics involved (*e.g.* the morphology and dynamics of dunes and dune fields) and make long-term predictions possible.

There are two distinct approaches in natural sciences; reductionism and universalism. Reductionism is a classic and probably the most convincing approach, in which observed phenomena are repeatedly reduced to a deeper level, hopefully to the fundamental processes (first principles). To how deep a level it is satisfactory to reduce is a question. In addition, the reductionist approach is almost always hampered by mathematical difficulties both analytically and numerically, due, for example, to the non-linearity of the system and limitations of computational power, respectively. Scaling-up processes are usually associated with some assumptions (simplifications), such as continuity, approximations and many kinds of symmetry (Richards, 1996). However, any step up from such simplifications makes the problem very difficult in a mathematical respect.

On the other hand, universalism is an approach that attempts to understand complex phenomena by using universal properties common to many systems. For example, concepts of entropy (Leopold and Langbein, 1962) and the least action principle (see for example Huang and Nanson, 2000) have been imported from physics and tested to explain geomorphic, mostly fluvial, phenomena. However, universalism is usually best applied to non-linear open systems. Universalism may be quite different from the reductionist approach. Given that there is a uni-

versal aspect, which is independent of microscopic details, we only need to study the simplest model (prototype) that shows such a universal property (Bak, 1996). Some key words are chaos, self-organised pattern, fractals and self-organised criticality (Phillips, 1996).

Chaos: complexity in nature may arise from systems governed by variables with many degrees of freedom, and/or from stochasticity. However, even if the system is deterministic with only a few degrees of freedom, long-term prediction is still sometimes not possible when the system is chaotic. The time-evolution of a deterministic system can usually be written in the form of a set of differential equations. But being able to write down an equation that governs the system does not necessarily mean that its dynamics are completely understood. Strictly speaking, chaos is defined as a long-term response. The sensitivity to initial conditions is the most important property of chaos (Ruelle, 1991), and to test this, it is essential to keep all the other conditions constant. For these reasons, in the study of chaos, well-defined experiments have been carried out for rapidly varying systems, which do not usually occur in geomorphology. Complex transient behaviour should be considered differently from chaos (Steven R. Bishop, talk in the Institution of Civil Engineers (London), 27 September 2000). Furthermore, it is known that the transition from a stable state through an oscillatory state (limit cycle) to chaos can (usually) be classified into three characteristic and universal routes: Feigenbaum's, Manneville-Pomeau's, and Ruelle-Takens-Newhouse's. Feigenbaum's route is the transition to chaos after an infinite cascade of period doubling. Manneville-Pomeau's route is the intermittent transition to chaos. Ruelle-Takens-Newhouse's route is the transition to chaos after three bifurcations (Schuster, 1988, table 12). So when assessing whether the system under consideration is really showing chaos, it is important to examine the behaviour near the bifurcation points by changing the parameters. However this usually is not practically possible in large-scale geomorphic systems. If we speculate, for example, that the dune pattern in a desert is governed by how many times wind direction changes in a year, we cannot conduct a field experiment to test such a hypothesis.



Self-organised pattern: some systems which are comprised of many interacting degrees of freedom can spontaneously form a distinct pattern (self-organised pattern) such as periodic rolls and grids. Mathematically, lattice dynamics, such as Coupled Map Lattice (CML) (Kaneko, 1993) and Cellular Automata (CA) (Wolfram, 1986), have been studied as prototypes that generate such patterns. CML can correspond to the spatially and temporally discretised partial differential equations, where the time evolution of quantities (state) defined on each lattice site is simulated following rules. If the state of the system is also discretised, that is the CA. However it is not an easy task to derive CML or CA from the original fundamental equation of the system. Consequently, we set the rules based on physical considerations for each case (*e.g.* Bak, 1996). There is much circumstantial evidence that geomorphic systems do show chaos and/or self-organisation, such as in the formation of periglacial and nonperiglacial patterned ground, the evolution of beach cusps, and drainage network evolution (Hallet, 1990; Phillips, 1996, table 13.1, 13.2). Some of these patterns have been simulated by lattice dynamics (*e.g.* Werner and Fink, 1993; Murray and Paola, 1994). Universalism may provide us with insights into these kinds of geomorphology.

Fractals: fractals are another type of self-organised pattern. The word ‘fractal’ was coined by Mandelbrot (1983) to refer to scale-invariant geometries. For example, rivers in the Amazon (Takayasu, 1990) and the Norwegian coast (fjords) (Bak, 1996) have been shown to have fractal structures. Fractal structures can be seen in so many fields other than landscapes, for example, in the time series of price of commodity, that fractal-ity is thought to be one of the universal aspects of nature. However, the concept of fractals cannot address the dynamic origins of a phenomenon.

Self-organised criticality: some self-organising systems can reach the critical state, which is characterised by a sequence of punctuated catastrophic events of all sizes. This is known as Self-Organised Criticality (SOC), which was demonstrated first with the sand-pile prototype (Bak *et al.*, 1987). SOC can create fractal structures. Unlike usual critical states as seen in phase transition in solids, SOC is

insensitive to order parameters (*e.g.* temperature, magnetic field in phase transition in solids). For this reason, SOC can be expected to be observed widely in many different systems. In geomorphology, SOC has been discussed in reference to turbidites (Bak, 1996).

Since there is some circumstantial evidence, it can be expected that our understanding of geomorphology may deepen with the concepts of chaos, self-organised pattern, fractals and self-organised criticality. The problem is that quantitative discussion and prediction is difficult if it is confined to these concepts alone. For systems whose basic equations are not known or slowly change with time, the impact of chaos remains at the level of scientific philosophy (Ruelle, 1991, chapter 12).

In the study of aeolian geomorphology, however, the reductionist approach does not seem to work well even for simplified problems (Werner, 1995, 1999). Mathematical difficulties, such as non-linearity in the Navier-Stokes equation, three-dimensional features of the system, and the discrete nature of sand grain motion, limit our choice of methods as follows.

In an extremely arid dune field, such as the Namib desert, vegetation does not need to be taken into account. In such a desert, landforms are the result only of recurring interactions between topography and sand motion induced by wind flow over the dune field and by gravity. In such a case, following the traditional path in physics, we would first develop a momentum conservation equation for the system comprised of air and sand, then monitor the time evolution of the system by solving this equation. However, such a fundamental equation has yet to be established. Even if we could consider wind flow and sand transport separately, it is extremely difficult to solve the Navier-Stokes equation, even in the case of an isolated single dune on a flat surface. In the case of a dune field comprising many dunes with different shapes, it is almost impossible to calculate the wind flow with the same accuracy as in the case of single dune. Furthermore, we have to solve these equations under moving boundary conditions as dunes grow in three-

dimensional space. Tracking dune evolution through conventional analysis that calculates wind flow over a dune field each time is therefore practically impossible.

To simulate dune fields, more phenomenological models are necessary. The patterns of dunes and ripples that grow on an initially flat surface are no doubt self-organised in a non-linear open system, because before dunes or ripples grow, the wind does not have any structure which resembles the resulting bedform pattern. In this respect, universalism may be a more effective approach to modelling. This might, in turn, contribute to non-linear physics. However, a wholly universal approach, which discusses only patterns qualitatively, is not adopted here. Models will be developed that are based on lattice dynamics. Yet they will seriously attempt to account for physical processes and scales, and aim at quantitative prediction. Phenomenological models, which are not based on detailed physical processes, but on simplified rules which, nevertheless correctly reflect observations, are necessary.

Kinematic modelling is a phenomenological, but not universal, approach to understanding nature, in which a theory is constructed based on empirically known facts and not on causality. This reduces the mathematical difficulties significantly. Models can then be developed using the geometric relations of the system, in which the symmetries associated with the observational facts play a significant role. Despite the neglect of causality, models like these can give deeper levels of understanding, since they give quantitative links between observed phenomena. Kinematic modelling has been an effective tool in the study of aeolian and, in particular, subaqueous bedforms (Allen, 1968, chapter 5). In other fields, it has been applied to gravitational and turbidity currents (Allen, 1970, chapter 6), and also to debris flows in relation to the headward surge profile (Hung, 2000). The explanatory and predictive success of this kind of approach can support and highlight the empirically known facts which are used as the assumptions in the model.

## 1.3 Scope

The dunes analysed in this thesis are free dunes, which are independent of any vegetation or underlying topography. Their geomorphology and related aeolian processes will be reviewed in chapter 2. In chapters 3 and 4, some local dynamics and features of single dunes will be analytically investigated in the kinematic sense. However, most of the work concerns dune-field morphodynamics, and is developed in chapters 5 and 6. This will heavily rely on computer simulations. Computer simulations now make three-dimensional study possible, where before mathematical difficulties precluded this approach. In the final chapter the results of both attempts are compared, rediscussed and the philosophical issues are re-examined in the light of the results presented.

## CHAPTER 2

# Introduction to desert dune geomorphology and aeolian processes

In this chapter, basic aeolian geomorphology and processes are briefly summarised, and previous studies of dune and dune-field modelling are reviewed. Subaqueous bedforms, which are thought to be related to aeolian dunes, are also discussed for the following two reasons: ripples and dunes in rivers resemble aeolian dunes in view both of their dynamics and morphology; and the study of subaqueous bedforms has progressed further than that of aeolian dunes.

### 2.1 Hierarchies in aeolian geomorphology

Dune fields show hierarchical structures (Wilson, 1972; Cooke *et al.*, 1993, chapter 24). Wilson classified these into three groups with respect to scale; ripples, dunes and draas, the last of which were termed, by Cooke *et al.*, mega dunes. Ripples, dunes and draas are typically  $10^{-2} - 10^{-1}$ ,  $10^1 - 10^2$ ,  $10^2 - 10^3$  m in wavelength, respectively (Wilson, 1972, figure 3). Ripples are the smallest member of the hierarchy and occur on most bare sand surfaces, including dunes, the

next largest member. In many areas these dunes are superimposed on larger draas. Wilson thought that these three features co-existed in quasi-equilibrium, and ripples did not grow into dunes, nor dunes into draas. This leads to the conclusion that the nuclei of draas must be larger than fully grown dunes, of which nuclei must be larger than fully grown ripples. Another explanation of the hierarchy may be the superimposition of dunes from different geological periods with different wind regimes (Warren and Allison, 1998). Dune size may however also be related to wind velocity (Cooke *et al.*, 1993, p346), and superimposition may have aerodynamic explanations (Lancaster, 1995, p191). In this thesis, only dunes and draas (mega dunes) are discussed further, because different dynamics work on ripples (see section 2.4.2).

## 2.2 Classification of simple (elementary) dunes

Dunes can be classified into two groups, free dunes and anchored dunes. Free dunes can grow and migrate freely in response to changes in wind speed and direction. Anchored dunes are pegged by vegetation or topography, and cannot migrate freely, though their forms are shaped by changes in wind speed and direction. Here, only free dunes are reviewed, since they are more fundamental aeolian features. Some findings from the study of free dunes may however also be applied to anchored dunes.

Free dunes can be further divided into three groups, depending on the alignments of their crest to the net sand transport: transverse, linear and star dunes. For transverse dunes, the net sand transport is normal to the crests. This group includes classic transverse dunes, barchan dunes and reversing dunes. For linear dunes the net sand transport is parallel to the crests. This group includes seif dunes and sand ridges. For star dunes, the net sand transport is towards a node. This group includes “star” (large) and network (smaller) dunes. Each dune type is described in detail below.

## Transverse dunes

**Dome dune:** an isolated, usually transverse dune with no slip face (Figure 2.1(a)).

**Barchan dune:** a free transverse dune with a crescentic plan-shape in which the crescent opens downwind (Figure 2.1(b)). More detailed morphometric descriptions are given in the next chapter (section 3.3.1).

**Transverse dune:** dune ridges with crests transverse to the dominant wind, which migrate, for the most part, in the direction of the dominant wind (Figure 2.1(c)).

**Reversing dunes:** transverse dunes that reverse in the direction as the wind changes through 180°.

## Linear dunes (Figure 2.1(d))

**Seif dune:** a sinuous, sharp-crested, linear dune.

**Sand ridge:** partly vegetated linear dune, usually larger than a seif.

## Star dunes

**Star dune:** a large pyramidal or dome-like dune with arms (Figure 2.1(e)).

**Network dune:** result of the overlap of a number of transverse dune systems, each aligned to a different wind in a complex annual regime (Figure 2.1(f)).

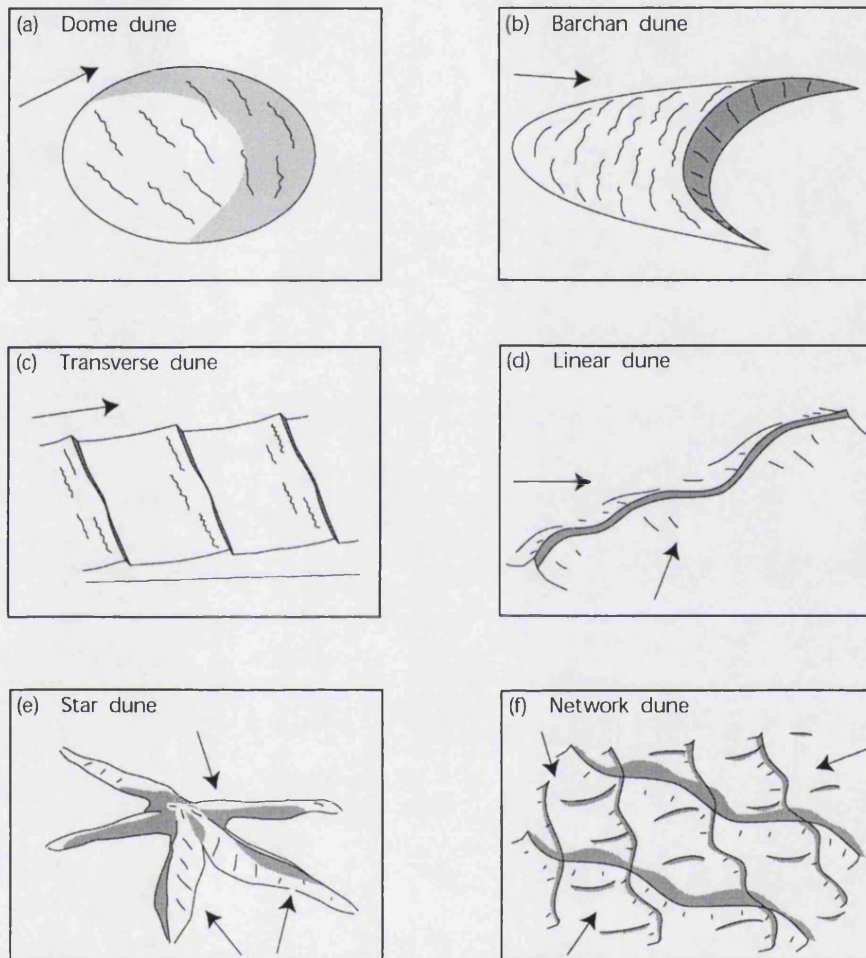


**Figure 2.1:** Schematic views of typical dunes: (a) dome dune, (b) barchan dune, (c) transverse dune, (d) linear dune, (e) star dune and (f) network dune ((a)–(e) after McKee, 1979b; (f) after Cooke *et al.*, 1993).



## 2.3 Formative environment of each type of dune

Although many factors, such as grain size and humidity, affect dune shape and alignment, the type of dune at a site is primarily determined by the wind regime. A useful terminology was given by Fryberger (1979). He categorised annual wind patterns into three main regimes; 'unimodal', 'bimodal' and 'complex', and subdivided 'unimodal' and 'bimodal' into two subregimes each. In 'unimodal' regimes winds blow from nearly one direction throughout the year. If the distribution is restricted to  $45^\circ$  it is called 'narrow unimodal', while if a distribution is larger than  $45^\circ$  it is called 'wide unimodal'. In 'bimodal' regimes the wind distribution comprises two modes. If the angle between the two modes is less than  $90^\circ$  it is called 'acute bimodal', while if the angle is greater than  $90^\circ$  it is called 'obtuse bimodal'. In 'complex' regimes the wind distribution comprises either more than two modes or no distinct mode.

The second important factor is thought to be sand availability; *i.e.* the amount of sand available for dune building. Wasson and Hyde (1983) developed a diagram of dune types with respect both to wind variability and to sand availability. Later this diagram was refined by Livingstone and Warren (1996, reproduced in Figure 2.2). These diagrams are accepted by many researchers.

Another type of relation between bedform alignment and directionally varying flows was proposed by Rubin and Hunter (1987). From theoretical considerations they claimed that bedforms are aligned such that the gross normal sand transport throughout the cycle of wind directional variation is maximum. This relation was confirmed with a series of flume experiments carried out by Rubin and Ikeda (1990), and supported with field observations of aeolian dunes by Lancaster (1991).

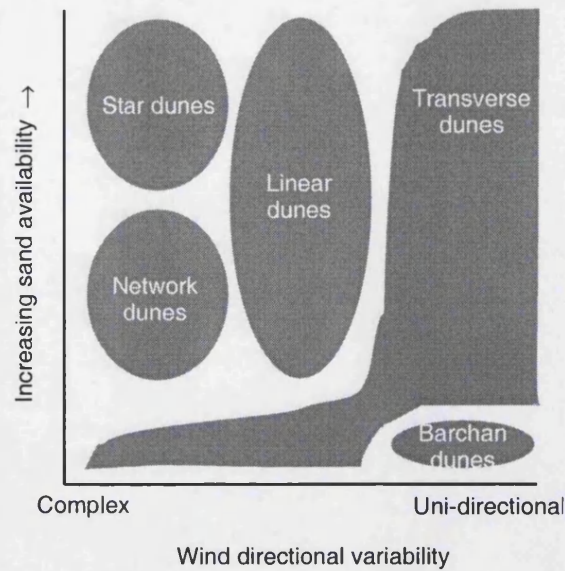


**Figure 2.2:** Dune type diagram with regard to sand availability and wind-direction variability (after Livingstone and Warren, 1996, figure 5.22).

## 2.4 Dune dynamics and sand transport induced by wind and by gravity

### 2.4.1 Sediment continuity equation

Dune dynamics, which describes changes of dune shape and dune migration is governed by the sediment (sand) continuity (conservation) equation:

$$\begin{aligned}
 0 &= \gamma \frac{\partial \eta}{\partial t} + \frac{\partial q}{\partial x} + \frac{\partial q}{\partial y} \\
 &= \gamma \frac{\partial \eta}{\partial t} + \nabla q,
 \end{aligned} \tag{2.1}$$

where  $t$  is time,  $x$  and  $y$  are horizontal distances,  $\gamma$  is the bulk density of sand in  $\text{kg m}^{-3}$ ,  $\eta$  is surface elevation in m and  $q$  is sand flux in  $\text{kg m}^{-2} \text{s}^{-1}$ . According to equation (2.1), erosion occurs when the sand flux ( $q$ ) diverges ( $\nabla q > 0$ ), and deposition occurs when it converges ( $\nabla q < 0$ ).

Transverse dunes and barchan dunes, which migrate downwind ( $+x$  direction, say) without changing their shapes, are often discussed in two-dimensional space.

In this approximation, combining the geometric considerations and the sediment conservation equation leads to the well-known condition that a shape-invariant dune must follow:

$$\gamma c_d \frac{\partial \eta}{\partial x} = \frac{\partial q}{\partial x}, \quad (2.2)$$

where  $c_d$  is dune migration speed (celerity) in  $\text{m s}^{-1}$  (Bagnold, 1941; Zeman and Jensen, 1988; see section 3.2.1 with Figure 3.3 for derivation). Equation (2.2) is applicable also to ripples and mega dunes, if they migrate without change in their shape. In the cases of dunes and mega dunes, equation (2.2) results in the well-known wind speedup over the windward slope of a dune (see section 2.4.4), through, for example, Bagnold's sand transport equation described below (section 2.4.3). However, it should be noted here that equations (2.1) and (2.2) are universal, so that they can be applied also to bedforms in other environments, such as ripples and dunes in a river.

## 2.4.2 Sand motion induced by wind

From his wind tunnel experiments, Bagnold (1941) proposed that there were three distinct types of sand motion induced by wind; creep, saltation and suspension. Creep was the rolling or sliding motion of sand grains in contact with the sand surface. Saltation was the ballistic, short-distance jump of sand grains, induced by wind shear or the impact of another saltating grain. In saltation, the sand grains typically rose a few centimetres and flew forward many centimetres, and ultimately descended again to the surface. Suspension was the movement of sand grains kept aloft and transported long distances following turbulent eddies in the wind. These three forms of motion occur if the wind shear stress exceeds a specific value, the threshold shear stress, and co-exist. Generally, creep, saltation and suspension apply to heavy, medium and light sand grains, respectively.

Observations using high-speed photography revealed that there is another type of sand motion, reptation (Mitha *et al.*, 1986). Reptation is the splash-like movement of sand grains thrown up by a descending saltating grain. Reptating grains

do not receive enough kinetic energy from the saltating particle to enter into saltation themselves (although some ejected grains do). Typically their mean ejection velocities are less than 1/10 of the impact velocity of the saltating grains. Anderson (1987a) found that ripple wavelength is not related to the saltation length, as was widely believed since Bagnold's work (1941), and that it is about six times long as the mean reptation length.

For dune dynamics, saltation is the dominant sand transport mechanism. In what follows, only saltation-dominated dynamics are discussed. However, for sand grains departing at the dune crest, modified saltation approaching a state of suspension could be expected due to the turbulence effect (Hunt and Nalpanis, 1985; Anderson, 1987b). The consequent long airborne trajectories of such grains may have a significant importance to dune dynamics (see section 2.4.6).

### 2.4.3 Sand transport formulae

Wind velocity over a flat surface can be expressed by the Kármán/Prandtl relations:

$$u_* = \frac{u_z}{5.75 \log\left(\frac{z}{z_0}\right)}, \quad (2.3)$$

where  $u_*$  is wind shear velocity,  $u_z$  is the velocity at the height of measurement ( $z$ ), 5.75 is a constant incorporating von Kármán's constant ( $\kappa \sim 0.4$ ) and  $z_0$  is the roughness length (referred to as roughness height in some literature). Shear velocity ( $u_*$ ) is another expression of shear stress ( $\tau$ ) given by

$$u_* = \sqrt{\frac{\tau}{\rho_a}}, \quad (2.4)$$

where  $\rho_a$  is air density.

Bagnold first studied sand transport in connection with this boundary flow pattern (1941). He established the following semi-empirical formula relating sand flux ( $q(x)$ ) with wind shear velocity ( $u_*(x)$ ), where  $x$  is horizontal distance.

$$q(x) = C_B \left(\frac{D_g}{D_r}\right)^{1/2} \left(\frac{\rho_a}{g}\right) u_*(x)^3, \quad (2.5)$$

where  $C_B$  is constant,  $D_g$  is sand grain diameter,  $D_r$  is a reference sand grain diameter of 0.25 mm,  $\rho_a$  is air density, and  $g$  is gravitational acceleration. Kawamura (1951) postulated that the shear stress acting on sand grains is due in part to the direct wind shear and also to impacting sand grains. This idea resulted in a different sand transport formula from Bagnold's (2.5), and it was the first to incorporate the threshold shear stress ( $u_{*t}$ ). According to Bagnold (1941) the threshold shear velocity is expressed as

$$u_{*t} = A \left( \frac{\rho_s - \rho_a}{\rho_a} g D_g \right)^{1/2} \approx 0.1 \left( \frac{\rho_s}{\rho_a} g D_g \right)^{1/2}, \quad (2.6)$$

where  $A$  is a constant ( $\approx 0.1$ ),  $\rho_s$  is sand density. Many formulae have since been proposed for sand transport (Greeley and Iversen 1985). Among others, Lettau and Lettau's formula:

$$\begin{aligned} q(x) &= C_{LL} \left( \frac{D_g}{D_r} \right)^{1/2} \left( \frac{\rho_a}{g} \right) u_* (x)^2 (u_* (x) - u_{*t}) & u_* (x) > u_{*t} \\ &= 0 & u_* (x) \leq u_{*t}, \end{aligned} \quad (2.7)$$

where  $C_{LL}$  is constant, is currently, the most widely used (Lettau and Lettau, 1978; Greeley and Iversen, 1985 pp.99-100). However, which formula best describes the actual sand transport is still in debate (Sherman *et al.*, 1998).

The wind and the sand grains interact with each other in transport. Once saltation occurs, saltating sand grains modify the log-linear profile of the wind expressed in equation (2.3). For example, roughness length ( $z_0$ ) increases from the static value of  $D_g/30$  (Bagnold, 1941) to one that depends on the surface shear velocity ( $u_*$ ):

$$z_0 = 0.02 \frac{u_*^2}{2g} \quad (2.8)$$

(Owen, 1964). Theoretical and experimental studies of the "Owen effect" were reviewed by Gillette (1999), whose review included the Raupach formula (Raupach, 1991), which is an extension of Owen's (2.8).

In the same way that roughness length ( $z_0$ ) is modified once saltation occurs, the threshold shear velocity becomes smaller, namely the "impact threshold shear velocity" (Bagnold, 1941). A slope correction to the threshold shear velocity, which was derived theoretically by Howard (1977), is another important modification in

view of dune dynamics. Though both field and laboratory experiments show that threshold shear stresses on upslope surfaces differ from those on downslope surfaces (Hardisty and Whitehouse, 1988a; 1988b, Iversen and Rasmussen, 1994), the significance of this effect is in debate as is mentioned again later (section 2.7.1).

#### 2.4.4 Wind flow over a dune

The most characteristic wind flow features over dunes are wind speedup on the windward slope and the reverse flow in the lee. Wind speedup has been noted, both in the field and in wind tunnel experiments (see for example Mulligan, 1988; Burkinshaw *et al.*, 1993; Frank and Kocurek, 1996b; Lancaster *et al.*, 1996; Wiggs *et al.*, 1996). Here it is worth recalling sand transport formulae (equations (2.5) and (2.7)). It is the surface shear velocity ( $u_*$ ), or more correctly the surface shear stress ( $\tau$ ), that causes sand transport, and is hence associated with the erosion/deposition pattern over the dune surface. Since the log-linear wind profile (2.3) is valid only on a flat surface, it is difficult to estimate the surface shear velocity on dune surfaces from the conventional wind data. This difficulty was recognised firmly by around 1996 (Frank and Kocurek, 1996b; Lancaster *et al.*, 1996; Wiggs *et al.*, 1996). Recently direct sand-flux measurement using sand traps has become popular, replacing the conventional wind-speed measurement using cup-anemometers (Lancaster *et al.*, 1996; Walker, 1999). The use of sand traps may be a more integrated measurement which accounts for the fluctuation in the surface shear velocity. Since sand flux is a cubic function of the surface shear velocity ( $q \sim u_*^3$ ), if only the average surface shear velocity is discussed, sand flux may be under-estimated. In this respect too, sand-trap measurements are thought to be superior to the use of anemometers.

Using sand traps, Lancaster and co-workers found that shear velocity increases linearly over a barchan dune, provided that the wind is strong enough such that the shear velocity significantly exceeds the threshold shear velocity (Lancaster *et*

*al.*, 1996, figure 10). However, this condition is not always satisfied. A non-linear increase of shear velocity was suggested by Frank and Kocurek (1996b, figure 3), though this was deduced from the conventional wind-speed measurement. Accurate observation and prediction of wind speedup and the associated increase in the surface shear velocity, which is more important, is a vital part of dune study. This is because, as seen in equation (2.2), the sand-flux increase over the windward slope of a dune is necessary to sustain the shape of the windward slope (Bagnold, 1941; Zeman and Jensen, 1988). The wind speed profile over the dune has been studied also by using a scaled dune model which was placed in a wind tunnel (*e.g.* Howard *et al.*, 1978; Wiggs *et al.*, 1996).

The surface slope changes abruptly at the dune crest. The angle of a slipface, as defined by the angle of repose of 30 – 33° for dry sand (Livingstone and Warren, 1996, p72; also see section 2.4.5), is too sharp for the oncoming wind to follow the topography. Consequently, the wind and the topography separate at the dune crest and the “separation zone” is formed, in which reverse flow occurs. The separation zone extends to the re-attachment point which is about four times the dune height in the lee of the dune crest (Frank and Kocurek, 1996a). This topic will be revisited at the end of this subsection.

Another characteristic of flow over dunes is the wind speed decline just upwind of the dune. This phenomenon is astonishing, since if we treat it simply this could make the dune migrate backwards, which is, of course, against observations in the field. To remedy this anomaly, enhanced turbulence just upwind of the dune may probably be invoked (Wiggs *et al.*, 1996; Van Boxel *et al.*, 1999).

Wind flow patterns over dunes have three-dimensional structures. Wind diversion around a barchan dune was well documented by Howard *et al.* (1978). Wind deflection at the crest was studied by Tsoar (1983) for linear dunes, and by Lancaster (1989) for star dunes.

The patterns of flow described above are idealised mean wind-flow patterns. In

the field, however, the wind profile and speed are not constant. According to Frank and Kocurek (1996a), for example, the wind flow re-attachment point varies from 1.6 to 5.4 dune heights downwind of the crest. Furthermore Knott reported that strong gusts blew in the mornings at Salah in Algeria, which may be important for dune initiation (Knott, 1979, referred to in Cooke *et al.*, 1993, p323; Lancaster, 1996).

#### 2.4.5 Avalanche and sand deposition on the lee face

A 10 m dune migrates typically  $10 - 30 \text{ m year}^{-1}$  (Cooke *et al.*, 1993, figure 23.24). The deposits created by migration form strata in which ancient dune migrations have been recorded. According to Hunter, there are three types of depositional modes: 1) ripple laminae; 2) grainfall laminae; and 3) grain flow laminae (hereafter termed avalanche) (Hunter, 1977a). Types 2 and 3 occur on slipfaces. An avalanche occurs when the sandy surface slope exceeds the angle of repose which is commonly  $30 - 33^\circ$  (Livingstone and Warren, 1996, p72). Theory and laboratory experiments suggest that this slipface is indeed not a smooth but a complicated surface, which is a consequence of avalanches of all sizes (Bak *et al.*, 1987; Bak 1996; see SOC in section 1.2). The top end of the slipface is called the brink. Brink and crest (the highest point of a dune) sometimes coincide, and are sometimes separate. The reason of this brink-crest coincidence/separation has been much debated, but is still obscure (see Cooke *et al.*, 1993, pp331–333). For barchan dunes and transverse dunes, which are strongly two-dimensional, the windward face is erosional and the leeward face is depositional.

Hunter (1985) discussed the alternating sequence of grainfalls and avalanche deposition on the lee slope of transverse dunes, and developed a kinematic model, which predicts some structural characteristics such as the spacing relation between grainfall and avalanche. In the model he assumed that the deposition rate due to grainfall on the lee slope is constant from the brink to a certain point, and exponentially decreases with distance downwind from that point. Though



evidence of these conditions may be preserved in strata, from which ancient dune migrations may be deduced, no quantitative comparison of this model to nature has yet been made.

Grainfall mainly comprises the saltating sand grains crossing the brink and then being deposited on the leeface. An expression for saltation length was developed by Anderson and Hallet (Anderson and Hallet, 1986). Following their study, Anderson (1988) studied this depositional process further, and re-examined Hunter's assumption in the previous paragraph. He found that a small bump forms on the slipface just leeward of the brink, unlike Hunter's assumption. This bump was observed in the field. Detailed field study of the sand deposition pattern on a slipface was reported with computer simulations by McDonald and Anderson (1995).

#### 2.4.6 Dune migration

It is widely believed that aeolian sand dunes migrate downwind without changing their shapes (Bagnold, 1941). Dune migration is a result of the erosion on the windward surface and the deposition on the slipface in the lee. Dune migration speed (celerity) is usually described by Bagnold's expression (Bagnold, 1941):

$$c_d = \frac{q(0)}{\gamma H}, \quad (2.9)$$

where  $q(0)$  is sand flux in  $\text{kg m}^{-1} \text{s}^{-1}$  at the dune crest,  $\gamma$  is sand bulk density in the dune in  $\text{kg m}^{-3}$ , and  $H$  is dune height in m. This inverse relation between migration speed ( $c_d$ ) and dune height ( $H$ ) has been amply confirmed by many researchers and is summarised by Cooke *et al.* (1993, figure 23.24). Wilson (1972) proposed a more refined expression of migration speed ( $c_d$ ):

$$c_d = \frac{q(0) - q(+\infty)}{\gamma H}, \quad (2.10)$$

where  $q(+\infty)$  is the outgoing sand flux not captured by the slip face, whose implications are discussed later (section 3.2.1).

Estimating migration speeds of dunes is one of the major challenges in aeolian geomorphology, since migration is one of the most hazardous aspects of dunes. Protecting a road from inexorably advancing dunes needs a continuous removal operation (Livingstone and Warren, 1996, p162). A recent field study in north-eastern Brazil found dunes migrating at speeds that were completely out of the range of those summarised by Cooke *et al.* (1993, figure 23.24). A dune of more than 50 m height was noted to migrate at a speed of more than 15 m year<sup>-1</sup> (Jimenez *et al.*, 1999). This suggests that the deduction based only on empirical knowledge, as in the summary by Cooke *et al.*, is sometimes misleading. However, no model has yet been proposed that can explain these field data systematically.

## 2.5 The structure and evolution of a dune field

Dune fields have spatial structure both in plan and in depth. Lancaster (1988) found that dune-to-dune spacing (wavelength) scales with dune height. Dune-to-dune spacing is thought to be regulated by the secondary wind flow that is in turn generated by dunes themselves. The longitudinal spacing between transverse dunes (measured in the direction perpendicular to the dune trend) is thought to be related to the size of the wind separation zone in the lee of the dune (see section 2.4.4), while the lateral spacing between linear dunes (also measured in the direction perpendicular to the dune trend) may be associated with helical roll vortices (Lancaster, 1995, pp185–190). Dune-to-dune spacing may also be controlled by sand grain size as noted by Wilson (1972).

The vertical structure (strata) is the record of the evolution of a dune-field and the dunes within it. Kocurek *et al.* (1992) described dune field evolution in Padre Island, Texas. Mature barchan dunes with a slipface grew from a flat sand surface, and decayed again to a flat surface annually. Lancaster (1996) studied sand patches (protodunes) in detail, and found that they are initiated in an area of spatially and temporally fluctuating wind shear velocity.

The interpretation of the internal structure of dune fields is not an easy task, for it requires consideration based on the sediment state comprised of sediment supply, sediment availability and the transport capacity of the wind (Kocurek and Lancaster, 1999). Dune fields show many types of strata (Hunter, 1977b). In many cases of migrating transverse bedforms, only the sediment deposited on each lee slope and not eroded during the passage of a following dune may be preserved as cross-stratified strata. Therefore cross-strata analysis needs an understanding of the collective motions of dunes.

The surface between older and newer bedforms is called a bounding surface. Brookfield (1977) related the order of bounding surfaces and dune field dynamics. "First order surfaces mark the movement of dunes. Second and third order surfaces are related to the migration of dunes and local airflow instabilities respectively". The bounding surface is seldom horizontal, in which case each subsequent dune climbs over the one before. This is known as bedform climbing, which may be an important correction when comparing simulation results of dune field evolution to ancient records of dune fields. Rubin and Hunter (1982) considered climbing dune fields as net-depositional areas. They discussed the dynamics of two-dimensional dune trains migrating downwind with decreasing size or number, which contribute to sand accumulation resulting in a climbing dune field. They showed that under certain conditions, the thickness of a climbing transverse stratum is a function of dune height and the rate of downwind decrease in the transport rate. Using this relation, they estimated heights of ancient dunes recorded in the Navajo, De Chelly and Entrada Sandstones, and concluded that they might be more than a few hundred meters.

Until recently, the internal structure of a dune has been reconstructed from the stratigraphic knowledge gained from an outcrop or a trench in the field, but ground-penetrating-radar, a recently developed technique, now enables the investigation of the three-dimensional internal structure of dunes without physical penetration. Using this technique, Bristow *et al.* (2000) showed that a so-called linear dune can migrate laterally (in the direction perpendicular to the dune trend).

In addition to these stratigraphic analyses, absolute dating techniques can now provide us with significant information about the formation dynamics of dunes and dune fields over long periods of time. While radiocarbon ( $^{14}\text{C}$ ) can date only to 40,000 years (Livingstone and Warren, 1996, p132), optical (luminescence) dating techniques “can provide reliable ages for aeolian sediments ranging in age from a few hundred to a few hundred thousand years” (Singhvi and Wintle, 1999). Studying aeolian deposits in the Last Glacial Maximum is particularly important since in that period there were higher winds than at present, so that many of our present aeolian bedforms may have originated then (Warren and Allison, 1998).

## **2.6 Analytical studies of emergence and shape of dunes**

Important progress has been made in the theoretical study of subaqueous dunes. There are some distinct differences between the environments of aeolian and subaqueous dunes and ripples. For example, there is the free surface between air and water, which appears to play an important role in dune formation under the water. Waves on this free surface are thought to cause anti-dunes, the subaqueous, dune-like bedforms which, however, migrate upcurrent (Yalin, 1977, pp220-222). Another major difference is that water is much denser than air, so that the fall velocity of particles is much lower, and consequently suspended sand grains play a significant role in subaqueous dune formation. Still there are many similarities between the two types of bedform in morphology and in dynamics.

### **2.6.1 Linear instability analysis**

Ripples and dunes are considered to form when a previously plane bed destabilises after which undulations with a certain range of wavelengths grow. Stability analysis of a plane bed under water dates back to Kennedy (1963), and has more

recently been reviewed by McLean (1990). Anderson (1987a) applied this analysis to the formation of aeolian ripples, and succeeded in calculating the relation between ripple wavelength and the mean reptation length. Non-linear analyses for aeolian ripples have also been made (Prigozhin, 1999; Valance and Rioual, 1999).

Stam (1996) developed a two dimensional dune model combining linear approximation of Bagnold's sand transport formula (2.5) and the wind flow theory developed by Jackson and Hunt (1975), which is introduced in more detail with mathematical expressions in the next chapter (section 3.3.2). He showed that combining the Jackson-Hunt theory and the linearised Bagnold formula leads to the phase difference between topography and shear stress, which is thought to be necessary when dunes grow from a plane bed with a small undulation (Kennedy, 1963; McLean, 1990). There are three drawbacks in his model. First, only sinusoidal migrating patterns can be analysed. Second, due to linearisation, dunes show exponential growth without reducing their migration speeds. These two drawbacks are not avoidable in linear instability analysis. And last, the model shows that all wavelength components are unstable, and that the shorter the wavelength, the more quickly its component grows. Consequently shorter-wavelength components dominate, and a dune profile cannot be maintained.

Later Stam developed a numerical model incorporating avalanching, which he expected to suppress short-wavelength components, into his analytical model (Stam, 1997). However the resulting dunes still did not resemble natural dunes.

## 2.6.2 Kinematic analysis

This is an approach to modelling that focusses on the geometry of moving objects, here ripples and dunes. Kinematic discussion in dune geomorphology dates back to Exner<sup>1</sup> (referred to in Cooke *et al.*, 1993, p328), who attempted to explain the

---

<sup>1</sup>in Exner, F.M. 1920. 'Zür Physik der Dünen', *Akademie der Wissenschaften, Wien, Mathematisch-Naturwissenschaft-liche Klasse, Abteilung 1*, 129, 929–952. Since the author

asymmetric profile of a dune in the wind direction. Fredsøe (1982) estimated the equilibrium shape and dimensions of a sequence of subaqueous dunes including their height and wavelength, using the current flow pattern downcurrent of a step whose height is the same as the dune considered. Applying linear stability analysis he found that the estimated shape was stable. The resulting shape was at least qualitatively acceptable. In his paper, Fredsøe (1982) presented an equation that he conjectured the equilibrium dune must follow:

$$\frac{h(x)}{H} = \frac{q(x)}{q(0)}, \quad (2.11)$$

where  $h(x)$  is the surface height at  $x$ ,  $H$  is the dune height,  $q(x)$  is the sand flux at  $x$  and  $q(0)$  is the sand flux at the crest. Using this equation, Lancaster (1985) predicted the dune surface profile for various wind speeds upwind of the dune, together with his field-measured sand transport data.

Compared to the study of aeolian dunes, well defined experiments on subaqueous dunes are relatively easy, using flumes. When the mean current velocity is increased, an originally plane bed changes to dunes migrating downcurrent. Further increases of mean current velocity lead to another plane bed called the upper-regime plane bed. Ultimately the increase of mean current velocity results in antidunes migrating upcurrent, which are strongly related to the existence of the free surface between the air and the water, and are thought to be unlikely to occur subaerially. These changes among dunes, plane bed and antidunes also depend on the sand grain size. Increasing grain size makes these changes occur at higher current velocities. The morphological diagram against stream power and grain size was given by Allen (1970, figure 2.6). Engelund and Fredsøe (1974) discussed the kinematics of subaqueous dunes and succeeded in describing the transition from dunes to plane bed. They thought that the transition occurred when the dominant sand transport mode changed from bedload transport, which corresponds to saltation and creep in aeolian processes, to suspension. This scheme was supported by recently conducted flume experiments (Bennett *et al.*, 1998). This dune-to-plane-bed transition may be more universal. Looking wider afield, could not track this paper, it is not included in the references list.

since the air on Venus is extremely dense (Greeley and Iversen, 1985, p28), aeolian processes and geomorphology on Venus are similar to subaqueous ones on Earth. Using a wind tunnel which simulated Venusian atmosphere, Bougan and Greeley (1985) demonstrated the possibility of a transition from dunes to upper plane bed on Venus.

### 2.6.3 Difficulties in analytical studies

The previously reviewed analyses have been carried out for the two-dimensional geometry of dunes, representing transverse dunes at right angles to the flow. In his book, however, Allen (1968) emphasised the importance of three dimensional flow patterns on ripple and dune patterns. These three-dimensional patterns affect not only the shape of single dunes but also the alignment of dune systems. For example, the pattern of out-of-phase transverse bedforms (the common pattern), where neighbouring bedforms downwind are arranged such that they are half a wavelength shifted sideways (see Figure 4.16), is said to be strongly associated to three-dimensionally diverted local wind flow (Wilson, 1970 referred to in Cooke *et al.*, 1993, figure 26.1). These three-dimensional current flows over bedforms have been studied with flume experiments, and related observations were made in the desert (see section 2.4.4). However, mathematical formulations of these patterns have proved difficult.

## 2.7 Computer modelling of dunes and dune fields

There have been many attempts to model dune evolution and migration. They can be divided into two types. In the first type, which is based on detailed physical processes, the aim is to reproduce an isolated dune on a flat surface. In the other type, which is based on more abstract mathematical rules, the aim is to model a dune field, in which many dunes grow, vanish, migrate and interact

with each other.

### 2.7.1 Models dealing with an isolated dune on a flat surface

The fundamental framework of this type of model was established by Howard *et al.* (1978). They attempted to model sand transport over a mature barchan dune in the Salton Sea dune field in California. Sand transport was estimated from field-measured topography together with wind direction and speed data which were measured both in the field, and in the laboratory with a scaled model dune. The resulting erosion/deposition patterns derived from the spatial pattern of sand transport were similar to those observed in the field and those predicted by the assumption of equilibrium. They found some important results: 1) the best results are obtained without assuming delay between shear stress and the sand transport rate; 2) better results are obtained without a slope correction for the sand transport rate (see section 2.4.3); and 3) variations in surface shear are more important in determining windward side equilibrium than are the direct effects of sediment convergence and divergence.

Since their model depends on field-observed wind data, it cannot predict dune evolution. Following their study, many models simulating a dune evolution using wind flow simulators have been presented. These models, in general, iteratively carry out the four calculations shown in Figure 2.3. Simulations usually start from a simple, gentle, initial topography such as a conical sand pile.

Among the steps in Figure 2.3, the flow-field calculation is the most difficult. Jackson and Hunt (1975) presented an analytical expression of airflow over a low hill. Later field measurements confirmed the Jackson-Hunt theory, and are reviewed by Taylor (1987). The Jackson-Hunt theory predicts wind speedup over the windward slope of a low hill, which is one of the major characteristics of the wind flow over a dune. The Jackson-Hunt theory has been regarded as



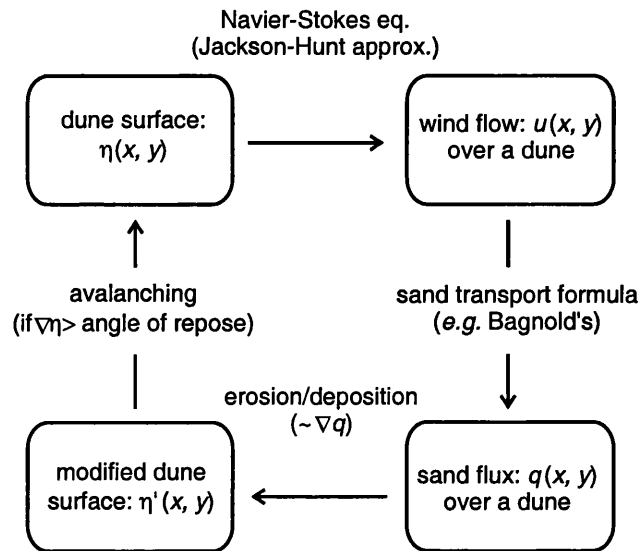


**Figure 2.3:** Flow chart for dune modelling in the conventional method.

If  $\eta'(x + dx, y + dx) = \eta(x, y)$ , the dune is at equilibrium. The dune migration speed is  $c_d = (dx/dt, dy/dt)$ .

one of the greatest achievements in the study of wind flow over terrain (Taylor, 1987). The merits of using the Jackson-Hunt theory are that: a) it gives clear insight about flow dynamics; and b) it allows for rapid calculations. However, this theory is strictly only valid for hills with gentle slopes not exceeding about  $3^\circ$  (Van Boxel *et al.*, 1999), although according to Walmsley and Howard (1985), the slope of ‘up to about 0.2 is probably acceptable’ ( $\tan^{-1} 0.2 = 11^\circ$ ). However it is definitely not applicable to the flow around a slipface in the lee of a dune. None of the flow models so far correctly calculates reverse flow over slipfaces. Other major limitations in the Jackson-Hunt theory is that it is applicable only to an isolated hill on a flat surface, such as a barchan dune, and that roughness length is constant all over the whole topography.

Modifying the Jackson-Hunt theory to make it applicable to a desert dune was first attempted by Walmsley and Howard (1985). Walmsley *et al.* (1982) developed a model of boundary-layer flow, MS3DJH/1.5, which is based on Mason and Sykes’ (1979) three-dimensional extension of the Jackson-Hunt theory (1975). Using the topographic data of the model dune in the Salton Sea dune

field in California, studied by Howard *et al.* (1978), Walmsley and Howard (1985) investigated the applicability of their model of wind flow to a barchan dune. The average windward slope angle of this dune is about  $8^\circ$ , and the dune has a slip-face in its lee. They concluded that the theory was reliable for the wind flow over the windward slope of the dune. Howard and Walmsley (1985) then incorporated this flow model with Howard's 1978 dune model. During the simulation, however, numerical instability occurred very early, and the resulting dune did not resemble the natural one.

Another drawback of using models based on the Jackson-Hunt theory for dunes is that the models predict the decline in the surface shear velocity just upwind of the dune, leading to the backwards migration of the dune, which, of course, is against observations in nature. Later, Weng *et al.* (1991) developed a three-dimensional wind flow model, FLOWSTAR, based on a revision by Hunt *et al.* (1988) to the Jackson-Hunt theory. However, there was still the decline in the surface shear velocity just upwind of the dune.

Wippermann and Gross (1986) thought that Howard and Walmsley's failure came from the use of an analytical wind flow model which was limited to terrain of low slope ( $< 0.2$ ). Instead, Wippermann and Gross used a numerical wind flow model developed by Gross<sup>2</sup>, FITNAH (Flow over Irregular Terrain with Natural and Anthropogenic Heat Sources). This non-hydrostatic, first-closure numerical wind-flow model can simulate even the reverse flow in the lee of the dune. Shear velocity is computed using the logarithmic wind profile. As well as sand transport induced by wind, avalanching is introduced on the slipface. Although the model includes an operation to smooth the surface, and the question of equilibrium shape was not solved, Wippermann and Gross succeeded in reproducing a barchan dune with good geometrical agreement to dunes in the Pampa de la Joya, Peru (Finkel, 1959). They also showed that under strong wind conditions, the barchan dune

---

<sup>2</sup>in Gross, G. 1985. 'An explanation of the Maloja-Serpent by numerical simulation', *Contr. Phys. Atm*, **58**, 441–457. Since the author could not track this paper, it is not included in the references list.

becomes lower and more elongated, while under light wind conditions, it remains high and wider. This tendency coincides with Melton's (1940) qualitative picture of the influence of wind speed on barchan dune shape. However, Warren (1988) found that the network dunes in Oman became steeper during a period of strong wind. It is not clear which picture is correct or in what wind and sand conditions.

Despite this remarkable success in reproducing barchan dune patterns, some of the assumptions used by Wipermann and Gross are crude, and revisions need to be introduced into their model. For example, the derivation of friction velocity from the logarithmic wind profile is only valid if the surface is uniform and flat. Zeman and Jensen (1987) developed a two-dimensional wind flow model, which is a second-order-closure type, and discussed the effect of streamline curvature on turbulence strength, which is not negligible if the slope exceeds  $3 - 5^\circ$  (Van Boxel *et al.*, 1999). Using their wind flow model, Zeman and Jensen (1988) attempted to simulate two-dimensional dune evolution, and to see if there is an equilibrium form. However simulations resulted in the dune migrating backwards, which is, needless to say, unsuccessful.

Although Zeman and Jensen's attempt was unsuccessful, the importance of using a second-order-closure wind flow model has been recognised, since the effect of streamline curvature on turbulence strength was emphasised by Wiggs *et al.* (1996) through their field measurements and wind tunnel study. Van Boxel *et al.* (1999) developed a two-dimensional, second-order-closure model, based on Zeman and Jensen's model (1987). Van Boxel *et al.* pointed out the importance of the enhanced turbulence associated with streamline curvature. Using this wind flow model, Van Dijk *et al.* (1999) developed a two-dimensional model which numerically simulates dune evolution. They demonstrated the growth of the asymmetric two-dimensional dune with a slipface in the lee from an initial single, symmetric, "sine-shaped" topography (the exact function was not specified). The resulting dune reached an equilibrium dune height, although the toe of the windward slope did not move, so that the windward slope kept elongating. They also showed that using first-order-closure wind-flow calculations results in dunes decreasing their

heights.

In general, while much effort has been made to calculate correctly the wind flow over the windward surface, few attempts have been made to model the grain-fall dynamics in the lee. It is not evident whether a continuum treatment, which is expressed in the differential form (2.1), can be applied at the dune crest, where the surface slope changes abruptly.

## 2.7.2 Models dealing with dune field dynamics

Since the models reviewed above are mostly based on the Jackson-Hunt theory or on the intensive Computer Fluid Dynamics (CFD) calculations, they have been applied only to isolated single dunes on flat surfaces. In many cases, however, transverse dunes form closely connected dune trains. Extending the modelling to a dune field, where many dunes grow, migrate and interact, is not an easy task. It is, for example, extremely difficult to calculate three dimensional wind patterns over many different temporary forms of dune, such as partially connected dunes. To simulate dune fields, we need more phenomenological models based not on detailed physical processes, but on simplified rules which, however, should correctly reflect observational facts.

Use of such simulation models has the merit of dimensionality. Most analytical studies and simulation models based on CFD, as seen above, discuss only two-dimensional dunes transverse to the wind, because dealing with three-dimensional features is mathematically difficult and computationally intensive. On the other hand, developing a computer-simulation model in three dimensions is not so difficult. Such computer-simulation models have been shown to be effective in explaining ripple formation (Nishimori and Ouchi, 1993; Anderson and Bunas, 1993; Landry and Werner, 1994).

Three models were proposed almost simultaneously, one by Nishimori and co-

workers (1993; 1998), another by Werner (1995), and the other by de Castro (1995). These models are mathematically different in formulation, but are all based on two-dimensional discrete dynamics. They attempt to simulate dune field dynamics on a two-dimensional lattice, where dunes emerge from an initial flat surface with a small undulation, and then grow.

Nishimori and Ouchi (1993) developed a dune-field model based on a two-dimensional Coupled Map Lattice, CML, which is a mathematical system of spatially connected local maps distributed on each lattice site. The model was an extension of that developed for ripples in the same paper. CML deals with a continuous variable on each lattice site, which here is the surface elevation (height). Periodic boundary conditions are applied both in the  $x$  and in the  $y$  directions. The model comprises wind-directional sand transport and diffusion. Diffusion is a deformational shaping (levelling) process by gravity, and is introduced instead of avalanching. The steeper the slope, the more sand is transported downwards. Since diffusion is a local, continuous process, it is easy to implement, although avalanching in nature is a global, discrete process (see section 2.4.5). Sand motion is represented by the exchange of a block of sand between lattice sites. Hereafter, this block is called a ‘slab’ following Werner (1995). Sand transport is set such that a slab is transported farther if eroded from the windward surface, and less far if from the lee surface. The map represents time evolution, so that the dune field evolves following deterministic dynamics. In terms of CML, local dynamics (mapping) represents erosion, and the spatial connection among lattice sites represents wind directional sand transport and subsequent deposition, plus diffusion. Nishimori and Ouchi succeeded in demonstrating the formation of a barchan dune field.

Later Nishimori *et al.* (1998) extended this idea to simulate various types of dunes under different environments. Two major revisions were made. They refined the wind-directional sand transport rule, considering the CFD-based wind-flow calculation over a two-dimensional dune. They also introduced wind-directional change by periodically shuffling three sand transport directions perpendicular to

each other, resulting in three types of wind regimes; uni-, bi- and tri-directional. Together with these revisions, they investigated the effects of sand availability, that is the amount of sand being able to be moved. They succeeded in demonstrating the emergence of barchan, transverse, linear and star dunes corresponding to difference in wind regime and sand availability. The simulated transverse dunes and linear dunes have terminations (defects, Y-junctions), which are also observed in nature. They also developed a diagram for relating dune shape, wind directional variability, and sand availability, which is roughly identical to those based on empirical knowledge (see section 2.3). A discrepancy with this approach, however, is that the empirical observations show that in the bi-directional wind regime with a large amount of sand, linear dunes emerge, while the simulation reproduces transverse dunes (Wasson and Hyde, 1983; Livingstone and Warren, 1996, figure 5.22 on p80). Nishimori *et al.* not only demonstrated dune and dune field morphology, but also some aspects of their dynamics. For example smaller barchans moved faster than bigger ones (Cooke *et al.*, 1993, figure 23.24). Dune-dune interactions such as coalescence (Kocurek *et al.*, 1992), and smaller dunes running up and down larger dunes also occurred.

Werner (1995) developed a slightly different dune field model. Unlike Nishimori's model, the dynamics in Werner's model are stochastic, and the dune field consists of three-dimensionally discrete sand slabs, so that height, which is proportional to the number of sand slabs piled on each lattice site, is discrete. Periodic boundary conditions are adopted. An erosion site is randomly chosen, and the eroded slab is transported down over a specific number of lattice sites. Based on Bagnold's (1941) observation, a depositional probability difference is introduced between sites with at least one slab and sites without any slab. Furthermore, a shadow zone of  $15^\circ$ , in which the deposition probability is unity regardless of whether there is a slab or not, is introduced, which corresponds to the reattachment point downwind which is set at four times the dune height from the dune crest (following Frank and Kocurek, 1996a). These are the rules for wind-directional transport. Furthermore, avalanching occurs on the steepest descent if the gradient between two adjacent lattice sites exceeds  $30^\circ$ . A change in wind direction was simu-

lated by periodically altering sand slab transport directions. Werner succeeded in demonstrating barchan, transverse, linear and star-like dunes, changing wind directional variability, and sand availability, though for some simulations such as the one for transverse dunes, the presumed sand depth was not thought to be sufficient (*cf.* Wasson and Hyde, 1983; Livingstone and Warren, 1996, figure 5.22 on p80). Like those demonstrated by Nishimori *et al.* (1998), the transverse dunes and linear dunes simulated by Werner had terminations, whose motions may significantly contribute to the dune alignment to the wind (Werner and Kocurek, 1997), and to dune-to-dune spacing (Werner and Kocurek, 1999). Werner also demonstrated some aspects of dune and dune field dynamics; dune-dune interactions such as coalescence; and small barchans being “calved” from the horns of larger barchans. He showed that dune shape was insensitive to wind-directional deviation. Examining the resulting patterns in detail, even qualitatively, some problems can be found. For example, the cross-sectional views of simulated barchans and transverse dunes are much more symmetric than those of real dunes.

For directions not parallel to the dominant wind, both Nishimori and co-workers and Werner assumed only gravitational sand transport, although sand transport by the wind diverted around dunes, or sharply deflected at the crest, has been observed in nature on barchan dunes (Howard *et al.*, 1978), linear dunes (Tsoar, 1983) and star dunes (Lancaster, 1989).

Neither paper quantitatively discussed the comparison between simulated patterns and real dune field patterns. This is thought to be because of the difficulty of scaling the dynamics in the model to the processes in nature. Another problem is that both models cannot deal with a net-depositional dune field leading to bedform climbing since they adopted periodic boundary conditions.

de Castro (1995) developed a model to simulate the coastal dune field comprising alternating sequences of transverse dunes and vegetation areas. The basis of the model resembles Werner's. However, some simulation rules adopted in de Castro's

paper, such as random choice of the transport distance between the two limits and enforcement of the maximum climbing slope angle of  $4^\circ$ , are questionable and the model does not seem to be applicable to desert dune fields. Nevertheless, it is unfortunate that de Castro's paper has not attracted much attention so far. In a geomorphological sense, this model might be considered to be more advanced than those by Nishimori *et al.* and by Werner, because of the following two distinct characters. The model was developed by considering both spatial and temporal scales in nature. Moreover, instead of enforcing a periodic boundary condition, the model deals with an open dune field with a constant sand supply from the sea.

Generally in computer simulations, dune-like patterns can be easily obtained with various rules, in other words, models are not unique. Hence it is very important to examine if the simulation rules correctly reflect real physics in nature. In chapters 5 and 6, we will aim to develop a dune-field model with qualitative and quantitative agreement with nature, where we will pay particular attention to temporal and spatial scales.



## CHAPTER 3

# Modelling a transverse and a barchan dune

### 3.1 Introduction: shape and migration speed

Although many dunes are known to change their shape continually (Hesp and Hastings, 1998), some aspects of their migration can be discussed under an assumption of equilibrium. In conditions of unidirectional constant winds and sand supply, it is well known that transverse and barchan dunes migrate downwind without changing their shapes (Bagnold, 1941; Coursin, 1964; Long and Sharp, 1964; Hastenrath, 1967; Howard *et al.*, 1978; Fryberger *et al.*, 1984; Al-Hinai and Moore, 1987; see also section 2.4.6). This dynamic equilibrium is a consequence of the interaction between the form and the processes, known as *morphodynamics* (Livingstone and Warren, 1996, pp77–79). Considering the shape of barchan dunes, there are two distinct characteristics which may indicate that they are at equilibrium: a) the cross-sectional shape perpendicular to the wind (depicted as B-B' in Figure 3.1) is height independent (Hesp and Hastings, 1998; Sauermann *et al.*, 2000); whereas b) the cross-sectional shape parallel to the wind (A-A'), *i.e.* the profile, is height dependent: the higher the dune, the steeper the windward slope (Finkel, 1959; Long and Sharp, 1964; Hastenrath, 1967; Sauermann *et al.*, 2000).

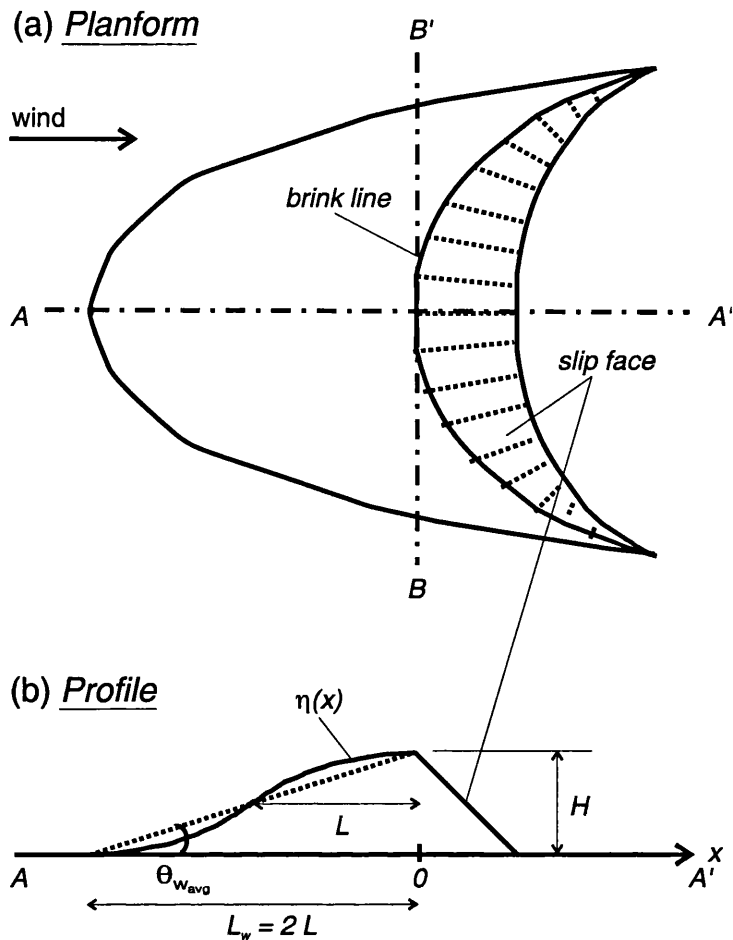


**Figure 3.1:** Schematic views of a barchan dune (a) from top and (b) from side.

The shape of a dune at equilibrium is still not well understood. Howard *et al.* (1978) deduced some requirements that must be satisfied by the equilibrium shape of a barchan dune and the wind flow over it, and checked the validity of these requirements using limited field data (see section 2.7.1). Without more empirical data, however, their model cannot predict the surface profile of the dune, hence the above two characteristics a) and b) remain unsolved.

The evolution of the dune surface profile has previously been calculated by iteratively solving the interaction between the topography and the wind flow as schematically viewed in the block flow chart of Figure 3.2 (Howard and Walmsley, 1985; Wippermann and Gross, 1985; Zeman and Jensen, 1988; Stam, 1997; Van Dijk *et al.*, 1999; see section 2.7.1 for details). In this type of modelling, the

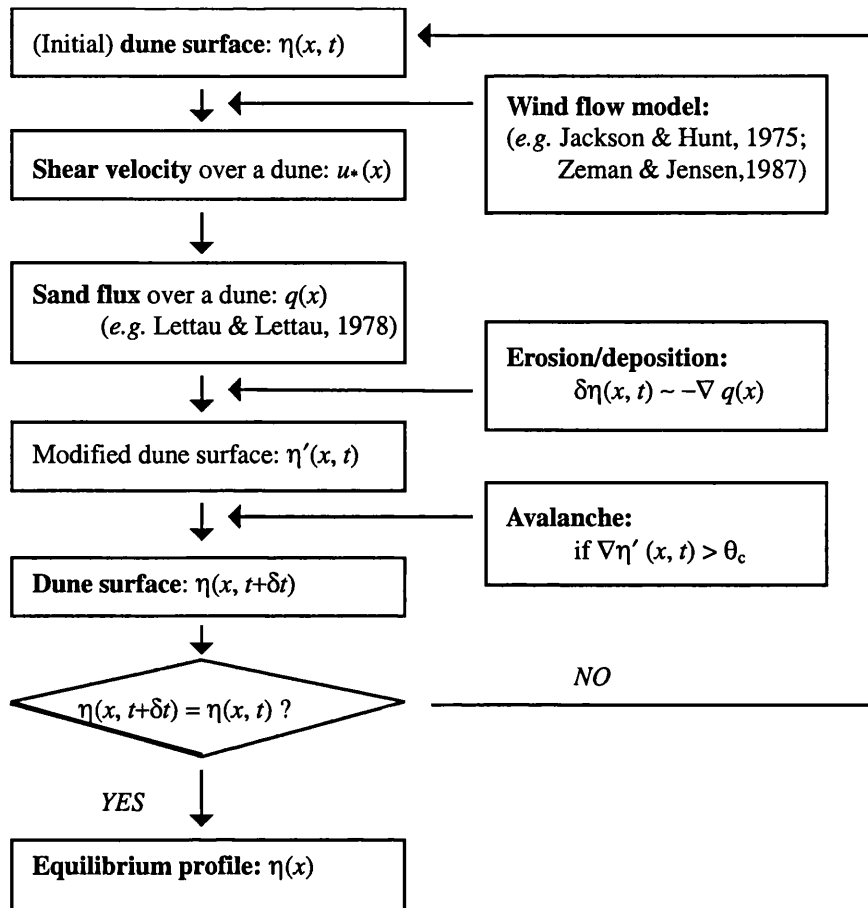


**Figure 3.2:** Flow chart for dune modelling in the conventional method.

equilibrium surface profiles are defined as those that do not show any change after successive iterations. However, complete equilibrium has not yet been achieved using this approach. The three-dimensional barchan dune simulated by Wippermann and Gross (1985) showed a continual decrease in height and elongation in the windward slope with time. Although Van Dijk *et al.* (1999) showed a height saturation for the two-dimensional dune, the windward slope continued to elongate.

While still restricting the problem to dunes at equilibrium, a different approach is possible, where the dune surface profile is solved as a boundary-condition problem. On the assumption of morphological conservation, Zeman and Jensen (1988) developed such a model, but with limited success due in part to the difficulties in wind-flow calculation.

Dune migration speed ( $c_d$ ) is usually described with the Bagnold formula for dune migration speed (2.9):

$$c_d = \frac{q(0)}{\gamma H},$$

where  $q(0)$  is sand flux at the dune crest,  $\gamma$  is sand bulk density in the dune, and  $H$  is dune height (Bagnold, 1941). A more accurate expression is the Wilson formula (2.10):

$$c_d = \frac{q(0) - q(+\infty)}{\gamma H},$$

where  $q(+\infty)$  is the outgoing sand flux not captured by the slip face (Wilson, 1972; section 2.4.6). We can now introduce the concept of sand trapping efficiency ( $T_E$ , dimensionless), which is the proportion of moving sand trapped in the dune slip face to the total amount of sand crossing the dune crest (Wilson, 1972; Cooke *et al.*, 1993, pp346–347). The Wilson formula (2.10) is then rewritten as

$$c_d = \frac{T_E q(0)}{\gamma H}. \quad (3.1)$$

$T_E$  is related to the pattern of deposition of sand on the slip face which was modelled by Anderson (1988) and McDonald and Anderson (1995).

Sand flux ( $q(x)$ ) can be estimated from shear velocity ( $u_*(x)$ ) using the Bagnold formula for sand flux (2.5):

$$q(x) = C_B \left(\frac{D_g}{D_r}\right)^{1/2} \left(\frac{\rho_a}{g}\right) u_*(x)^3,$$

where  $C_B$  is a constant,  $D_g$  is sand grain diameter,  $D_r$  is reference grain diameter,  $\rho_a$  is air density,  $g$  is gravitational acceleration (Bagnold, 1941), or using the Lettau and Lettau formula (2.7):

$$\begin{aligned} q(x) &= C_{LL} \left(\frac{D_g}{D_r}\right)^{1/2} \left(\frac{\rho_a}{g}\right) u_*(x)^2 (u_*(x) - u_{*t}) & u_*(x) > u_{*t} \\ &= 0 & u_*(x) \leq u_{*t}, \end{aligned}$$

where  $C_{LL}$  is a constant and  $u_{*t}$  is the threshold shear velocity, below which no saltation occurs (Lettau and Lettau, 1978). The two formulae (2.5) and (2.7) give almost identical results for the cases where  $u_*(x) \gg u_{*t}$  (see for example Fryberger, 1979, figure 92).

Both the Bagnold (2.9) and the Wilson (2.10; 3.1) formulae for dune migration speed were derived as a consequence of the assumption of shape invariance. In such conditions, as Zeman and Jensen (1988) noted, the outgoing and the incoming sand fluxes must be the same:

$$q(+\infty) = q(-\infty). \quad (3.2)$$

If otherwise, dunes shrink ( $q(+\infty) > q(-\infty)$ ) or grow ( $q(+\infty) < q(-\infty)$ ). Consequently, the Bagnold formula (2.9), which does not take into account the outgoing sand flux ( $q(+\infty)$ ), suffers not only inaccuracy, but also inconsistency in its derivation.

The Wilson formula (2.10; 3.1), which is consistent in its derivation, is still not satisfactory. It suffers lack of predictive power. There are many dunes in a dune field, each being different in height, as will be seen in section 3.3.1. It is practically impossible to know the shear velocity at the crest ( $u_*(0)$ ) for each dune. On an ideal flat surface, it is true, wind speed ( $u$ ) and shear velocity ( $u_*$ ) are connected by the Kármán-Prandtl formula (2.3):

$$u_* = \frac{u_z}{5.75 \log\left(\frac{z}{z_0}\right)},$$

where  $u_z$  is the velocity at the height of measurement ( $z$ ), 5.75 is a constant incorporating von Kármán's constant ( $\kappa \sim 0.4$ ) and  $z_0$  is the roughness length. But in order to use wind data collected at nearby meteorological stations to predict qualitatively (semi-quantitatively) dune migration speed, a model that links dune migration speed and shear velocity on the level surface is necessary. For quantitative estimations, wind data collected closer to the dunes are necessary.

The first half of this chapter (section 3.2) shows that only by assuming an equilibrium condition and by estimating the sand trapping efficiency ( $T_E$ ), can a self-consistent model that describes transverse dune migration be developed. The following section (3.2) shows how the sand trapping efficiency ( $T_E$ ) depends on wind shear velocity ( $u_*$ ) and dune height ( $H$ ), and consequently how  $T_E$  influences dune migration speed ( $c_d$ ). The discussion is developed by combining and extending Zeman and Jensen's (1988) approach and Anderson's (1988) microscale

analysis of sand grain deposition on the slip face. Throughout the first half of the next section (3.2.1) the importance of the equilibrium assumption, wind speedup over the windward surface of a dune and sand trapping efficiency ( $T_E$ ) are repeatedly emphasised. They are shown to be strongly connected.

In the second half (section 3.3), after examining field data of the windward surface profile of barchan dunes, the model is further extended by introducing the wind-flow theory developed by Jackson and Hunt (1975). This introduction enables the estimation of the surface profile of a dune at equilibrium, as a boundary-condition problem.

## 3.2 Migration speed of transverse dunes and sand trapping efficiency

### 3.2.1 Migration speed of transverse dunes at equilibrium

Since sand flux ( $q$ ) can be related to shear velocity ( $u_*$ ) via equation (2.5) or (2.7), dune migration speed ( $c_d$ ) in (3.1) can be calculated using the shear velocity at the crest ( $u_*(0)$ ). However this section shows that  $c_d$  can be related to the shear velocity on a level surface ( $u_*(-\infty)$ ), rather than to  $u_*(0)$ , if dune-shape invariance (equilibrium) is assumed. It also shows that the replacement of  $u_*(-\infty)$  for  $u_*(0)$  implicates the well-known wind speedup phenomenon on the windward surface of dunes (section 2.4.4).

The discussion below follows Zeman and Jensen (1988). If it is assumed that the dune form is unchanged during downwind migration ( $+x$  direction), the following simple geometric relations must hold:

$$\begin{aligned}\tan \alpha &= \frac{\partial \eta}{\partial x}, \\ c_d \delta t \frac{\partial \eta}{\partial x} &= -\frac{\partial \eta}{\partial t} \delta t,\end{aligned}$$

where  $\alpha$  is local slope,  $\eta$  is surface elevation and  $t$  is time (see Figure 3.3(a) and (b)). The advection equation can be described as

$$\frac{\partial \eta}{\partial t} + c_d \frac{\partial \eta}{\partial x} = 0. \quad (3.3)$$

The sediment continuity equation (2.1), in two dimensions, which must always be satisfied regardless of dune form, is

$$\gamma \frac{\partial \eta}{\partial t} + \frac{\partial q}{\partial x} = 0. \quad (3.4)$$

Combining equations (3.3) and (3.4) leads to equation (2.2):

$$\gamma c_d \frac{\partial \eta}{\partial x} = \frac{\partial q}{\partial x}.$$

Equation (2.2), which was also derived by Bagnold (1941), must always be satisfied when discussing the migration of shape-invariant dunes. Integrating (2.2) from  $x = -\infty$  to  $x = 0$ , we get

$$q(0) - q(-\infty) = \gamma c_d H. \quad (3.5)$$

$x = 0$  at the dune crest, and dune height ( $H$ ) is  $\eta(0)$ .

Equations (3.3), (2.2) and (3.5) were derived by Zeman and Jensen (1988). They are applied below to the derivation of an analytical formulation relating dune migration speed ( $c_d$ ), sand trapping efficiency ( $T_E$ ), sand flux on a level surface ( $q(-\infty)$ ), and shear velocity on a level surface ( $u_*(-\infty)$ ). Substituting (3.1) into (3.5), we get

$$q(0) = \frac{q(-\infty)}{1 - T_E}. \quad (3.6)$$

By estimating sand trapping efficiency ( $T_E$ ) and assuming an appropriate sand flux formula such as equation (2.5) or (2.7), equation (3.6) allows dune migration speed ( $c_d$ ) to be calculated from shear velocity on a level surface ( $u_*(-\infty)$ ). Shear velocity ( $u_*$ ) is easier to estimate on a level surface than at the crest, since on such a surface, unlike at the crest, the log-linear wind profile expressed by equation (2.3) is well maintained.

By definition, sand trapping efficiency ( $T_E$ ) varies from 0.0 to 1.0. Since the sand flux at the crest has a finite value, equation (3.6) shows that where sand trapping

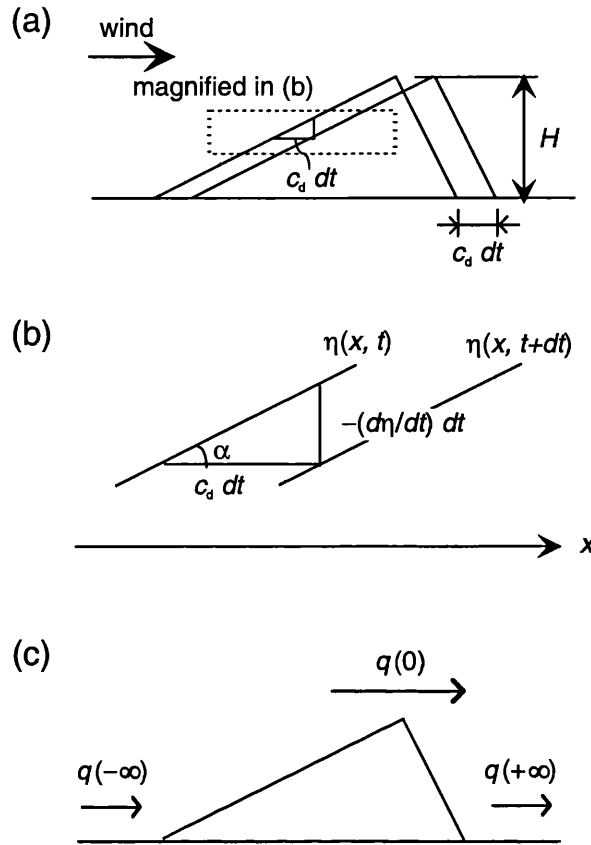


**Figure 3.3:** Cross-sectional geometry of a migrating shape-invariant transverse dune: (a) global view (b) magnified view of windward surface (c) sand flux ( $q(x)$ ) over a dune.

efficiency ( $T_E$ ) is nearly 1.0, sand flux on a level surface ( $q(-\infty)$ ) is almost equal to 0.0, so that the shear velocity on a level surface ( $u_*(\infty)$ ) is almost equal to the threshold shear velocity ( $u_{*t}$ ).

It is shown below that equation (3.6) is the direct result of the assumption of equilibrium (Figure 3.3(c)<sup>1</sup>). According to the definition of trapping efficiency ( $T_E$ ),

$$q(+\infty) = (1 - T_E) q(0). \quad (3.7)$$

<sup>1</sup>Usually in Figure 3.3(c),  $q(0) > q(-\infty) (= q(+\infty))$  because of the wind-speedup effect (more precisely, the shear-velocity-increase effect) as will be discussed in the next page (see also section 2.4.4). According to the sediment continuity equation (2.1), however,  $q(0) < q(-\infty) (= q(+\infty))$  may be applied to an anti-dune migrating upcurrent under the water, which is out of the scope of this thesis (see sections 2.4.1 and 2.6).



As an equilibrium dune form is assumed here,

$$q(+\infty) = q(-\infty).$$

Combining equations (3.7) and (3.2), we again get equation (3.6).

For mathematical simplicity, in the rest of this section sand flux ( $q$ ) is defined with Bagnold's formula (2.5). Substituting (2.5) into (2.2), we get

$$\frac{\partial \eta}{\partial x} = \left(\frac{1}{c_d \gamma}\right) C_B \left(\frac{D_g}{D_r}\right)^{1/2} \left(\frac{\rho_a}{g}\right) \frac{\partial(u_*^3)}{\partial x}. \quad (3.8)$$

Integrating (3.8), we get

$$u_*(x)^3 = u_*(-\infty)^3 + \frac{\eta(x)}{\left(\frac{C_B}{c_d \gamma}\right) \left(\frac{D_g}{D_r}\right)^{1/2} \left(\frac{\rho_a}{g}\right)}, \quad (3.9)$$

$$u_*(0)^3 = u_*(-\infty)^3 + \frac{H}{\left(\frac{C_B}{c_d \gamma}\right) \left(\frac{D_g}{D_r}\right)^{1/2} \left(\frac{\rho_a}{g}\right)}.$$

Equation (3.9) shows that shear velocity increases as the wind climbs the windward surface of a dune, as found empirically on a barchan dune by Lancaster (1996, figure 10). Since the vertical wind profile on the windward surface of a dune is not log-linear as expressed in equation (2.3), this increase in shear velocity does not necessarily mean an increase in wind speed at any height. Yet, this increase in shear velocity is thought to relate to the well-known wind speedup over a dune, which has been observed both in the field and in experiments (see for example Mulligan, 1988; Lancaster, 1995; Wiggs *et al.*, 1996; see also section 2.4.4). Wind speedup was also theoretically predicted by Jackson and Hunt (1975), who considered wind flow over a gentle hill.

Substituting (2.5) into (3.6), we get

$$u_*(0)^3 = \frac{u_*(-\infty)^3}{1 - T_E}. \quad (3.10)$$

Equation (3.10) shows that, at equilibrium, sand trapping efficiency ( $T_E$ ) is related to the shear velocity increase over the dune. If sand trapping efficiency ( $T_E$ ) is small, shear velocity increase is small, and if  $T_E$  is large the increase is large. If  $T_E \simeq 1.0$ , the use of equation (3.10) is not valid and equation (3.6) should be

used instead, together with a sand flux formula which incorporates the threshold shear velocity ( $u_{*t}$ ), such as Lettau and Lettau's (2.7). Note that sand trapping efficiency ( $T_E$ ) is itself a function of shear velocity on a level surface ( $u_*(-\infty)$ ), so that equation (3.10) does not mean a linear relationship between the shear velocities at the crest ( $u_*(0)$ ) and on a level surface ( $u_*(-\infty)$ ).

Substituting (2.5) and (3.6) into (3.1) we get the detailed form of the relation for dune migration speed ( $c_d$ ), with regard to shear velocity on a level surface ( $u_*(-\infty)$ ) and sand trapping efficiency ( $T_E$ ):

$$c_d = \left(\frac{1}{\gamma H}\right) C_B \left(\frac{D_g}{D_r}\right)^{1/2} \left(\frac{\rho_a}{g}\right) u_*(-\infty)^3 \left(\frac{T_E}{1 - T_E}\right). \quad (3.11)$$

Although in chapter 4, numerical calculations are carried out using a more accurate but very lengthy form of the expression for  $c_d$ , derived using Lettau and Lettau's formula (2.7), the overall trend is thought to be well described with (3.11).

### 3.2.2 Sand trapping efficiency

In this section analytical expressions of sand trapping efficiency ( $T_E$ ) are derived with regard to the shear velocity at the dune crest ( $u_*(0)$ ), dune height ( $H$ ) and sand grain diameter ( $D_g$ ). The discussion follows Anderson's (1988) study of sand deposition on the slip face near the crest. The equation numbers in his paper are given below as in the form of "[A88 (xxx)]". Since there are some miscalculations in Anderson's paper, some of his equations are recalculated below. Figure 3.4 shows the model and co-ordinate system used here. The  $x$ -axis is set differently from Anderson's. Following Anderson (1988), the region downwind of the crest ( $x > 0$ ) is considered to be comprised of the saltation zone ( $x > 0, z > 0$ ) and the lee zone ( $x > 0, z < 0$ ). The saltation zone is the zone of saltation alone where the force of the wind and gravity act together, and the lee zone is the zone where grains are accelerated only by gravity.

The number of grains crossing the  $z = 0$  plane through the window  $[x_0, x_0 + dx_0]$ ,

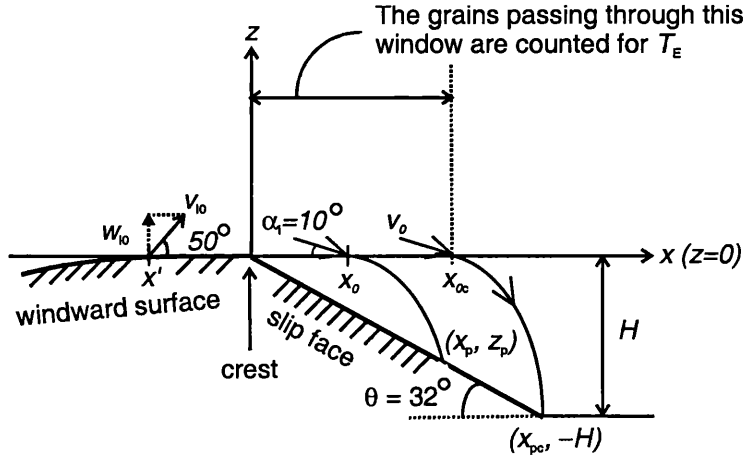


**Figure 3.4:** Model and co-ordinate system used in calculation of sand trapping efficiency ( $T_E$ ).

having originated in the upwind window of the dune crest  $[x', x' + dx']$  is

$$[N_{x_0} | x'] dx_0 = N_0(x') P[\lambda = (x_0 - x')] dx' dx_0$$

[A88, (6)], where

$$P[\lambda = (x_0 - x')] = (x_0 - x')^{(1/d)-1} / (d c^{1/d} v l_0) \exp\{-(x_0 - x')^{1/d} / c^{1/d} v l_0\}, \quad (3.12)$$

$$c = 0.36 (D_g/0.25)^{-0.5} (u_*/0.5)^{0.5}, \quad (3.13)$$

$$d = 2.0 (u_*/0.5)^{0.4}, \quad (3.14)$$

and  $D_g$  is sand grain diameter in mm,  $u_*$  is shear velocity in  $\text{m s}^{-1}$ , and  $v l_0$  is mean grain lift-off velocity in  $\text{m s}^{-1}$ . These three equations correspond to [A88, (7); corrected], [A88, (3); a part of] and [A88, (3); a part of]<sup>2</sup>.  $v l_0$  can be derived through the calculation of mean vertical lift-off velocity,  $w l_0$  (Anderson

<sup>2</sup>Equation (3.12) can be derived from the following two relations:

$$P[w l_0] \sim \exp[-w l_0 / \langle w l_0 \rangle_{\text{mean}}]$$

and

$$\lambda = c v l_0^d,$$

which are [A88, (5); modified] and [A88, (3); a part of], respectively. In addition,  $P[\lambda] \sim P[v l_0] \sim P[w l_0]$  and  $v l_0 \sim w l_0$  are assumed, neither being described explicitly in Anderson's (1988) paper.

and Hallet, 1986):

$$wl_0 = 0.64 u_* (0.25/D_g)^{1.5}, \quad (3.15)$$

this being [A88, (5b)] in Anderson's paper. According to White and Schulz (1977)

$$vl_0 = wl_0 / \sin(50^\circ).$$

In the following argument shear velocity ( $u_*$ ) in (3.13), (3.14) and (3.15) is approximated with that at the crest ( $u_*(0)$ ). Equation (3.12) is different from that introduced by Anderson (1988) by the factor of  $1/d$ . It is because the condition:

$$\int_0^{+\infty} P(\lambda) d\lambda = 1$$

should be satisfied, that the  $1/d$  factor is necessary.

The total number of grains crossing all downwind windows will then be the sum over all possible upwind origin sites, yielding the integral:

$$N_{x_0} = \int_{-\infty}^0 N_0(x') P[\lambda = (x_0 - x')] dx' \quad (3.16)$$

[A88, (8)]. Assuming that the surface just upwind of the crest is gentle enough so that  $N_0(x') = N_0 = \text{const.}$ , and substituting (3.12) into (3.16), we get

$$N_{x_0} = N_0 \exp(-x_0^{1/d}/c^{1/d} vl_0) \quad (3.17)$$

[A88, (9); corrected]. Equation (3.17) is different from that derived by Anderson (1988), because of the factor introduced above.

Of all the sand grains crossing the  $z = 0$  plane, only those crossing through the window  $[0, x_{0c}]$  are assumed to be captured on the slip face, hence contributing to sand trapping efficiency ( $T_E$ ). Integrating (3.17), we can calculate all those grains crossing through the window  $[0, x_{0c}]$

$$\int_0^{x_{0c}} N_{x_0} dx_0 = \int_0^{x_{0c}} N_0 \exp(-x_0^{1/d}/c^{1/d} vl_0) dx_0.$$

The ratio of those sand grains to all sand grains crossing the dune crest, *i.e.* the sand trapping efficiency ( $T_E$ ) is:

$$\begin{aligned} T_E &= \int_0^{x_{0c}} N_{x_0} dx_0 / \int_0^{+\infty} N_{x_0} dx_0 \\ &= \int_0^{x_{0c}} \exp(-x_0^{1/d}/c^{1/d} vl_0) dx_0 / \int_0^{+\infty} \exp(-x_0^{1/d}/c^{1/d} vl_0) dx_0. \end{aligned} \quad (3.18)$$

The denominator of (3.18) can now be more analytically expressed. Replacing  $c^{1/d} v l_0 = G_1^{-1}$  and  $1/d = G_2$ , and then using the gamma function formula:

$$\int_0^{+\infty} \exp(-G_1 x^{G_2}) dx = \Gamma(1/G_2) / \{G_2 G_1^{1/G_2}\},$$

we get

$$\text{the denominator of (3.18)} = \Gamma(d) / \{(1/d) (c^{1/d} v l_0)^{-d}\}. \quad (3.19)$$

Substituting (3.19) into (3.18), we get the analytical expression of sand trapping efficiency ( $T_E$ ) with regard to  $x_{0c}$ :

$$\begin{aligned} T_E &= \int_0^{x_{0c}} N_{x_0} dx_0 / \int_0^{+\infty} N_{x_0} dx_0 \\ &= \int_0^{x_{0c}} \exp(-x_0^{1/d} / c^{1/d} v l_0) dx_0 / \Gamma(d) d c v l_0^d. \end{aligned} \quad (3.20)$$

The relation between dune height ( $H$ ) and the corresponding integral limit ( $x_{0c}$ ) in equation (3.20) can now be calculated. Given that sand grains enter the lee region at a point  $x_0$  in the  $z = 0$  plane with a speed  $v_0$  and at an angle with the horizontal of  $\alpha_i$ , they land at a site  $(x_p, z_p)$  on the slip face, which is described by

$$x_p(t) = x_0 + [v_0 \cos \alpha_i] t, \quad (3.21)$$

$$z_p(t) = -[v_0 \sin \alpha_i] t - (1/2) g t^2, \quad (3.22)$$

where  $t$  is time in  $s$ . Since  $(x_p, z_p)$  is on the slip face,

$$z_p(t) = -x_p(t) \tan \theta. \quad (3.23)$$

Solving (3.21), (3.22), and (3.23), we get

$$x_p(t) = x_0 + \{(1 - \gamma)/(2\beta)\} + [\{(1 - \gamma)/(2\beta)\}^2 + x_0/\beta]^{1/2}, \quad (3.24)$$

where

$$\gamma = \tan \alpha_i / \tan \theta, \quad (3.25)$$

$$\beta = g / (2 v_0^2 \cos^2 \alpha_i \tan \theta). \quad (3.26)$$

Equation (3.24), (3.25), and (3.26) are different from the corresponding expressions derived by Anderson (1988), because of the different co-ordinate system.

Since  $x_{pc}$  ( $x_p$  corresponding to  $x_{0c}$ ) is the bottom of the slip face,

$$x_{pc} = H / \tan \theta. \quad (3.27)$$

Substituting (3.27) into (3.24), we get the relationship between  $x_{0c}$  and  $H$ :

$$H/\tan \theta = x_{0c} + \{(1 - \gamma)/(2\beta)\} + [\{(1 - \gamma)/(2\beta)\}^2 + x_{0c}/\beta]^{1/2}. \quad (3.28)$$

Combining (3.20) and (3.28), we could draw the curves for the relation between sand trapping efficiency ( $T_E$ ) and dune height ( $H$ ). The only problem remaining is the derivation of sand grain speed at  $(x_{0c}, z_o)$  ( $v_0$ ).

The distribution of  $v_0$  has its maximum probability with the smallest value of  $v_0 = v_*$ , and decays almost exponentially (Anderson, 1988). This smallest and most probable speed ( $v_*$ ) corresponds to the shortest saltation trajectory between the crest and  $x_{0c}$ . Since sand grains are integrated with respect to their landing points, this distribution has an influence only close to the bottom of the slip face ( $x_p$ ). Considering (3.17), this effect is not large. All grains coming to  $x_{0c}$  are assumed to have been ejected at the crest, giving them the same speed ( $v_*$ ), which is the smallest and most probable one because it corresponds to the shortest saltation trajectory. According to Anderson (1988),

$$v_* = a x_{0c}^b \quad [= v_0 \text{ in (3.26)}], \quad (3.29)$$

where

$$a = 5.8 (u_*(0)/0.5)^{0.4} (D_g/0.25)^{-0.2}, \quad (3.30)$$

$$b = 0.48 (u_*(0)/0.5)^{0.2}. \quad (3.31)$$

These three equations correspond to [A88, (2)].

In summary, sand trapping efficiency ( $T_E$ ) can be described as a function of shear velocity at the dune crest ( $u_*(0)$ ), dune height ( $H$ ) and sand grain diameter ( $D_g$ ):

$$T_E = T_{E_0}(u_*(0), H, D_g). \quad (3.32)$$

If an equilibrium shape is assumed (as discussed in section 3.2.1) shear velocity at the dune crest ( $u_*(0)$ ) is related to that on a level surface ( $u_*(-\infty)$ ) by equation (3.6) and, for example, Lettau and Lettau's sand flux formula (2.7):

$$q(u_*(0)) = \frac{q(u_*(-\infty))}{1 - T_E}.$$

In such conditions, sand trapping efficiency ( $T_E$ ) can be rephrased as a function of shear velocity on a level surface ( $u_*(-\infty)$ ), dune height ( $H$ ) and sand grain diameter ( $D_g$ ):

$$T_E = T_{E-\infty}(u_*(-\infty), H, D_g). \quad (3.33)$$

Consequently, dune migration speed ( $c_d$ ) is described as

$$c_d(u_*(-\infty), H, D_g) = \frac{T_E(u_*(-\infty), H, D_g) q(u_*(-\infty), H, D_g)}{\gamma H}. \quad (3.34)$$

Note that the discussion developed above does not assume any particular windward surface shape, except that the surface just upwind of the crest is horizontal for a long enough distance.

### 3.3 Windward slope profile of a barchan dune

In section 3.2.2, the shear velocity at the dune crest ( $u_*(0)$ ) was linked to dune height, sand grain diameter and shear velocity upwind of the dune ( $H, D_g, u_*(-\infty)$ ). The calculation in section 3.2.2 is performed only by estimating the sand trapping efficiency of the dune. The windward slope profile is unknown throughout the calculation, and to estimate the profile a discussion based on fluid dynamics is strictly necessary. For this inverse problem of predicting the topography from the wind flow, the boundary conditions on surface height and shear velocity profiles ( $\eta(x), u_*(x)$ ) are as follows:  $\eta(-\infty) = 0, \eta(0) = H; u_*(-\infty), u_*(0)$  (Figure 3.5).

Although attempts based on computational fluid dynamics have been made to calculate the wind flow over a dune (most recently by Van Boxel *et al.*, 1999; see also section 2.7.1), the flow is known to be described approximately by the (modified) Jackson-Hunt theory (1975). The Jackson-Hunt theory gives an analytical solution for the wind flow over a dune, so that it can highlight the physics more clearly. The applicability of the Jackson-Hunt theory to a barchan dune was investigated by Walmsley and Howard (1985), using the topographic data of a real dune. They concluded that the theory is reliable for the wind flow over the windward slope of the dune (for details, see section 2.7.1). Since its presentation,

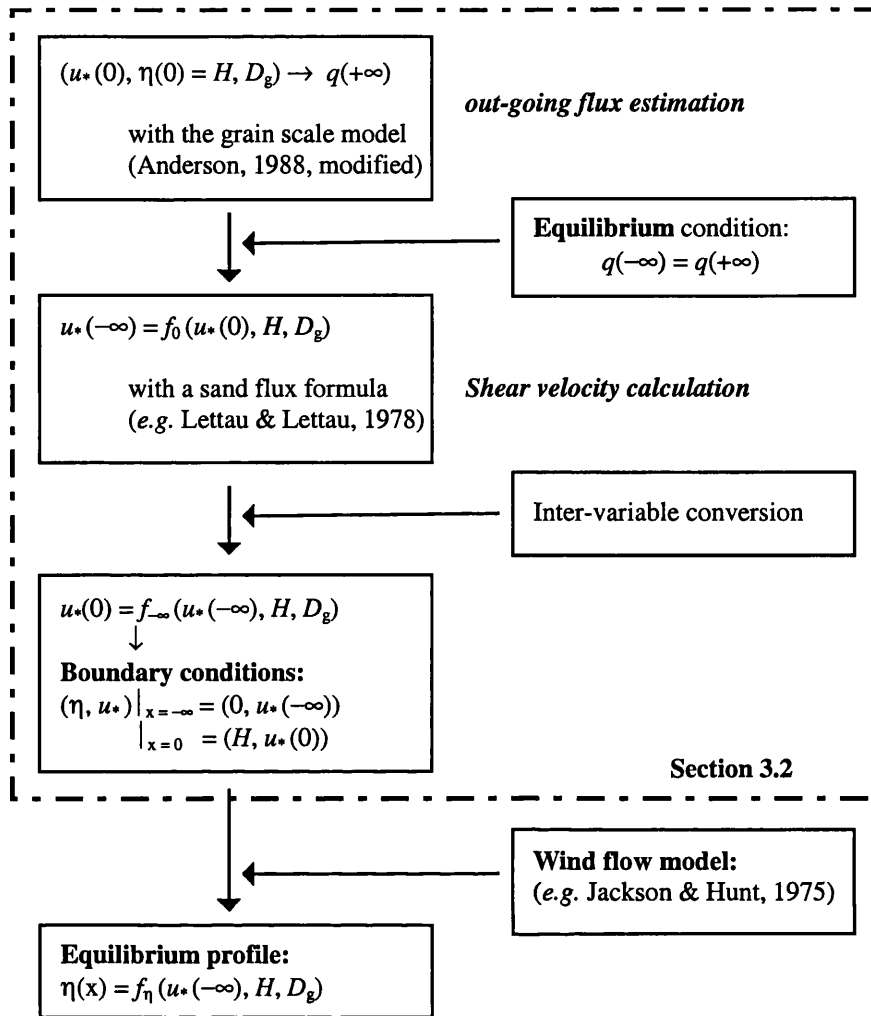


**Figure 3.5:** Flow chart for dune modelling in the new approach examined in this thesis.

the Jackson-Hunt theory has been continuously revised (see for example Hunt *et al.*, 1988; Weng *et al.*, 1991; for reviews see Taylor *et al.*, 1987; Belcher and Hunt, 1998). The most recent revision is that developed by Weng *et al.* (1991), who also discuss the applicability of the theory to a barchan dune. However, the use of the expression for the surface shear stress derived by Weng *et al.* is questionable, since it does not satisfy the symmetry condition of the Fourier transform (Weng *et al.*, 1991, equation (2.14a)).

In the following, the original Jackson-Hunt theory (1975) is incorporated into the dune-migration model developed in the previous section (3.2) for the estimation of the windward slope profile from three quantities: dune height, sand grain



diameter and shear velocity upwind of the dune ( $H, D_g, u_*(-\infty)$ ). The Jackson-Hunt theory considers a hill that has gentle windward and leeward slopes unlike a dune which has a slipface in the lee. Nonetheless, the theory is thought to be applicable to a dune with a few allowance for the air flow pattern over the dune, which is described in section 3.3.2 (see also section 2.7.1).

### 3.3.1 Windward slope profile of barchan dunes in the field

The windward slope angle of a barchan dune is typically said to range between  $4-11^\circ$  (Hesp and Hastings, 1998) or  $2-10^\circ$  (Lancaster, 1995, p52). The slope is concave at the base, steepest in mid-slope and convex at the crest (Figure 3.1). The relationship between the average windward slope angle ( $\theta_{w,avg}$ ) and dune height ( $H$ ) for some dune fields are plotted in Figure 3.6, using field data from Finkel (1959), Long and Sharp (1964), Hastenrath (1967) and Sauermann *et al.* (2000). The average windward slope angles ( $\theta_{w,avg}$ ) were calculated simply by dividing dune height ( $H$ ) by the windward slope length ( $L_w$ ) (see Figure 3.1). All sets of data show in general that the windward slope angle ( $\theta_{w,avg}$ ) increases as dune height ( $H$ ) increases.

Figure 3.6 shows that the change in the average windward slope angle as dune height increases in the data of Long and Sharp (1964) is about half that shown by the data of Hastenrath (1967). In a uni-directional wind regime, the sand grain size and wind speed are thought to be the two most important factors that govern dune dynamics (section 3.2.2). Hastenrath (1967) reported that in the dune field in southern Peru which he studied, the sand was well sorted and its grain diameter ( $D_g$ ) was between 0.125 and 0.177 mm. In contrast, in the dune field near Salton Sea, California, the sand was poorly sorted with  $D_g = 0.250$  mm (Long and Sharp, 1964, table 2). Neither paper provided details of the wind speed.

Finkel (1959) studied the same dune field as Hastenrath (1967). He reported that

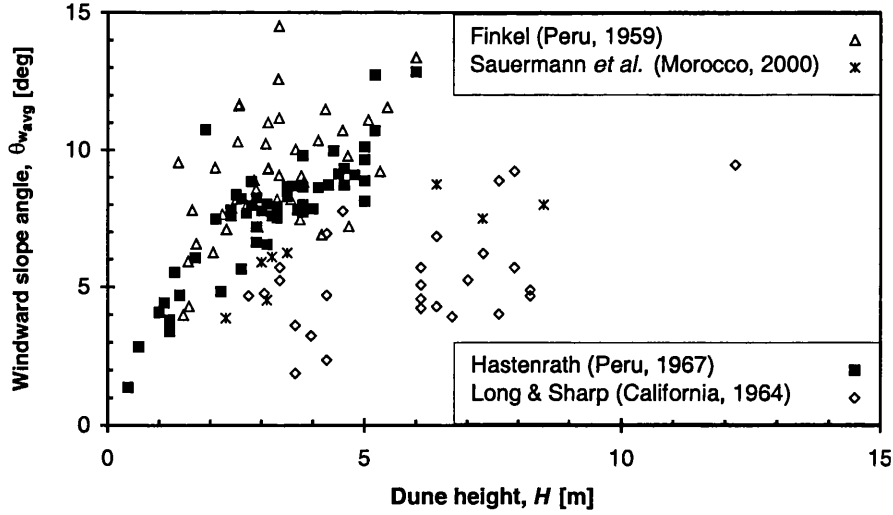


**Figure 3.6:** Measured data of dune height ( $H$ ) and the average angle of windward slope ( $\theta_{w,avg}$ ) taken from Finkel (1959), Long and Sharp (1964), Hastenrath (1967) and Sauermann *et al.* (2000).

the grain diameter ( $D_g$ ) was between 0.208 and 0.420 mm, which gives a mean value of 0.314 mm. The threshold shear velocity ( $u_{*t}$ ) corresponding to 0.314 mm is calculated as  $0.26 \text{ m s}^{-1}$  from the Bagnold (1941) formula for the threshold shear velocity (2.6):

$$u_{*t} = A \left( \frac{\rho_s - \rho_a}{\rho_a} g D_g \right)^{1/2} \approx 0.1 \left( \frac{\rho_s}{\rho_a} g D_g \right)^{1/2},$$

where  $A$  is a constant ( $\approx 0.1$ ),  $\rho_s$  is sand density and  $g$  is gravitational acceleration. Finkel introduced a ‘shape factor’ of 0.75, without definition, which gave the ‘effective particle diameter’ of 0.24 mm, with  $u_{*t} = 0.23 \text{ m s}^{-1}$ . Finkel also analysed the wind data recorded at the nearest meteorological station, which was 33 km northeast, and found that the ‘equivalent effective wind’ velocity could be calculated as  $5.32 \text{ m s}^{-1}$ . Surface shear velocity over a flat surface can be estimated with the Kármán/Prandtl relations (2.3):

$$u_* = \frac{u_z}{5.75 \log\left(\frac{z}{z_0}\right)},$$

where  $u_z$  is the velocity at the height of measurement ( $z$ ) and  $z_0$  is the roughness length. Finkel did not mention the measurement height ( $z$ ), although to analyse his field data Finkel used Bagnold’s (1941) theory in which the standard height

is 1 m. If assuming the standard height of 10 m, which was specified by the World Meteorological Organization (Fryberger, 1979, p143), together with the roughness length ( $z_0$ ) of 1 mm, the wind velocity of  $5.32 \text{ m s}^{-1}$  results in a surface shear velocity ( $u_*$ ) of  $0.23 \text{ m s}^{-1}$ , which is less than or equal to the threshold shear velocities estimated above. As the sand grain diameter reported by Hastenrath showed the ‘good agreement’ with another survey conducted by Amstutz and Chico in the same region (Hastenrath, 1967, p311), this thesis utilises Hastenrath’s data.

Since Sauermann *et al.* (2000) did not report any data on sand grain size, grading or wind speed, dunes in southern Morocco will not be discussed more in this thesis (Data on wind direction and speed during 1956–1959 and sand grain diameter in the same area are in Oulehri (1992).).

### 3.3.2 Wind-flow modelling with the Jackson-Hunt theory

In the analysis developed by Jackson and Hunt (1975), the topography of a dune is characterised by two length scales: dune height ( $H$ ) and the half distance ( $L$ ) between two sites whose height is half the dune height (see Figure 3.1). The surface profile of the topography ( $\eta(x)$ ) is then expressed in the following non-dimensional form:

$$\begin{aligned}\eta(x) &= Hf(x/L) \\ &= Hf(\xi),\end{aligned}$$

where the dune crest is set to  $x = 0$ . In the Jackson-Hunt theory, each quantity, for example the surface profile ( $f(\xi)$ ), is given in the form of Fourier transform ( $\hat{f}(k)$ ), which is defined as

$$f(\xi) = \frac{1}{2\pi} \int_{-\infty}^{+\infty} \hat{f}(k) e^{ik\xi} dk. \quad (3.35)$$

The Jackson-Hunt theory is a linear perturbation method of analysis, where each quantity is expanded about the perturbation variable ( $\varepsilon$ ), which is much less than

1.0. The surface shear stress ( $\tau(\xi)$ ) is written as

$$\tau(\xi) = \tau_0(1 + \varepsilon\tau_d(\xi)), \quad (3.36)$$

where  $\tau_0$  is the surface shear stress on the flat surface far enough upwind of the dune and  $\tau_d(\xi)$  represents the spatial variation in the surface shear stress. According to Jackson and Hunt, the perturbation variable ( $\varepsilon$ ) can be calculated from the following relation:

$$\varepsilon = \frac{H \ln^2(L/z_0)}{L \kappa \ln(l/z_0)}, \quad (3.37)$$

where  $\kappa$  is von Kármán's constant ( $\sim 0.4$ ),  $z_0$  is the roughness length, which is a function of shear velocity (see section 2.4.3), and  $l$  is defined as the inner-layer thickness, which, according to Jackson and Hunt, can be numerically calculated from the following relation:

$$\frac{l}{L} \ln\left(\frac{l}{z_0}\right) = 2\kappa^2. \quad (3.38)$$

From equation (3.37), equation (3.36) can be re-written at  $\xi = 0$  as

$$\frac{\tau(0) - \tau_0}{\tau_0} = \tau_d(0) \varepsilon \sim \tau_d(0) \frac{H}{L}.$$

Accordingly, if the windward slope is height-independent ( $H/L = \text{const.}$ ), the normalised increase in the shear stress at the dune crest ( $(\tau(0) - \tau_0)/\tau_0$ ) is expected to be almost constant.

Stam (1996, 1997) developed a two-dimensional dune model combining a linear approximation of Bagnold's sand transport formula (2.5) and the Jackson-Hunt theory (see section 2.6.1). According to Stam (1996), the Fourier transform of the surface shear stress ( $\tau_d(\xi)$ ):

$$\tau_d(\xi) = \frac{1}{2\pi} \int_{-\infty}^{+\infty} \hat{\tau}_d(k) e^{ik\xi} dk \quad (3.39)$$

can be approximated as

$$\hat{\tau}_d(k) = -\kappa|k| \hat{f}(k) \frac{\ln(z(k)) - i\phi}{(\ln(z(k)))^2 + \phi^2}, \quad (3.40)$$

where  $i = \sqrt{-1}$ ,

$$\begin{aligned}\phi &= +\frac{\pi}{4} \quad (k \geq 0) \\ &= -\frac{\pi}{4} \quad (k < 0).\end{aligned}\tag{3.41}$$

and

$$z(k) = 2\sqrt{\frac{z_0}{l}|k|}.\tag{3.42}$$

In the lee of the slipface of the dune, a reverse flow occurs, which the Jackson-Hunt theory cannot model. The leeward wind flow is very difficult to calculate correctly even using a computational fluid model (Van Boxel *et al.*, 1999). A practical remedy is to define the separation zone downwind of the slipface, and calculate the wind flow over the topography comprised of the windward surface and this separation zone (Zeman and Jensen, 1988; Van Dijk *et al.*, 1999). This thesis adopts a similar treatment. The wind flow over a dune with a slipface is replaced with that over a symmetrical gentle topography, whose windward surface represents that of the dune in consideration. The following subsections consider a cosine and Gaussian function to represent the windward slope of the dune, which changes from concave to convex between the base and the crest (Figures 3.1 and 3.7). One merit of using these functions is that the Fourier transform of the surface profiles ( $\hat{f}(k)$ ) can be analytically solved.

The windward slope length ( $L_w$ ), which will be estimated in the present paper, is defined as double the horizontal length scale ( $2L$ ). This definition is precise in the case of a cosine hill, and acceptable in the case of a Gaussian hill because

$$\eta(2L) = 0.06 H.$$

The shear velocity ratio ( $u_*(0)/u_*(-\infty)$ ) can be estimated for a given set of dune height, sand grain diameter and shear velocity upwind of the dune ( $H, D_g, u_*(-\infty)$ ) (section 3.2.2; Figure 3.5). Since shear velocity ( $u_*$ ) and shear stress ( $\tau$ ) are linked by equation (2.4):

$$u_* = \sqrt{\frac{\tau}{\rho_a}},$$

where  $\rho_a$  is air density, from equation (3.36), the shear velocity ratio can be written as

$$\frac{u_*(0)}{u_*(-\infty)} = \sqrt{1 + \varepsilon \tau_d(0)}. \quad (3.43)$$

### Cosine-hill approximation

Following Stam (1996), with the corrections that height ( $H$ ) and the characteristic horizontal distance ( $L$ ) in his model should be  $H/2$  and  $L/4$ , the dune profile is assumed to be approximated as a cosine function:

$$\begin{aligned} \eta(x) &= H \frac{1}{2} [\cos(\frac{\pi x}{2L}) + 1] \\ &= H f(\xi), \end{aligned}$$

where the non-dimensional surface profile ( $f(\xi)$ ) can be rephrased as

$$f(\xi) = \frac{e^{+i\frac{\pi}{2}\xi} + e^{-i\frac{\pi}{2}\xi}}{4} + \frac{1}{2} \quad (3.44)$$

(Figure 3.7(a)). Since the Jackson-Hunt theory can deal only with an isolated mound on a level surface, only the largest Fourier components of the dune surface profile will be discussed.

Applying equation (3.35) to equation (3.44),

$$f(\xi) = \frac{1}{2\pi} \left\{ \frac{\pi}{2} e^{+i\frac{\pi}{2}\xi} + \frac{\pi}{2} e^{-i\frac{\pi}{2}\xi} + \pi e^0 \right\},$$

so that

$$\begin{aligned} \hat{f}(k) &= \frac{\pi}{2} \quad (k = \pm \frac{\pi}{2}) \\ &= \pi \quad (k = 0) \\ &= 0 \quad (k = \text{otherwise}). \end{aligned} \quad (3.45)$$

Stam analysed a sinusoidal topography with  $k = 1$  (Stam, 1997, table 1), but this does not correctly represent the features of this topography, hence we use  $k = \pm \frac{\pi}{2}$  and  $k = \pi$  as in equation (3.45). Substituting equations (3.40)–(3.42)

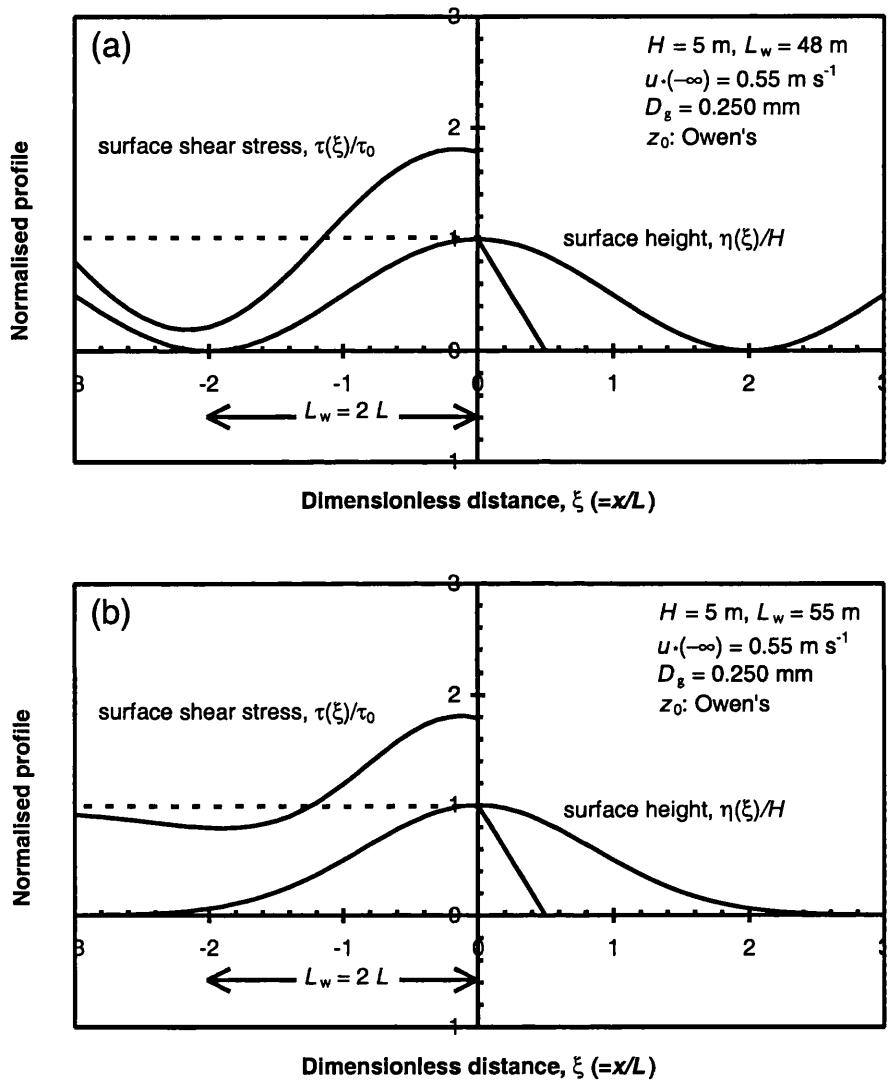


**Figure 3.7:** The normalised surface profiles ( $f(\xi)$ ) of (a) a cosine hill and (b) a Gaussian hill, and examples of normalised surface shear stress profiles ( $\tau(\xi)/\tau_0$ ) over them. The slip face is drawn just for reference, but is not used for any wind-flow calculation in this thesis.

and (3.45) into equation (3.39),

$$\begin{aligned}
\tau_d(\xi) &= \frac{1}{2\pi} \left[ -\kappa \frac{\pi}{2} \frac{\pi}{2} \frac{\ln(z(\frac{\pi}{2})) - i\frac{\pi}{4}}{(\ln(z(\frac{\pi}{2})))^2 + (\frac{\pi}{4})^2} e^{+i\frac{\pi}{2}\xi} - \kappa \frac{\pi}{2} \frac{\pi}{2} \frac{\ln(z(\frac{\pi}{2})) + i\frac{\pi}{4}}{(\ln(z(\frac{\pi}{2})))^2 + (\frac{\pi}{4})^2} e^{-i\frac{\pi}{2}\xi} + 0 \right] \\
&= \frac{\pi\kappa}{8} \frac{1}{(\ln(z(\frac{\pi}{2})))^2 + (\frac{\pi}{4})^2} \left[ (-\ln(z(\frac{\pi}{2}))) + i\frac{\pi}{4} \right] e^{+i\frac{\pi}{2}\xi} + (-\ln(z(\frac{\pi}{2}))) - i\frac{\pi}{4} e^{-i\frac{\pi}{2}\xi} \\
&= \frac{\pi\kappa}{8} \left\{ (\ln(z(\frac{\pi}{2})))^2 + (\frac{\pi}{4})^2 \right\}^{-1/2} \left[ e^{+i\theta} e^{+i\frac{\pi}{2}\xi} + e^{-i\theta} e^{-i\frac{\pi}{2}\xi} \right] \\
&= \frac{\pi\kappa}{4} \left[ (\ln(z(\frac{\pi}{2})))^2 + (\frac{\pi}{4})^2 \right]^{-1/2} \cos\left(\frac{\pi}{2}\xi + \theta_{\text{ph}}\right), \tag{3.46}
\end{aligned}$$

where

$$\theta_{\text{ph}} = \tan^{-1}\left(\frac{\pi/4}{-\ln(z(\frac{\pi}{2}))}\right)$$

is the phase difference between the topography ( $f(\xi)$ ) and the surface shear stress ( $\tau(\xi)$ ).

If the dune is at equilibrium, the sand flux and the topography ( $f(\xi)$ ) must be in phase (Zeman and Jensen, 1988, equation (10); see also Fredsøe, 1982). This requirement means that if the topography ( $f(\xi)$ ) and surface shear stress ( $\tau(\xi)$ ) are not in phase ( $\theta_{\text{ph}} \neq 0$ ), there must be another mechanism.

### Gaussian-hill approximation

A Gaussian function may also be considered to represent the windward slope (see Weng *et al.*, 1991). Here following Zeman and Jensen (1988),

$$\begin{aligned}
\eta(x) &= H \exp\left\{-\left(\frac{x}{L}\right)^2 \ln(2)\right\} \\
&= H f(\xi). \tag{3.47}
\end{aligned}$$

$\ln(2)$  in equation (3.47) is introduced so that the height at  $x = L$  is half the dune height ( $H/2$ ) (Figure 3.7(b)). From equation (3.47), the local gradient of the windward slope ( $\partial\eta(x)/\partial x$ ) is

$$\begin{aligned}
\frac{\partial\eta(x)}{\partial x} &= -\left(\frac{\ln(2)}{L^2}\right) 2xH \exp\left\{-\left(\frac{\ln(2)}{L^2}\right)x^2\right\} \\
&= -\left(\frac{2\ln(2)}{L^2}\right)x\eta(x). \tag{3.48}
\end{aligned}$$



From equation (3.48), the local curvature of the windward slope ( $\partial^2\eta(x)/\partial x^2$ ) is then

$$\begin{aligned}
\frac{\partial^2\eta(x)}{\partial x^2} &= \frac{\partial}{\partial x}\left[-\left(\frac{2\ln(2)}{L^2}\right)x\eta(x)\right] \\
&= -\frac{2\ln(2)}{L^2}\left[\eta(x) + x\frac{\partial\eta(x)}{\partial x}\right] \\
&= -\frac{2\ln(2)}{L^2}\left[\eta(x) + -\left(\frac{2\ln(2)}{L^2}\right)x^2\eta(x)\right] \\
&= -\frac{2\ln(2)}{L^2}\left(1 - \frac{2\ln(2)}{L^2}x^2\right)\eta(x). \tag{3.49}
\end{aligned}$$

Since the maximum windward slope angle ( $\theta_{w_{\max}}$ ) is at the position where the curvature is zero, from equation (3.49),

$$x = -L\sqrt{\frac{1}{2\ln(2)}}. \tag{3.50}$$

Substituting equation (3.50) into equation (3.48), the maximum slope gradient ( $\partial\eta(x)/\partial x|_{\max}$ ) is

$$\begin{aligned}
\frac{\partial\eta(x)}{\partial x}\Big|_{\max} &= -\frac{2\ln(2)}{L^2}\left(-L\sqrt{\frac{1}{2\ln(2)}}\right)H \exp\left\{-\left(\frac{\ln(2)}{L^2}\right)\frac{L^2}{2\ln(2)}\right\} \\
&= \frac{H}{L}\sqrt{\frac{2\ln(2)}{e}}. \tag{3.51}
\end{aligned}$$

Here, following Stam (1996), the approximated form of surface shear stress ( $\tau(\xi)$ ) is given below. By using a Fourier transform formula:

$$\int_{-\infty}^{+\infty} \exp^{-ax^2} \exp^{-ikx} dx = \sqrt{\frac{\pi}{a}} \exp^{-k^2/4a},$$

where  $a$  is a constant,

$$\hat{f}(k) = \sqrt{\frac{\pi}{\ln(2)}} \exp^{-k^2/4\ln(2)}. \tag{3.52}$$

Substituting equations (3.40)–(3.42) and (3.52) into equation (3.39),

$$\begin{aligned}
\tau_d(\xi) &= \frac{1}{2\pi} \int_{-\infty}^{+\infty} -\kappa |k| \sqrt{\frac{\pi}{\ln(2)}} \exp^{-k^2/4 \ln(2)} \frac{\ln(z(k)) - i\phi}{(\ln(z(k)))^2 + \phi^2} e^{ik\xi} dk \\
&= \frac{\kappa}{2} \sqrt{\frac{1}{\pi \ln(2)}} \int_{-\infty}^{+\infty} |k| \exp^{-k^2/4 \ln(2)} \frac{-\ln(z(k)) + i\phi}{(-\ln(z(k)))^2 + \phi^2} e^{ik\xi} dk \\
&= \frac{\kappa}{2} \sqrt{\frac{1}{\pi \ln(2)}} \int_{-\infty}^{+\infty} |k| \exp^{-k^2/4 \ln(2)} \frac{-\ln(z(k)) + i\phi}{(-\ln(z(k)))^2 + \phi^2} (\cos(k\xi) + i \sin(k\xi)) dk \\
&= \frac{\kappa}{2} \sqrt{\frac{1}{\pi \ln(2)}} \left[ \int_{-\infty}^{+\infty} |k| \exp^{-k^2/4 \ln(2)} \frac{(-\ln(z(k))) \cos(k\xi) - \phi \sin(k\xi)}{(-\ln(z(k)))^2 + \phi^2} dk \right. \\
&\quad \left. + i \int_{-\infty}^{+\infty} |k| \exp^{-k^2/4 \ln(2)} \frac{\phi \cos(k\xi) + (-\ln(z(k))) \sin(k\xi)}{(-\ln(z(k)))^2 + \phi^2} dk \right]. \tag{3.53}
\end{aligned}$$

In equation (3.53), the imaginary part of the integrand is ‘*odd*’, so that the corresponding integral is ‘*zero*’. On the other hand, the real part of the integrand is ‘*even*’. Equation (3.53) is then,

$$\tau_d(\xi) = \kappa \sqrt{\frac{1}{\pi \ln(2)}} \int_0^{+\infty} k \exp^{-k^2/4 \ln(2)} \frac{(-\ln(z(k))) \cos(k\xi) - (\pi/4) \sin(k\xi)}{(-\ln(z(k)))^2 + (\pi/4)^2} dk. \tag{3.54}$$

### 3.4 Conclusions in this chapter

In this chapter, a new one-way scheme has been presented to model the surface profile and migration speed of dunes, which focusses only on dunes at equilibrium.

In section 3.2, a model which describes transverse dune migration in equilibrium was developed. By extending Zeman and Jensen’s (1988) approach, it was shown that equilibrium dune migration speed must take into account sand trapping efficiency ( $T_E$ ), and that  $T_E$  is strongly related to the wind speedup over the windward surface of a dune. An expression for sand trapping efficiency was analytically derived by extending Anderson’s (1988) microscale analysis of sand grain deposition on the slip face, with some corrections.

In section 3.3, field data in southern Peru reported by both Finkel (1959) and Has-

tenrath (1967), in California by Long and Sharp (1964) and in southern Morocco by Sauermann *et al.* (2000) show that as a dune becomes higher the windward slope becomes steeper. Following this, the model developed in section 3.2 has been further extended by incorporating the wind-flow theory developed by Jackson and Hunt (1975). The proposed model can describe the surface profile for given dune height, sand grain diameter and shear velocity upwind of the dune ( $H, D_g, u_*(-\infty)$ ). The model will be evaluated numerically in the next chapter.

## CHAPTER 4

# Model results and comparison to nature

### 4.1 Migration speed

In this section numerical estimates are introduced for the relations between dune migration speed ( $c_d$ ) and sand trapping efficiency ( $T_E$ ). Initially the model that does not incorporate the wind-flow theory (section 3.2) is used alongside observational data. The full model with the Jackson-Hunt theory (1975) will then be evaluated in the subsequent two sections (4.2 and 4.3). Table 4.1 shows the values and constants used here. The threshold velocity ( $u_{*t}$ ) is calculated with Bagnold's (1941) threshold shear velocity formula (2.6).

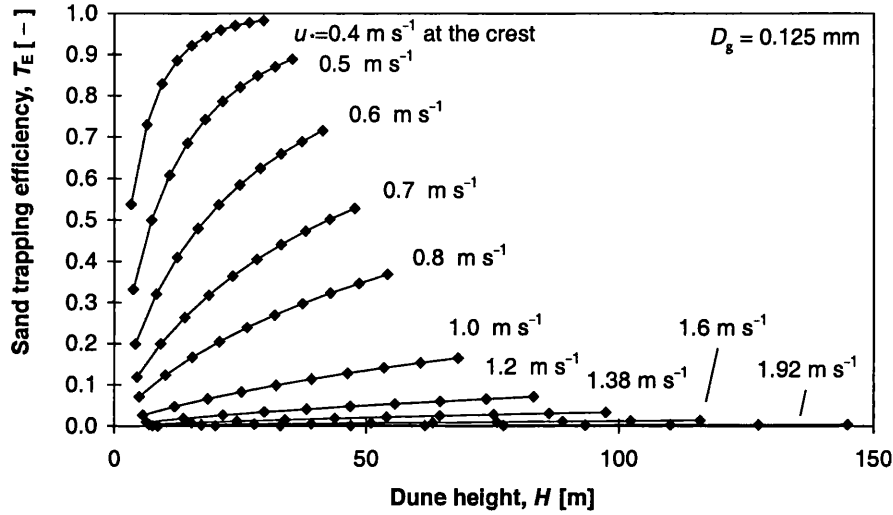
#### 4.1.1 Numerical calculations and comparison to nature

Figure 4.1 shows the relations between sand trapping efficiency ( $T_E$ ) and dune height ( $H$ ), calculated for various shear velocities at the dune crest ( $u_*(0)$ ). These correspond to the functional relationship in (3.32). For low shear velocities, such as  $u_*(0) = 0.4 \text{ m s}^{-1}$ , sand trapping efficiency ( $T_E$ ) rapidly increases as dune height ( $H$ ) increases. However as  $u_*(0)$  increases further, the rate of increase of

quantity / constant	value	unit
sand grain diameter ( $D_g$ )		
in section 4.1	0.125	mm
in section 4.2	0.150	mm
in sections 4.2 and 4.3	0.250	mm
reference diameter ( $D_r$ )	0.25*	mm
air density ( $\rho_a$ )	1.2*	kg m <sup>-3</sup>
sand grain density ( $\rho_s$ )	2,650*	kg m <sup>-3</sup>
sand bulk density ( $\gamma$ )	1,670	kg m <sup>-3</sup>
gravitational acceleration ( $g$ )	9.8	m s <sup>-2</sup>
sand grain incident angle ( $\alpha_i$ )	10	deg
slip face angle ( $\theta$ )	32	deg
coefficient in Lettau and Lettau's formula ( $C_{LL}$ )	4.2*	–
roughness length ( $z_0$ )		
in sections 4.1–4.3	the Owen formula (2.8)	
in sections 4.2 and 4.3	1	mm
measurement height of wind velocity	10	m
threshold shear velocity ( $u_{*t}$ ) (equation (2.6))		
$D_g = 0.125$ mm	0.16	m s <sup>-1</sup>
$D_g = 0.150$ mm	0.18	m s <sup>-1</sup>
$D_g = 0.250$ mm	0.23	m s <sup>-1</sup>

\* after Howard *et al.* (1978)

**Table 4.1:** Values and constants used for numerical calculation.



**Figure 4.1:** Relations between sand trapping efficiency ( $T_E$ ) and dune height ( $H$ ) calculated for various shear velocities at the dune crest ( $u_*(0)$ ).

$T_E$  declines rapidly, and in the case of  $u_*(0) = 1.92 \text{ m s}^{-1}$ ,  $T_E$  is virtually 0.0, even for dunes higher than 150 m. It should be noted here that these results are valid regardless of whether dunes are in equilibrium or not. In these calculations of sand trapping efficiency ( $T_E$ ), only the Anderson model was used, and the equilibrium condition expressed in equation (3.2) has not been assumed. However assuming that dunes are in equilibrium, equation (3.10) shows that, with  $T_E = 0.0$ , there is no increase in shear velocity (probably no wind speedup) over the dune, meaning no net erosion or deposition anywhere on the dune, and consequently no dune migration, which of course can be directly concluded from equation (3.1). The physical origin of wind speedup is that the terrain intruding into the boundary-layer flow compresses the streamlines. No wind speedup means that the windward surface of the dune is so gentle, or even flat, that streamlines are not compressed. According to Jackson and Hunt (1975), wind velocity at the crest ( $u(0)$ ) can be approximated according to

$$\frac{u(0) - u(-\infty)}{u(-\infty)} \sim 2 \frac{H}{L_w},$$

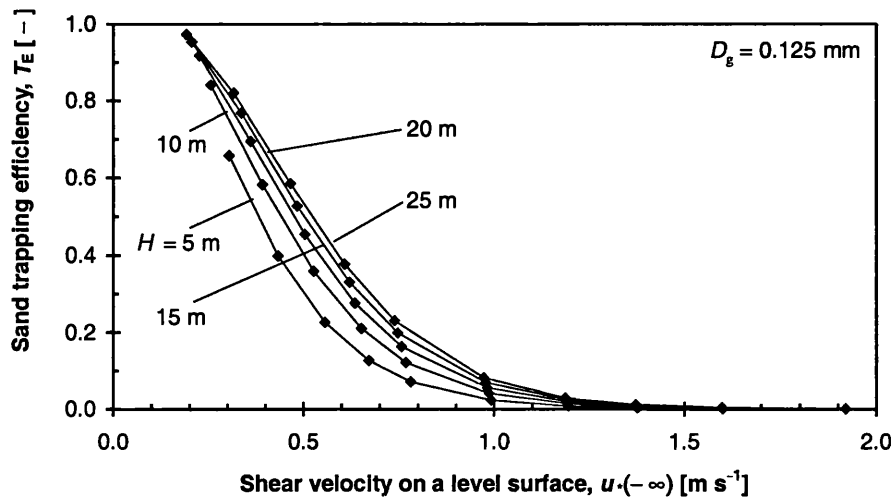
where  $L_w$  is the horizontal distance between the toe (windward bottom) of the dune and the crest. In this extreme case ( $u_*(0) = 1.92 \text{ m s}^{-1}$ ,  $H = 150 \text{ m}$ ), therefore, it can be estimated that only dunes with  $L_w \gg 3,000 \text{ m}$ , which corresponds

to the windward slope angle of less than  $3^\circ$ , can exist in equilibrium.

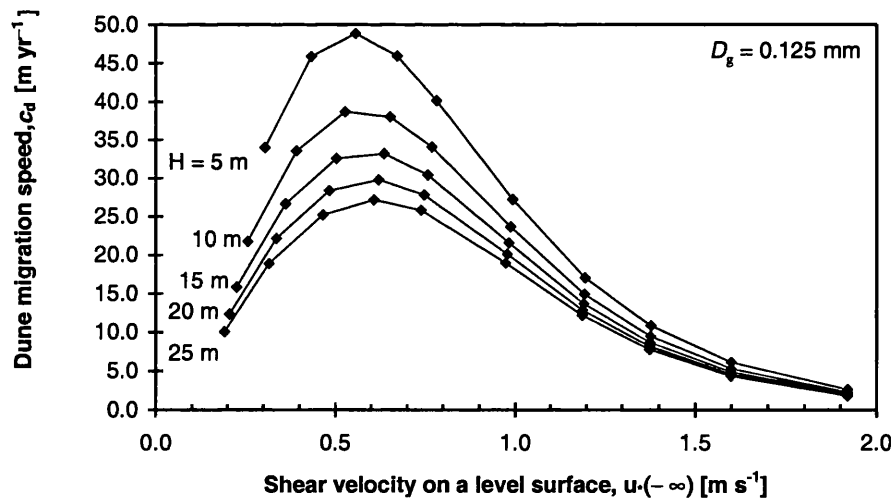
With equation (3.6) and with Lettau and Lettau's sand flux formula (2.7), Figure 4.1 can be converted to relations between sand trapping efficiency ( $T_E$ ) and shear velocity on a level surface ( $u_*(-\infty)$ ) for various dune heights ( $H$ ) (Figure 4.2). These are derived from the functional relationship in (3.33). Though sand trapping efficiency ( $T_E$ ) depends on dune height ( $H$ ), as seen in Figure 4.1, it can be said from Figure 4.2 that  $T_E$  is mainly determined by shear velocity ( $u_*(-\infty)$ ), and rapidly decreases as  $u_*(-\infty)$  increases.

Figure 4.3 shows the relations between dune migration speed ( $c_d$ ) and shear velocity on a level surface ( $u_*(-\infty)$ ), for various dune heights ( $H$ ). For each dune height ( $H$ ), dune migration speed ( $c_d$ ) first increases, and then decreases monotonically after reaching the maximum, as the shear velocity on a level surface ( $u_*(-\infty)$ ) increases. It can be said from equation (3.11) that the first increase is due to the increase of sand flux ( $q$ ), proportional to  $u_*(-\infty)^3$ , and that the subsequent decrease is due to the decrease of sand trapping efficiency ( $T_E$ ). In field observations, wind velocity ( $u_z(-\infty)$ ) is more commonly measured than shear velocity ( $u_*(-\infty)$ ), and most wind velocity data are recorded at 10-m height (Fryberger, 1979). Figure 4.4 shows calculated dune migration speed ( $c_d$ ) against wind velocity at 10-m height on a level surface ( $u_{10m}(-\infty)$ ) for various dune heights ( $H$ ).  $u_{10m}(-\infty)$  is calculated from the Kármán/Prandtl relations (2.3).

Figure 4.5 shows an example of the relation between shear velocity at the dune crest ( $u_*(0)$ ) and dune height ( $H$ ). Shear velocity on a level surface ( $u_*(-\infty)$ ) and the threshold shear velocity ( $u_{*t}$ ) are  $0.4 \text{ m s}^{-1}$  and  $0.16 \text{ m s}^{-1}$ , respectively. Curve a) is derived from Lettau and Lettau's sand flux formula (2.7). Curve b) is derived from equation (3.10), which does not take into account the threshold shear velocity ( $u_{*t}$ ). There is no significant difference between the two curves because  $u_*(-\infty)$  of  $0.4 \text{ m s}^{-1}$  is sufficiently larger than  $u_{*t}$  of  $0.16 \text{ m s}^{-1}$ . The model validity could be examined by comparing these results to field data. Shear velocity at the dune crest ( $u_*(0)$ ) is estimated only from sand trapping efficiency



**Figure 4.2:** Relations between sand trapping efficiency ( $T_E$ ) and shear velocity on a level surface ( $u_*(-\infty)$ ) for various dune heights ( $H$ ).



**Figure 4.3:** Relations between dune migration speed ( $c_d$ ) and shear velocity on a level surface ( $u_*(-\infty)$ ), for various dune heights ( $H$ ).



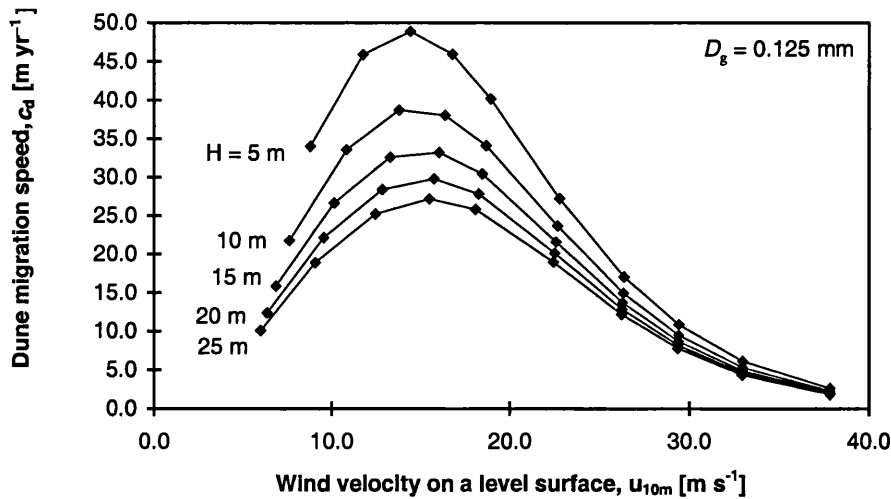


**Figure 4.4:** Relations between dune migration speed ( $c_d$ ) and wind velocity at 10 m height on a level surface ( $u_{10m}(-\infty)$ ) for various dune heights ( $H$ ).

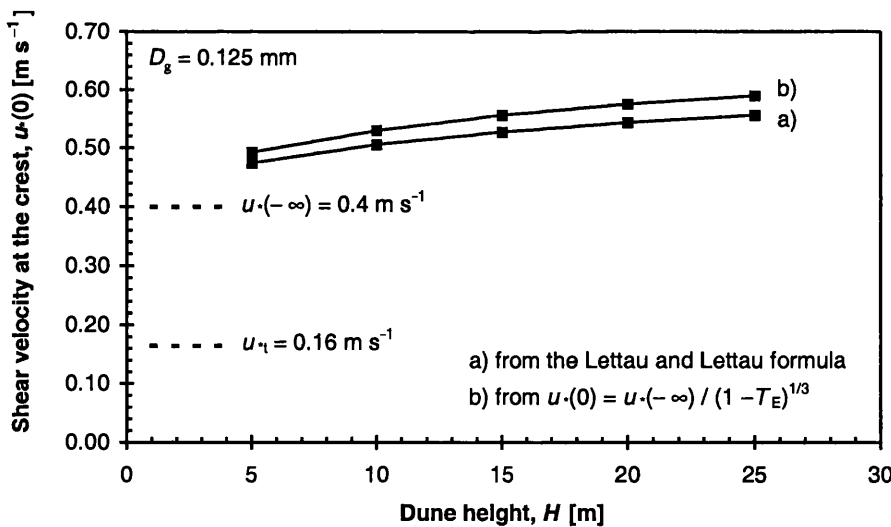


**Figure 4.5:** Relations between shear velocity at the dune crest ( $u_*(0)$ ) and dune height ( $H$ ). Shear velocity on a level surface ( $u_*(-\infty)$ ) and the threshold shear velocity ( $u_{*t}$ ) are  $0.4 \text{ m s}^{-1}$  and  $0.16 \text{ m s}^{-1}$ , respectively. Curve a) is derived from Lettau and Lettau's sand flux formula (2.7). Curve b) is derived from equation (3.10).

$(T_E)$ , for a given shear velocity on a level surface ( $u_*(-\infty)$ ). The profile of the windward surface is unknown here, and may be different for each dune height ( $H$ ) (this will be examined in the next section (4.2)).

Figure 4.6 shows the relations between dune migration speed ( $c_d$ ) and dune height ( $H$ ) for various shear velocities on a level surface ( $u_*(-\infty)$ ). In Figure 4.6(a) dune migration speed ( $c_d$ ) is plotted against the inverse of dune height ( $1/H$ ) on a linear scale. In Figure 4.6(b),  $c_d$  is plotted against  $H$  on a logarithmic scale. Although dune migration speed ( $c_d$ ) increases monotonically as dune height ( $H$ ) decreases, as seen in Figure 4.6(a),  $c_d$  is not proportional to the inverse of dune height ( $1/H$ ), but is rather a convex function of  $1/H$ . For low dunes, small sand trapping efficiency ( $T_E$ ) suppresses  $c_d$ , whereas for high dunes, wind speedup and large  $T_E$  resist the decrease of  $c_d$ . Consequently, if linear regression analysis were to be applied to the relation between  $c_d$  and  $1/H$ , only for readily observable dune height ( $H$ ), the trend line would cross the  $c_d$ -axis with a positive intercept:

$$c_d = a_{c_d} + b_{c_d} \frac{1}{H} \quad (a_{c_d} > 0, b_{c_d} > 0). \quad (4.1)$$

Table 4.2 shows some published data<sup>1</sup> analysed using equation (4.1). Except for the results of Al-Hinai and Moore (1987), the data show positive intercepts. Figure 4.7 shows an example  $c_d - 1/H$  plot, in which data collected by Hastenrath (1967) in southern Peru in 1955 and in 1958 are analysed. As seen in Figure 4.6(b)  $c_d$  is proportional to  $\log H$  rather than to  $1/H$ .

---

<sup>1</sup>In table 3 of Long and Sharp's (1964) paper, the height of 'Dune 13' is given as 10 feet, whereas in table 1 it is given as 40 feet. They used the data in table 3 of their paper to construct their figures 3, 4 and 5. But in all three figures, 'Dune 13' is regarded as 40 feet high as in table 1. Consideration of the windward surface length of 'Dune 13' in table 1 and these three figures leads to the conclusion that the height of 'Dune 13' in table 3 was misprinted.

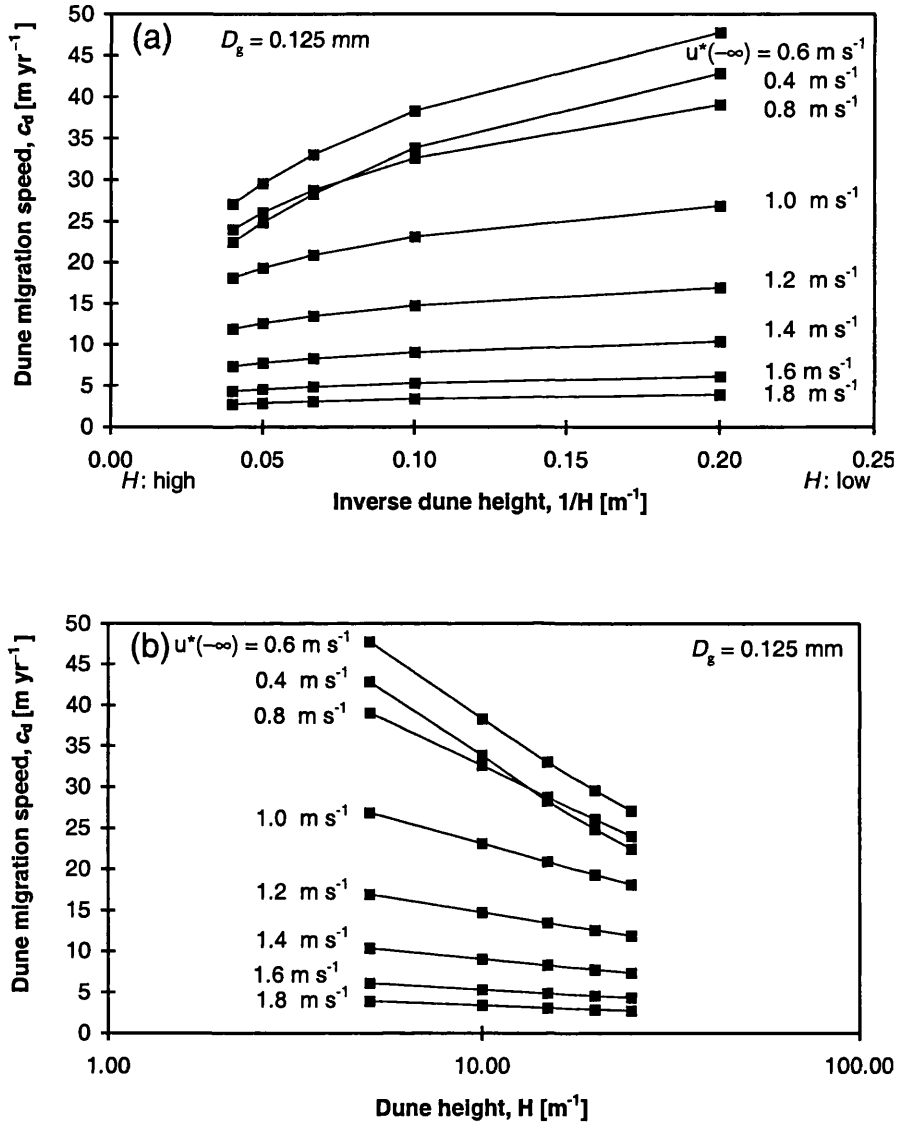


**Figure 4.6:** Relations between dune migration speed ( $c_d$ ) and dune height ( $H$ ), for various shear velocities on a level surface ( $u_*^{(-\infty)}$ ). In a)  $c_d$  is plotted against the inverse of dune height ( $1/H$ ) on a linear scale. In b),  $c_d$  is plotted against  $H$  on a logarithmic scale.

source	dunes	$H_{\min}$	$H_{\max}$	$a_{c_d}$	$b_{c_d}$	$R^2$
Al-Hinai and Moore (1987)						
(field measurement)	6	10.0	19.0	-1.8	103.2	0.93
(aerial photo)	6	10.0	19.0	-4.2	125.2	0.90
Coursin (1964)	44	3.0	17.0	10.6	169.1	0.80
Long and Sharp (1964)						
(7-year data)	27	2.7	12.2	11.7	75.9	0.59
(15-year data)	19	3.4	12.2	13.0	21.0	0.17
(22-year data)	19	3.4	12.2	12.9	34.6	0.43
Fryberger <i>et al.</i> (1984)	19	11.7	47.1	6.0	43.3	0.60
Hastenrath (1967)						
(1955-58)	42	1.2	6.0	8.1	19.3	0.67
(1958-64)	50	0.4	6.0	25.9	12.7	0.37
this model						
$u_*(-\infty) = 0.4 \text{ m s}^{-1}$	5	5	25	19.2	122.9	0.96
$u_*(-\infty) = 0.6 \text{ m s}^{-1}$	5	5	25	23.8	124.4	0.97
$u_*(-\infty) = 0.8 \text{ m s}^{-1}$	5	5	25	21.9	89.4	0.95
$u_*(-\infty) = 1.0 \text{ m s}^{-1}$	5	5	25	16.9	52.0	0.95
$u_*(-\infty) = 1.2 \text{ m s}^{-1}$	5	5	25	11.2	30.0	0.96
$u_*(-\infty) = 1.4 \text{ m s}^{-1}$	5	5	25	6.9	17.9	0.96
$u_*(-\infty) = 1.6 \text{ m s}^{-1}$	5	5	25	4.1	10.6	0.96
$u_*(-\infty) = 1.8 \text{ m s}^{-1}$	5	5	25	2.6	6.9	0.97

$$* c_d = a_{c_d} + b_{c_d} \frac{1}{H}; \quad c_d \text{ (m year}^{-1}\text{)}, H \text{ (m)}$$

**Table 4.2:** Some published dune migration data and model results.

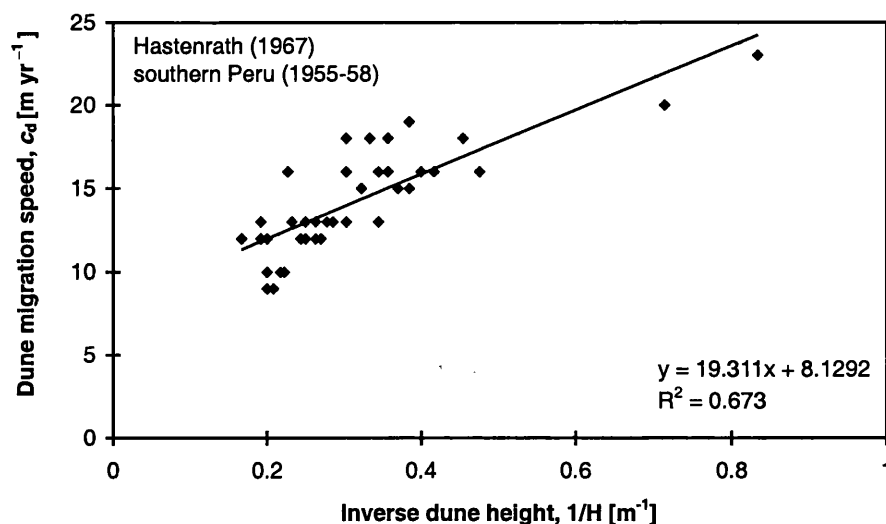


**Figure 4.7:** An example relation between dune migration speed ( $c_d$ ) and the inverse dune height ( $1/H$ ). Data collected by Hastenrath (1967) in southern Peru in 1955 and in 1958 are analysed. Sand grain diameter ( $D_g$ ) is between 0.125 and 0.177 mm (see sections 3.3.1 and 4.2.3).

#### 4.1.2 Model applicability to subaqueous and terrestrial aeolian dunes (section 2.6.2)

It is well known that the transition from dunes to a plane bed (upper-regime plane bed) on a subaqueous bed occurs with the increase of flow velocity and/or with the decrease of sand grain diameter (Allen, 1970, figure 2.6; see also section 2.6.2). The same dune-to-plane-bed transition has been observed in an experiment simulating aeolian conditions on Venus, on which the atmosphere is extremely dense (Bougan and Greeley, 1985; reproduced in Figure 4.8). As described and discussed by Bougan and Greeley, the transition from dunes to a plane bed on Venus seems to be similar to the behaviour of subaqueous bedforms on Earth. The transition to a plane bed in such systems is generally believed to be mainly due to the change in the transport mode, *i.e.* from saltation to suspension (Bougan and Greeley, 1985; Engelund and Fredsøe, 1974).

Sand grains discharged from the crest of a subaerial dune with high velocities act almost as if they were in suspension, due to their long flying distances. So

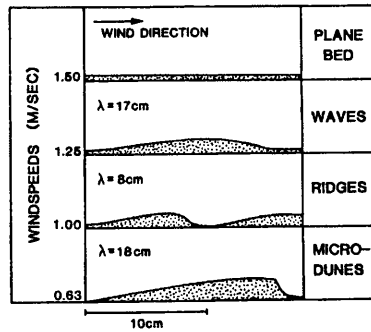


**Figure 4.8:** Bedforms formed in the wind tunnel that simulated Venusian atmosphere (transferred from Bougan and Greeley, 1985).

the model developed in the previous chapter, based as it is on the derivation of saltation distance against flow velocity, could be applied to the transition from dunes to plane bed in both subaqueous and planetary aeolian bedforms, with the replacement of some coefficients. Since sand trapping efficiency ( $T_E$ ) decreases with the increase of flow velocity and/or with the decrease of sand grain diameter (equations (3.29) to (3.31)), the decrease of  $T_E$  could be interpreted as the transport mode changing from saltation to suspension. Hence the dune-to-plane-bed transition, which was described on Allen's diagram with two parameters (flow velocity and sand grain diameter) (Allen, 1970, figure 2.6), could alternatively be systematically explained in terms of sand trapping efficiency ( $T_E$ ). Though sand trapping efficiency ( $T_E$ ) in our model is estimated through the calculation of saltation length assuming the existence of a slip face, the overall trend would be the same in the case without a slip face (this expectation will be supported in section 4.3).

A possible scheme is as follows. When sand trapping efficiency ( $T_E$ ) is close to 1.0, migrating dunes can be expected to develop. As flow velocity increases, sand trapping efficiency ( $T_E$ ) decreases (Figure 4.2), and dunes change to wave-like dune patterns without slip faces and with more symmetrical cross-sectional shapes (Bougan and Greeley, 1985; figure 4.8), since sand grains in suspension are deposited more equally on windward and on leeward surfaces. As sand trapping efficiency ( $T_E$ ) approaches to 0.0, a plane bed appears.

### 4.1.3 Model limitations and future work

Since the work of Howard and Walmsley (1985), dune dynamics models have been constructed based on the Navier-Stokes equation (see section 2.7.1), which is a partial differential equation, so that the degrees of freedom are infinite. When discussing only a specific and macroscopic feature, however, only a model can be constructed with a few important variables. The model that has so far been developed here describes transverse dune migration with four variables: dune height; sand grain diameter; shear velocities on a level surface and at the crest ( $\eta(0) = H, D_g, u_*(-\infty), u_*(0)$ ). Furthermore, by assuming an equilibrium condition (symmetry) these four variables are mutually related, and the degrees of freedom are reduced to three.

A drawback of these simplifications is that the model cannot predict the windward surface profile of the migrating dune for a given combination of shear velocity on a level surface, sand grain diameter and dune height ( $u_*(-\infty), D_g, H$ ). The model also cannot predict whether there is an upper limit for dune height ( $H$ ), for a given combination of ( $u_*(-\infty), D_g$ ). This is because the model has been developed by assuming that dunes are in equilibrium for all the combinations of ( $u_*(-\infty), D_g, H$ ). These problems will be overcome by incorporating the wind-flow theory (Jackson and Hunt, 1975; section 2.7.1), as will be seen in the next section.

The modelling of dunes without slip faces would require a modification of the approach (this would probably not make significant difference in results, see section 4.3). Another limitation may be the absence of any consideration of wake or wind re-circulation in the lee of the dune (for details see section 2.4.4). It is still uncertain, however, how much of the sand that falls between the bottom of the slip face and the re-attachment point is subsequently trapped on the slip face.

In this chapter, the idealised equilibrium state has been discussed, where wind speed ( $u(0)$ ), hence the shear stress ( $u_*(0)$ ) are constant in terms of time ( $t$ ).

In the field, however, the wind profile and speed are not constant. According to Frank and Kocurek (1996), for example, the wind flow re-attachment point varies from 1.6 to 5.4 dune heights downwind of the crest. Furthermore Knott reported that strong gusts blew in the mornings at Salah in Algeria (Knott, 1979, referred to in Cooke *et al.*, 1993, p323). In most of the literature, only average values of wind speed and the wind profiles are reported. However, short-term wind fluctuations, especially at the crest, may be essential to keep the dune in equilibrium. If only the averaged wind speed at the crest ( $u(0)$ ) is used, sand trapping efficiency ( $T_E$ ) is probably overestimated under modest wind conditions. Similarly, long saltation paths, which are modified by turbulence and approach a state of suspension, may also be important, and without allowance for them the sand trapping efficiency ( $T_E$ ) would be overestimated. An improved estimate may be obtained with some integrated function. Experimentally, a promising approach would be to mount sand traps in the lee of the dune, as did Walker (1999). If mounted upwind of the dune where sand flux is also well saturated, the model validity could be examined with these data. A good set of empirical data of shear stress fluctuation at the crest would not be difficult to incorporate into the model.

## 4.2 Windward surface morphology

Using numerical calculations, this section discusses the applicability of the model with the Jackson-Hunt theory (1975) (the proposed new scheme for dune modelling depicted in Figure 3.5). More specifically, the discussion concerns whether, and how well, the model can explain the height-dependent characteristic of a barchan dune: the higher the dune, the steeper the windward slope (see section 3.3.1).

Figure 4.9 shows the calculated relationship between the normalised increase in the shear stress at the dune crest ( $(\tau(0) - \tau_0)/\tau_0$ ) and dune height ( $H$ ) for various



shear velocities on a flat surface ( $u_*(-\infty)$ ). The assumed grain diameter here is 0.150 mm.  $(\tau(0) - \tau_0)/\tau_0$  increases as  $H$  increases, which in turn affects the height-dependent profile: the higher the dune, the steeper the windward slope. It should be noted here that no wind-flow theory has been used in these calculations. This trend is analysed more quantitatively in the following with the model using the Jackson-Hunt theory.

In the following numerical calculations, the windward slope length ( $L_w$ ) is estimated as follows. First, the inner-layer thickness ( $l$ ) is calculated from equation (3.38) for various possible horizontal length scales ( $L$ ). The roughness length ( $z_0$ ) may be either calculated using the Owen formula (2.8)<sup>2</sup>:

$$z_0 = 0.02 \frac{u_*^2}{2g},$$

or set to 1 mm (Walmsley and Howard, 1985; Weng *et al.*, 1991). Once the inner-layer thickness ( $l$ ) is known, the perturbation variable ( $\varepsilon$ ) can be calculated from equation (3.37), and the surface shear stress correction term ( $\tau_d(\xi)$ ) for a given dune height ( $H$ ) can be calculated either from equation (3.46) or from equation (3.54). Consequently, the windward slope length ( $L_w$ ) can be estimated from equation (3.43).

Dune migration speed ( $c_d$ ) can be described as in equation (3.34). The average bulk sand density ( $\gamma$ ) in the dune field in southern Peru is calculated here to be 1319 kg m<sup>-3</sup> from data presented by Hastenrath (1967, table 4). Assuming spherical quartz sand, this density value corresponds to the porosity of 0.50, which is just outside the theoretical range of 0.26 to 0.48 (Pye and Tsoar, 1990, p64). In the following calculations, a porosity value of 0.37 is assumed, which is the mean value of the theoretical range. The bulk sand density ( $\gamma$ ) is then found to be 1670 kg m<sup>-3</sup>, which is almost the same as that for a dune in Sinai (Pye and

---

<sup>2</sup>Gillette (1999) quoted a recent formula developed by Raupach (1991) (section 2.4.3). The Raupach formula gives a smaller value for the roughness length ( $z_0$ ) to that estimated with the Owen formula (2.8), if the same value as Gillette (1999) assumed for his parameter is used in the Raupach formula. However the difference between the outcomes of these two formulae is small, since in the present calculations only  $\log z_0$  is used (see section 3.3.2).

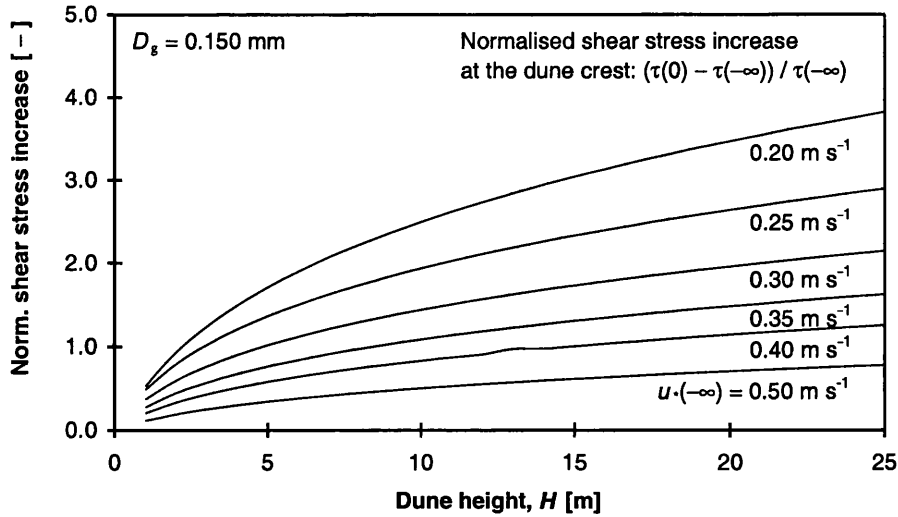


**Figure 4.9:** The calculated relation between the normalised increase in the shear stress at the dune crest ( $\frac{\tau(0) - \tau_0}{\tau_0}$ ) and dune height ( $H$ ) for various shear velocities on the level surface ( $u_*(-\infty)$ ). A sand grain diameter ( $D_g$ ) of 0.150 mm is assumed.

Tsoar, 1990, p64).

#### 4.2.1 General characteristics

Table 4.3 shows the results of the calculations for the windward slope length ( $L_w$ ), the average windward slope ( $\theta_{w_{avg}}$ ), the maximum windward slope ( $\theta_{w_{max}}$ ), the inner-layer thickness ( $l$ ), perturbation variable ( $\varepsilon$ ), the surface shear stress correction term at the dune crest ( $\tau_d(0)$ ) and the phase shift ( $\theta_{ph}$ ) for cosine-hill and Gaussian-hill approximations. The assumed sand grain diameter ( $D_g$ ) and the shear velocity upwind of the dune ( $u_*(-\infty)$ ) are 0.250 mm and 0.55 m s<sup>-1</sup>, respectively. The values do not show a significant difference when the roughness length ( $z_0$ ) is calculated from the Owen formula (2.8) or set to 1 mm.

The estimated average windward slope ( $\theta_{w_{avg}}$ ) varies between 4.8° and 11.9°. According to Weng *et al.* (1991), the Jackson-Hunt theory underestimates the surface shear stress perturbation ( $\tau_d(\xi)$ ) for a given topography. If one of the re-

$H$ (m)	$\frac{u_*(0)}{u_*(-\infty)}$ (-)	$L_w$ (m)	$\theta_{w_{avg}}$ (deg)	$\theta_{w_{max}}$ (deg)	$l$ (m)	$\varepsilon$ (-)	$\tau_d(0)$ (-)	$\theta_{ph}$ (deg)	$z_0$ (m)
cosine hill									
5	1.34	48	5.9	9.3	0.96	8.2	0.095	14.2	$3.1 \times 10^{-4}$
10	1.44	69	8.2	12.8	1.32	11.7	0.091	13.5	(Owen's)
15	1.50	87	9.8	15.2	1.62	14.1	0.089	13.1	
20	1.54	104	10.9	16.8	1.91	16.0	0.087	12.8	
25	1.58	119	11.9	18.3	2.15	17.6	0.085	12.6	
Gaussian hill									
5	1.34	51	5.6	8.8	1.16	7.2	0.110	16.8	$1.0 \times 10^{-3}$
10	1.44	74	7.7	12.0	1.60	10.1	0.105	15.8	(fixed)
15	1.50	93	9.2	14.2	1.96	12.3	0.102	15.3	
20	1.54	111	10.2	15.8	2.30	13.9	0.099	14.9	
25	1.58	127	11.1	17.2	2.59	15.3	0.098	14.6	
Gaussian hill									
5	1.34	55	5.2	7.4	1.08	7.2	0.109	–	$3.1 \times 10^{-4}$
10	1.44	80	7.1	10.1	1.51	10.2	0.104	–	(Owen's)
15	1.50	101	8.4	12.0	1.86	12.3	0.102	–	
20	1.54	120	9.5	13.4	2.17	14.0	0.100	–	
25	1.58	138	10.3	14.5	2.46	15.3	0.098	–	
Gaussian hill									
5	1.34	59	4.8	6.9	1.31	6.3	0.126	–	$1.0 \times 10^{-3}$
10	1.44	85	6.7	9.5	1.81	8.9	0.120	–	(fixed)
15	1.50	108	7.9	11.2	2.24	10.7	0.116	–	
20	1.54	128	8.9	12.6	2.60	12.2	0.114	–	
25	1.58	146	9.7	13.7	2.93	13.5	0.112	–	

$u_*(-\infty) = 0.55 \text{ m s}^{-1}$ ;  $D_g = 0.250 \text{ mm}$ ;  $u_{*t} = 0.23 \text{ m s}^{-1}$

**Table 4.3:** Example results with a cosine hill and a Gaussian hill.

vised Jackson-Hunt theories were used (*e.g.* Hunt *et al.*, 1988; Weng *et al.*, 1991), a gentler windward slope profile would be expected. In both approximations, as a dune becomes higher, the windward slope becomes steeper, as seen in the published field data (Figure 3.6). This trend is thought not to be dependent on the choice of the approximate function for the surface profile ( $f(\xi)$ ), though it might be dependent because the surface profile ( $f(\xi)$ ) and the sand flux over it are not in phase in the present calculations, as will be seen later in this subsection (see also section 3.3.2). Thus a definite conclusion on whether this trend is independent on the choice of the approximate function for the surface profile ( $f(\xi)$ ) or not cannot be drawn.

The trend that the higher the dune the steeper the windward surface, is thought to be because the increases in dune height ( $H$ ) and in the average windward slope angle ( $\theta_{w_{avg}}$ ) have opposing effects in the outgoing sand flux ( $q(+\infty)$ ). At equilibrium, the incoming and outgoing sand flux must be the same ( $q(-\infty) = q(+\infty)$ ) (Zeman and Jensen, 1988; section 3.2.1). The higher the dune, the more likely the sand grains crossing the dune crest are to be captured by the slip face, *i.e.* the increase in the sand trapping efficiency ( $T_E$ ). This would decrease the outgoing sand flux ( $q(+\infty)$ ). However this is thought to be compensated for by the increase in the average windward slope angle ( $\theta_{w_{avg}}$ ), which leads to an increase in the shear velocity at the dune crest ( $u_*(0)$ ). As an increase in  $u_*(0)$  decreases sand trapping efficiency ( $T_E$ ), the outgoing sand flux ( $q(+\infty)$ ) increases. A self-adjusting mechanism, which maintains the equilibrium condition ( $q(-\infty) = q(+\infty)$ ), is apparently taking place.

For all dune heights ( $H$ ), phase shifts ( $\theta_{ph}$ ) are about  $+15^\circ$  in a cosine-hill approximation. Likewise in most calculations in the Gaussian-hill approximation,  $\tau_d(\xi)$  peaks at a site  $0.1\xi$  upwind of the crest ( $\xi = 0$ ). The threshold shear velocity ( $u_{*t}$ ) is known to be slope-dependent, and larger on the windward surface of the dune than on a level ground (Iversen and Rasmussen, 1994). This slope dependent increase in the threshold shear velocity ( $u_{*t}$ ) may compensate for the phase difference between the shear stress ( $\tau_d(\xi)$ ) and the topography ( $f(\xi)$ ), and

keep the dune at equilibrium<sup>3</sup>. The inertial effect of the saltating sand grains, which was introduced in the model of Van Dijk *et al.* (1999) as in the form of adaptation length, may also compensate this phase difference. In addition, cosine and Gaussian functions may not represent the best the windward slope of the dune.

The example profile of the normalised surface shear stress ( $\tau(\xi)/\tau_0$ ) to the dimensionless length ( $\xi$ ) is shown for a cosine-hill approximation in Figure 3.7(a), and for a Gaussian-hill approximation in Figure 3.7(b). In Figure 3.7(b)  $\tau_d(\xi)$  is less than 1.0 at the base of the dune. This is a well-known problem that occurs when applying the Jackson-Hunt theory to a dune. Without any correction, sand deposition would occur just upwind of the dune. As discussed by Wiggs *et al.* (1996) and Van Boxel *et al.* (1999), the streamline curvature effect may remedy this problem (see also Zeman and Jensen, 1987; 1988). Since however, the windward toe (bottom) of the dune simulated with this effect does not show any downwind movement (Van Dijk *et al.*, 1999, figure 3), it is not certain that the streamline curvature effect is enough.

Another problem is that the perturbation variable ( $\varepsilon$ ) is much larger than 1.0. Furthermore, even the product of the perturbation variable and the surface shear stress correction term ( $\varepsilon \tau_d(\xi)$ ) is comparable to 1.0. The higher the shear velocity on the level surface ( $u_*(-\infty)$ ), the smaller the perturbation variable ( $\varepsilon$ ), as the shear velocity ratio ( $u_*(0)/u_*(-\infty)$ ) becomes smaller. The present estimation is not the only case in which the perturbation variable ( $\varepsilon$ ) has been found to be larger than 1.0. In the 1980s, several wind speed measurements over low hills were

---

<sup>3</sup>This slope-dependence in threshold shear velocity ( $u_{*t}$ ) may be very important for shape-invariant, immobile (anchored) dunes, which are out of the scope of this thesis. Over those dunes, sand flux ( $q(x)$ ) must be constant, according to the concept of sediment continuity (see particularly equation (3.5)). However, if there is a bump, whatever the shape, shear velocity ( $u_*(x)$ ) would increase over it, hence an increase in sand flux ( $q$ ). This wind speedup effect on sand flux ( $q$ ) may be compensated for by the increase in the threshold shear velocity ( $u_{*t}(x)$ ) up the slope (*cf.* Lettau and Lettau's sand flux formula (2.7)). Consequently, immobile dunes are expected to have a concave windward surface.

carried out. These field measurements were taken as confirmation of the validity of the Jackson-Hunt theory, and are summarised in Taylor *et al.* (1987). Table 4.4 shows the perturbation variables ( $\varepsilon$ ) calculated for these field measurements from equation (3.37), using the values listed in Taylor *et al.* (1987). The values of  $\varepsilon$  in Table 4.4 are much larger than 1.0, and are comparable to the present model results in Table 4.3. Barchan dunes are thought to be equivalent to the ‘low hills’, that are the concern of the Jackson-Hunt theory.

In the following calculations, a Gaussian-hill approximation is used, which better describes an isolated barchan dune.

## 4.2.2 Calculations for dunes in southern Peru

For the following calculations for the dunes in southern Peru, the sand grain diameter ( $D_g$ ) is set to 0.150 mm. Figure 4.10 shows the relation between the windward slope angle ( $\theta_{w_{avg}}$ ) and dune height ( $H$ ) for various shear velocities on the level surface ( $u_*(-\infty)$ ). As  $u_*(-\infty)$  increases,  $\theta_{w_{avg}}$  decreases. This trend is thought to be related to the dune-to-plane-bed transition discussed earlier (section 4.1.2), which has been observed on river beds (see for example Allen, 1970) and in the wind tunnel which simulated Venusian atmosphere (Bougan and Greeley, 1985). Field data collected in southern Peru (Hastenrath, 1967) are also plotted, which correspond to estimates of  $u_*(-\infty) = 0.20 \text{ m s}^{-1}$  and  $0.25 \text{ m s}^{-1}$ .

One of drawbacks in the model which does not incorporate wind-flow theory is that it cannot predict whether there is an upper limit in dune height ( $H$ ) for a given set of sand grain diameter and shear velocity upwind of the dune ( $D_g, u_*(-\infty)$ ). Figure 4.11 shows the relation between the maximum windward slope angle ( $\theta_{w_{max}}$ ) and dune height ( $H$ ) calculated using equation (3.51) for various shear velocities on the level surface ( $u_*(-\infty)$ ). In the case of the shear velocity on a level surface ( $u_*(-\infty)$ ) of  $0.20 \text{ m s}^{-1}$ , the maximum windward slope angle exceeds the angle of repose of  $32^\circ$  when the dune height ( $H$ ) exceeds 20 m.

field	$z_0$ (m)	$H$ (m)	$L$ (m)	$\theta_{w_{avg}}$ (m)	$l$ (m)	$\epsilon$ (-)
Bungendore Ridge	0.002 – 0.005	7.5	75	2.9	3.4	3.7 – 3.5
Kettles Hill (84)	0.01	100	520	5.5	22	7.4
Askervein (82, 2.27)	0.03	116	380	8.7	19	10.6
Askervein (83, TU01B)	0.03	116	280	11.7	14	14.1
Black Mountain	1.14	170	275	17.2	28	14.5
Nyland Hill	$\sim 0.04$	70	100	19.3	6.3	21.2

after Taylor *et al.* (1987), except  $\theta_{w_{avg}}$  and  $\epsilon$  (see text).

**Table 4.4:** Some published field data of the flow over a low hill.

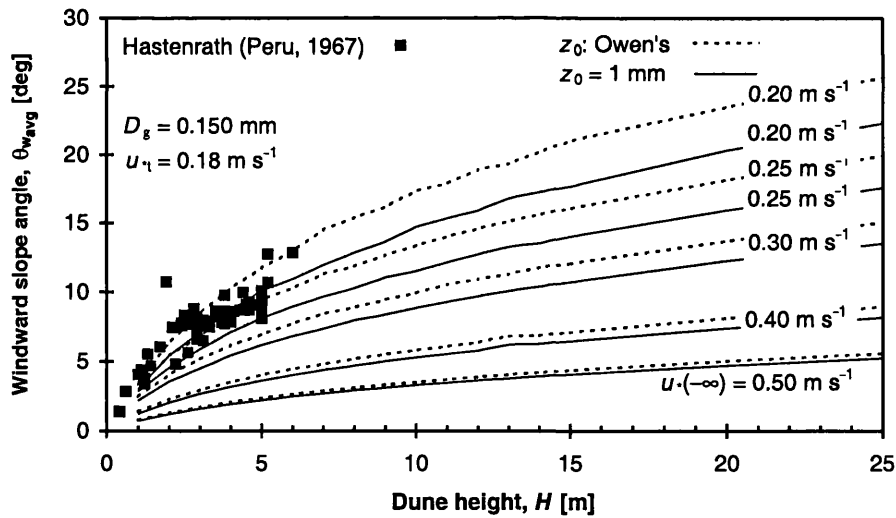


**Figure 4.10:** The calculated relation between the average windward slope angle ( $\theta_{w_{avg}}$ ) and dune height ( $H$ ) for various shear velocities on the level surface ( $u_*(-\infty)$ ). The sand grain diameter ( $D_g$ ) is taken as 0.15 mm and the roughness length ( $z_0$ ) was either calculated with the Owen formula (2.8) or set to 1 mm. Field data collected by Hastenrath (1967) are also plotted.

Although in this region, use of the Jackson-Hunt theory is against Walmsley and Howard's (1985) criterion of  $11^\circ$ , this figure implies why higher dunes are fewer in number in the contemporary environment, where modest winds blow.

Figure 4.12 shows the relation between dune migration speed ( $c_d$ ) and dune height ( $H$ ) for various shear velocities on a level surface ( $u_*(-\infty)$ ) derived from the model. Field data in the same region from 1958 to 1964 are also plotted (Hastenrath, 1967). Considering Figures 4.10 and 4.12, a wind whose shear velocity ( $u_*(-\infty)$ ) was around  $0.22 \text{ m s}^{-1}$  is thought to have been blowing in this field, though precise estimation needs an accurate value of bulk sand density ( $\gamma$ ), and consideration of wind fluctuations both in speed and in direction. This value is close to the shear velocity which was estimated above using Finkel's (1959) wind data with the assumption of the standard measurement height of 10 m.

For the shear velocities on a level surface ( $u_*(-\infty)$ ) of  $0.20 \text{ m s}^{-1}$  and below, dune migration speed ( $c_d$ ) increases as dune height ( $H$ ) increases up to 2 m. This is mainly because sand trapping efficiency ( $T_E$ ) in equation (3.34) sharply increases as dune height ( $H$ ) increases when  $H$  is small (section 4.1.1). In the region of this positive relation between dune migration speed ( $c_d$ ) and dune height ( $H$ ), zibar parabolic dunes would be expected to appear. A zibar parabolic dune is an active dune migrating downwind, which looks like a barchan dune, whose two horns, however, point towards the windward direction (Cooke *et al.*, 1993, pp395–396). Figure 4.13 shows schematic explanation of the origin of parabolic shape, contrasting barchan dune formation. Zibar dunes have coarse sand, which is thought to be equivalent here to small shear velocity in terms of sand transport capability. More quantitative discussion of this point, however, needs a revision in the modelling of sand trapping efficiency ( $T_E$ ) to suit dunes without a slipface (section 3.2.2).



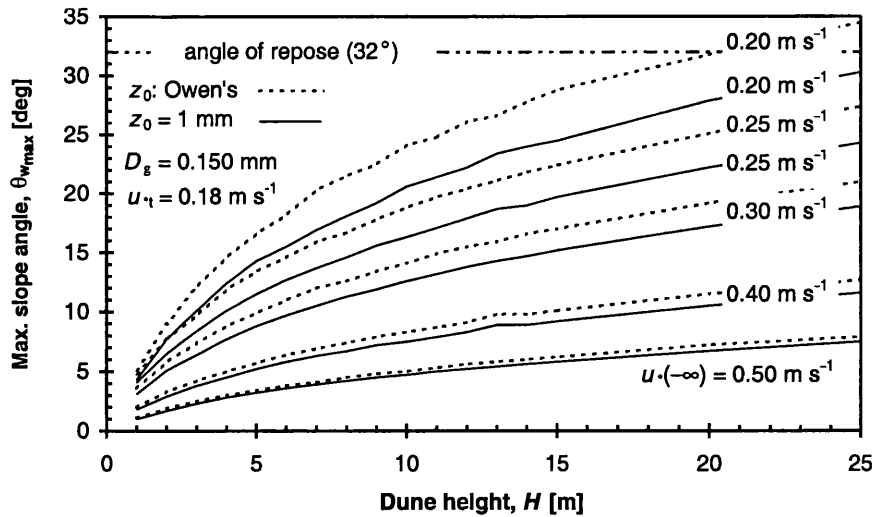


**Figure 4.11:** The relation between the maximum windward slope angle ( $\theta_{wmax}$ ) and dune height ( $H$ ) for various shear velocities on the level surface ( $u_*(-\infty)$ ).

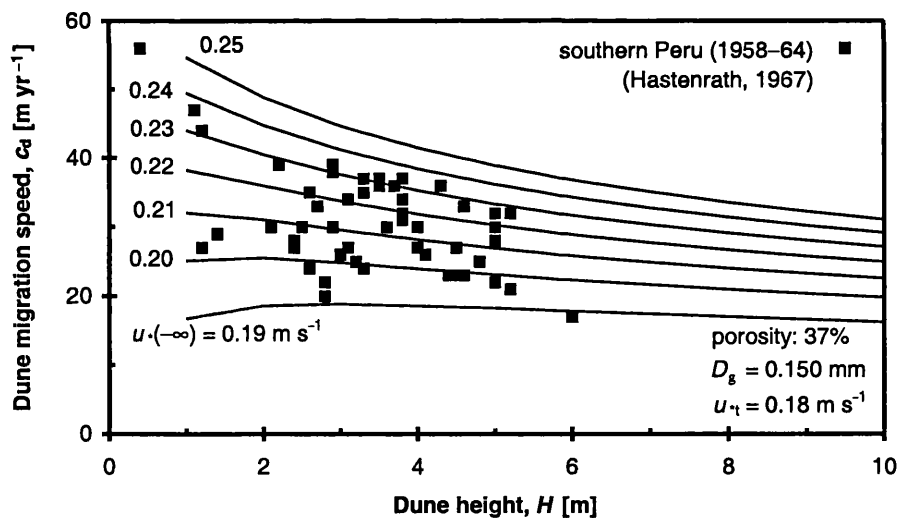


**Figure 4.12:** The relation between dune migration speed ( $c_d$ ) and dune height ( $H$ ) for some shear velocities on a level surface ( $u_*(-\infty)$ ) around  $0.22 \text{ m s}^{-1}$ , which best fits average windward slope angle ( $u_*(-\infty)$ ) data given by Hastenrath (1967). Sand grain diameter ( $D_g$ ) is assumed to be  $0.15 \text{ mm}$ . Field data from 1958 to 1964 are also plotted (Hastenrath, 1967).

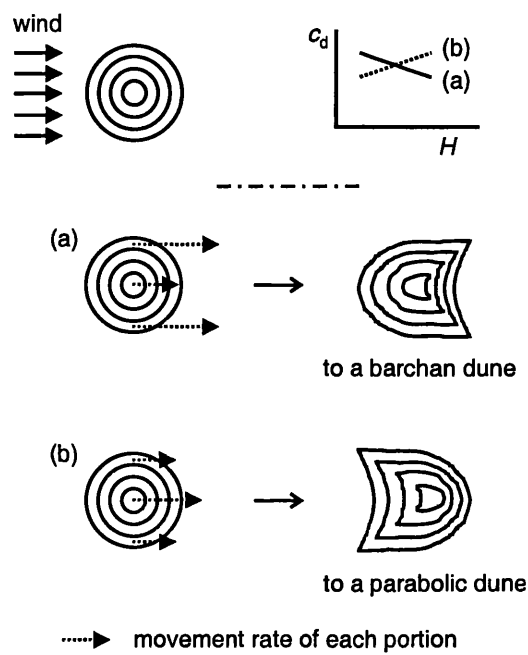


**Figure 4.13:** Schematic explanation of the origin of (a) barchan and (b) parabolic shapes. Inverse and positive relationships between dune migration speed ( $c_d$ ) and dune height ( $H$ ) may be associated with barchan and parabolic dunes, respectively.

### 4.2.3 Calculations for dunes in California

Using a sand grain diameter ( $D_g$ ) of 0.250 mm for dunes in California, Figure 4.14 shows the relation between windward slope angle ( $\theta_{w_{avg}}$ ) and dune height ( $H$ ) for various shear velocities on a level surface ( $u_*(-\infty)$ ). The field data collected by Long and Sharp (1964) are also plotted.

Figure 4.15 shows the relation between dune migration speed ( $c_d$ ) and dune height ( $H$ ) for the data in California (Long and Sharp, 1964; see also footnote in page 89) and for calculations with shear velocity on a level surface ( $u_*(-\infty)$ ) of  $0.55 \text{ m s}^{-1}$ , which best fits the windward slope angle data from California (Figure 4.14). Calculated values are more than ten times larger than field data, which could suggest that the estimated shear velocity on a level surface ( $u_*(-\infty)$ ) of  $0.55 \text{ m s}^{-1}$  is too large. However, another factor may be the poorly sorted sand in California, for which the threshold shear velocity ( $u_{*t}$ ) is effectively lower. If so, a revision to the model may be necessary. It may also be necessary to consider sand flux which is not fully saturated and the use of one of the modified Jackson-Hunt theories. Both of these would result in the smaller shear velocity on a level surface ( $u_*(-\infty)$ ).

Nevertheless, the following is thought to be worthy of mention. As seen above, in this model dune shape and migration speed are sensitive to sand grain diameter ( $D_g$ ). Experimentally even in the same dune field the values may vary significantly depending on how the measurements were performed. In southern Peru, as noted above, Hastenrath found sand grain diameter ( $D_g$ ) between 0.125 and 0.177 mm, which agrees with the survey results by Amstutz and Chico (Hastenrath, 1967, p311), whereas Finkel (1959) recorded measurements between 0.208 and 0.420 mm. Further data are needed to support or counter these results or the whole model.

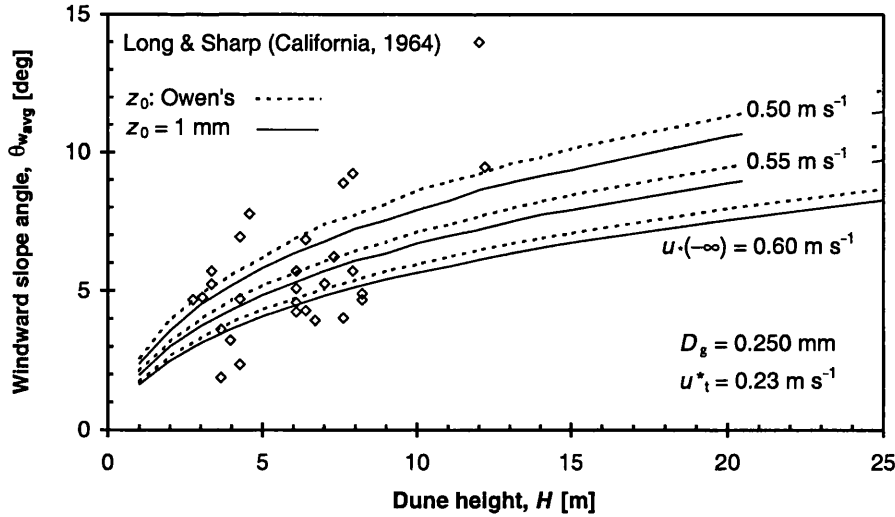
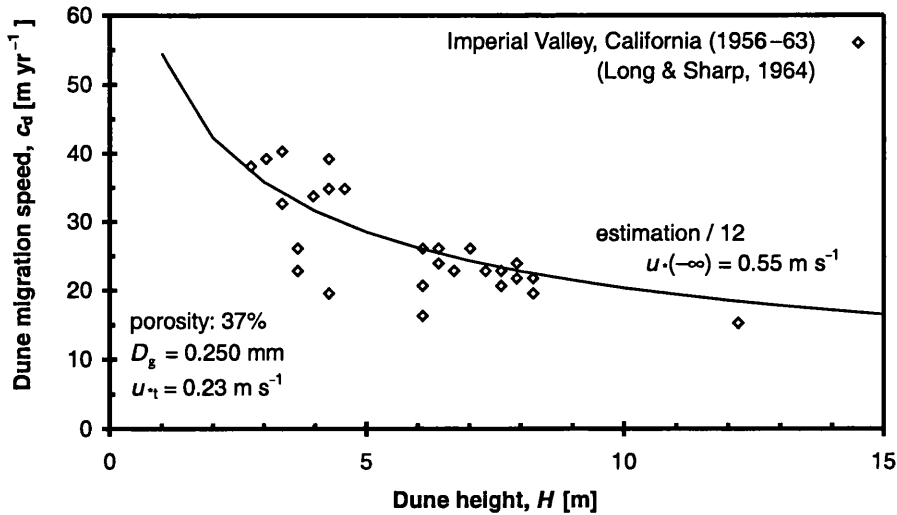


**Figure 4.14:** The relation between windward slope angle ( $\theta_{wavg}$ ) and dune height ( $H$ ) for various shear velocities on a level surface ( $u_x(-\infty)$ ). Sand grain diameter ( $D_g$ ) is 0.250 mm. Field data collected by Long and Sharp (1964) are also plotted.

#### 4.2.4 Towards a model of a three-dimensional dune

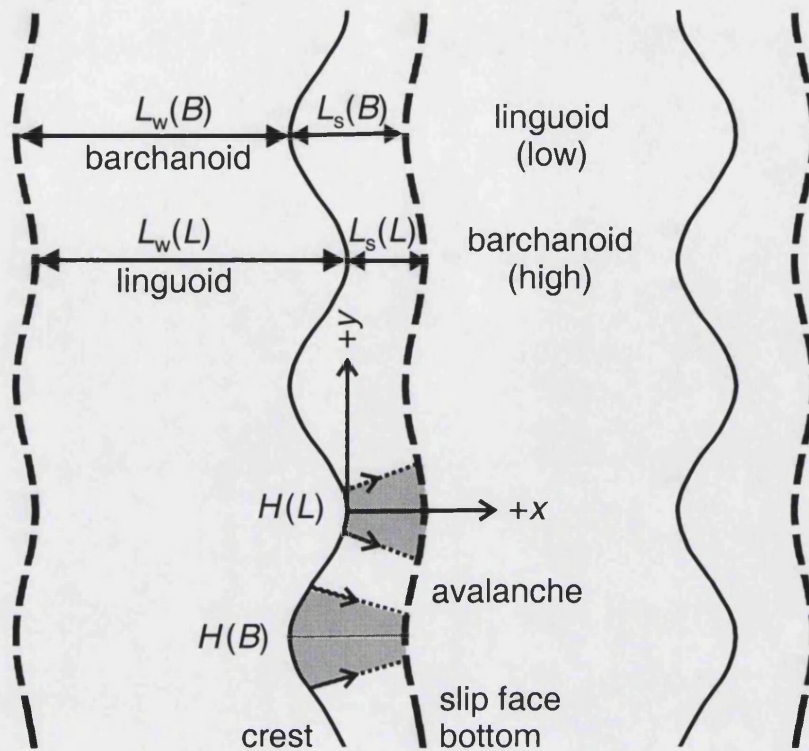
An expansion of the model to three dimensions would aim to explain the height-independent cross-sectional shape of a barchan dune, perpendicular to the wind (B-B' in Figure 3.1). However a barchan dune has a peculiar shape that is mathematically difficult to deal with. More specifically the model needs to estimate the sand trapping efficiency at every point on the brink line. A dune with a more easy-to-handle shape is a sinuous transverse dune comprised of higher barchanoid and lower linguoid parts, which are curved in the opposite direction to barchanoid parts (Figure 4.16; see also Cooke *et al.*, 1993, figure 23.1). Most transverse dunes are indeed sinuous.

Figure 4.6 shows that dune migration speed ( $c_d$ ) increases monotonically as dune height ( $H$ ) increases. The present model cannot explain why dunes of the barchanoid/linguoid pattern maintain their shapes during migration. When sinuous transverse dunes are at equilibrium, both barchanoid and linguoid parts must migrate at the same speed. Three possible mechanisms could be associated with



**Figure 4.15:** The relation between dune migration speed ( $c_d$ ) and dune height ( $H$ ) for data by Long and Sharp (1964) and for calculations with sand grain diameter ( $D_g$ ) of 0.250 mm and shear velocity on a level surface ( $u_*(-\infty)$ ) of  $0.55 \text{ m s}^{-1}$ , which best fits average windward slope angle ( $\theta_{\text{wavg}}$ ) data. The calculated relation has been drawn divided by 12 for Figure 4.15 because it is much larger than field data.

such a condition. (1) Howard *et al.* (1978, p312) noted that the effective height of a barchanoid section was less than the actual height because of the larger curvature at the crest than at the bottom of the slip face. The opposite curvature effect should work for linguoids. This would mean that barchanoids should move faster than predicted by the model and linguoids move more slowly. (2) Sinuosity in dunes must involve wind diversion, particularly on the windward surface (Howard *et al.*, 1978). Wind diversion may be opposite to the first mechanism in effect. In other words, barchanoid and linguoid parts may migrate more slowly and more quickly than predicted by the model, respectively, because with wind diversion, respective sand fluxes on barchanoid and linguoid parts may become smaller and larger than predicted by the model. (3) Figure 4.16 shows a typical transverse dune system, in which barchanoid and linguoid parts are alternately aligned in the wind direction. In this system, the windward slope of linguoid parts may be gentler than that estimated in the present model. The gentle linguoid slope may



**Figure 4.16:** Schematic plan view of the transverse dune system comprised of barchanoid and linguoid parts. Barchanoid parts are higher than linguoid parts ( $H(B) > H(L)$ ). In this configuration of barchanoid/linguoid sequence in the wind direction, windward slopes of barchanoid parts are shorter than those of linguoid parts ( $L_w(B) < L_w(L)$ ).

decrease the migration speed of linguoid parts, which is another mechanism that enables dunes to be at equilibrium.

Extending equations (3.7) and (3.2), and by considering the symmetries at the apexes of barchanoid and linguoid parts, the dynamics of barchanoid( $B$ )/linguoid ( $L$ ) pattern can be described as

$$\begin{aligned}
 q(0; B) &= q(+\infty; B)/(1 - T_E(B)) \\
 q(0; L) &= q(+\infty; L)/(1 - T_E(L)) \\
 q(+\infty; B) + q(+\infty; L) &= q(-\infty; B) + q(-\infty; L),
 \end{aligned}$$

where  $T_E(B)$  and  $T_E(L)$  may implicate wind speedup that has been reduced or

enhanced by wind diversion. In a barchanoid( $B$ )/linguoid( $L$ ) downwind sequence as in Figure 4.16, we can expect

$$\begin{aligned} q(+\infty; B) &\simeq q(-\infty; L) \\ q(+\infty; L) &\simeq q(-\infty; B). \end{aligned}$$

A barchan dune can be considered as the special type of sinuous transverse dune, where the linguoid height is zero.

In this section, the wind-directional profile of barchan dunes has been discussed. The full model that incorporates the Jackson-Hunt theory was found to be capable of explaining why the windward slope of higher dunes are steeper. By extending the model to suit sinuous transverse dunes, the model may also be able to explain why barchan dunes have a height-independent cross section, at right angles to the wind direction.

### 4.3 Shape and migration speed of proto-dunes <sup>4</sup>

Despite their simple shapes and formative environment, the initiation process of barchan dunes is not well understood. Some barchan dunes are thought to have been formed in the dense stream of sand downwind of the end of a preceding dune (Cooke *et al.*, 1993, p323). Alternatively a very low and gently-sloping sand mound (known as proto-dune, sand patch or ephemeral dune) is also thought, by some, to be the initial stage of a barchan dune (Lancaster, 1996; Cooke *et al.*, 1993, p325). According to Lancaster (1996), typical proto-dunes, observed in a dune field near Gobabeb, Namibia, are 0.05–0.10 m high. Their average wind-directional length and width are 12.71 m and 8.14 m, respectively.

The fact that even proto-dunes have lengths which are comparable to those of mature dunes may have significance. Dune fields show hierarchical structures

---

<sup>4</sup>Hiraku Nishimori was involved in this section.

from small to large: ripples, dunes and mega dunes (Wilson's draas), (Wilson, 1972; Livingstone and Warren, 1996, p79). Ripples occur on most bare sand surfaces, including dunes, and in many areas dunes are superimposed on mega dunes. Wilson thought that these three features co-existed in quasi-equilibrium, and ripples did not grow into dunes, nor dunes into mega dunes. This leads to the conclusion that the nuclei of mega dunes must be larger than fully grown dunes, of which nuclei must be larger than fully grown ripples (see section 2.1, which includes Warren and Allison's (1998) different idea).

In the following, we attempt to explain that proto-dunes can be seen as the lower limit of barchan dunes in respect both to their profile (cross-sectional shape in the wind direction) and to their migration speed.

In chapter 3, a model for the migration speed ( $c_d$ ) of a mature barchan dune, which has a slip face in the lee, was developed (section 3.2). With support of field studies, it predicts the following approximate formula (4.1):

$$c_d = a_{c_d} + \frac{b_{c_d}}{H},$$

where  $H$  is dune height,  $a_{c_d}$  and  $b_{c_d}$  are positive constants. Strictly, the logarithmic relation:

$$c_d = a_L - b_L \log H,$$

where  $a_L$  and  $b_L$  are positive constants, may be a better approximation (see Figure 4.6). When plotting field data in the  $c_d - \frac{1}{H}$  plane, and applying linear regression analysis, coefficients  $a_{c_d}$  and  $b_{c_d}$  correspond to the  $y$ -intercept and the slope, respectively (see section 4.1.1). Further incorporation of the wind-flow theory (Jackson and Hunt, 1975) allowed the model to be developed such that it predicted the windward slope profile (see section 3.3).

Figure 4.17 shows the calculated relation between the windward slope length ( $L_w$ ) and dune height ( $H$ ) for three shear velocities on a level surface ( $u_*(-\infty)$ ). The sand grain diameter ( $D_g$ ) is taken as 0.25 mm. These values are adjusted to those in the dune field near Gobabeb, Namibia (Lancaster, 1996). The roughness



length ( $z_0$ ) is calculated with Owen's formula (2.8). The natural extrapolation of the curve for  $u_*(-\infty) = 0.35 \text{ m s}^{-1}$  is 7.8 m, which is close to the average half length of a proto-dune measured by Lancaster (1996), which is  $12.7/2 = 6.4 \text{ m}$ .

Now we consider a dune that migrates downwind ( $+x$  direction) at a constant speed ( $c_d$ ) without changing its shape. The dune crest, height  $H$ , is set to  $x = 0$ . For migrating shape-invariant dunes, equation (3.5) holds:

$$q(0) - q(-\infty) = \gamma c_d H,$$

where  $q(x)$  is sand flux and  $\gamma$  is the sand bulk density in the dune (for derivation, see section 3.2.1).

In the analysis of wind flow developed by Jackson and Hunt (1975), the dune is characterised with two length scales: dune height ( $H$ ) and the half distance ( $L$ ) between two sites whose height is half the dune height.  $L$  can be related to half the windward surface length ( $L_w/2$ ) (section 3.3.2). According to Jackson and Hunt (1975), the increase of shear velocity at the crest:

$$\delta u_*(0) = u_*(0) - u_*(\infty)$$

can be related to the average dune slope:

$$\delta u_*(0) \sim \frac{H}{L_w}. \quad (4.2)$$

Although sand flux ( $q$ ) is proportional to cube of shear velocity ( $u_*^3$ ), if the shear velocity increase ( $\delta u_*$ ) is small enough, the sand flux ( $q$ ) can be linearised with regard to the shear velocity increase ( $\delta u_*$ ), so that,

$$q(0) - q(-\infty) \sim \delta u_*(0). \quad (4.3)$$

From equations (4.2) and (4.3),

$$q(0) - q(-\infty) \sim \frac{H}{L_w}. \quad (4.4)$$

Substituting equation (4.4) into equation (3.5), we get

$$c_d \sim \frac{1}{L_w}. \quad (4.5)$$

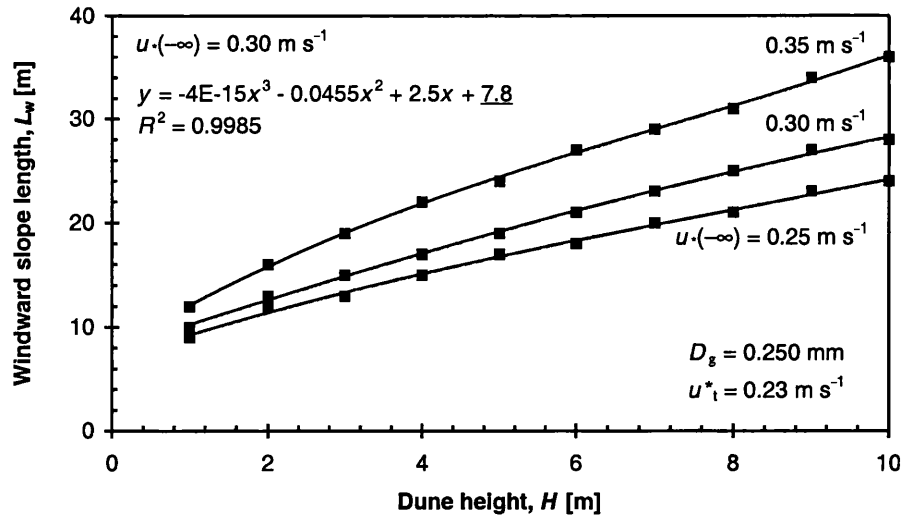


**Figure 4.17:** The calculated relation between the windward slope length ( $L_w$ ) and dune height ( $H$ ) for various shear velocities on the level surface ( $u_*(-\infty)$ ). The sand grain diameter ( $D_g$ ) is taken as 0.25 mm and the roughness length ( $z_0$ ) is calculated with Owen's formula (2.8).

Dune migration speed ( $c_d$ ) is usually discussed in respect to the dune height ( $H$ ). Equation (4.5), however, implies that for low dunes the wind directional length ( $L_{PD} = 2L_w$ ) may be a better index.

Since a proto-dune, whose height ( $H$ ) is nearly zero, has a length ( $L_{PD}$ ) of more than 10 m, from equation (4.5), dune migration speed ( $c_d$ ) must approach a finite value as dune height ( $H$ ) approaches zero. The migration speeds ( $c_d$ ) of a proto-dune observed in the dune field near Gobabeb, Namibia were about 1.0–1.4 m day<sup>-1</sup> = 365–511 m year<sup>-1</sup> when winds were strong (Lancaster, 1996). This may be regarded as a finite value, since according to Cooke *et al.* (1993, figure 23.24), the migration speed of 5-m high dunes is 10–60 m year<sup>-1</sup>.

Figure 4.18 shows the calculated relation between dune migration speed ( $c_d$ ) and dune height ( $H$ ) for three shear velocities on a level surface ( $u_*(-\infty)$ ). A sand grain diameter ( $D_g$ ) of 0.25 mm, the same value as in Figure 4.17, is assumed. For the bulk sand density ( $\gamma$ ), a figure of 1670 kg m<sup>-3</sup> is used (see section 4.2). The natural extrapolations of the curves in this figure are 135, 295 and 423 m year<sup>-1</sup>

for the shear velocity on a level surface ( $u_*(-\infty)$ ) of 0.25, 0.30 and 0.35 m s<sup>-1</sup>, respectively. The last estimation is comparable to field data referred to above, in which migration speeds were 365–511 m year<sup>-1</sup> when winds were strong. Figures 4.17 and 4.18 imply that the present model, which was developed by assuming a slip face, may be a good predictor even for dunes without slip face.

According to equation (4.1), however, the dune migration speed ( $c_d$ ) tends to infinity as dune height ( $H$ ) approaches zero. Generalising equation (4.1), we therefore propose the revised approximation formula:

$$c_d = a_{c_d} + \frac{b_{c_d}}{H + c_{c_d}}, \quad (4.6)$$

where  $c_{c_d}$  is also a positive constant. Constants  $a_{c_d}$  and  $b_{c_d}$  can be determined from field data in the same manner as in equation (4.1). The constant  $c_{c_d}$  can be determined by taking the migration speed of a proto-dune ( $H = 0$ ) as  $a_{c_d} + b_{c_d}/c_{c_d}$ . Equation (4.6) produces a finite value for dune migration speed ( $c_d$ ) as the dune height ( $H$ ) approaches zero. Furthermore, the inverse of equation (4.6) resembles the curves in Figure 4.17, which is consistent with equation (4.5).

For further analysis, more field studies on shape and migration speed of both proto-dunes and mature barchan dunes are necessary.

## 4.4 Conclusions in this chapter

In this chapter, the single-dune model which was developed in the previous chapter was evaluated (as in the flow chart in Figure 3.5).

In section 4.1, the basic model was discussed with numerical calculations, before incorporating wind-flow theory. For low shear velocities at the dune crest, such as  $u_*(0) = 0.4$  m s<sup>-1</sup>, sand trapping efficiency ( $T_E$ ) rapidly increases as dune height increases. However as  $u_*(0)$  increases further, the rate of increase of  $T_E$  declines rapidly, and for the case where  $u_*(0) = 1.92$  m s<sup>-1</sup>,  $T_E$  is virtually 0.0,

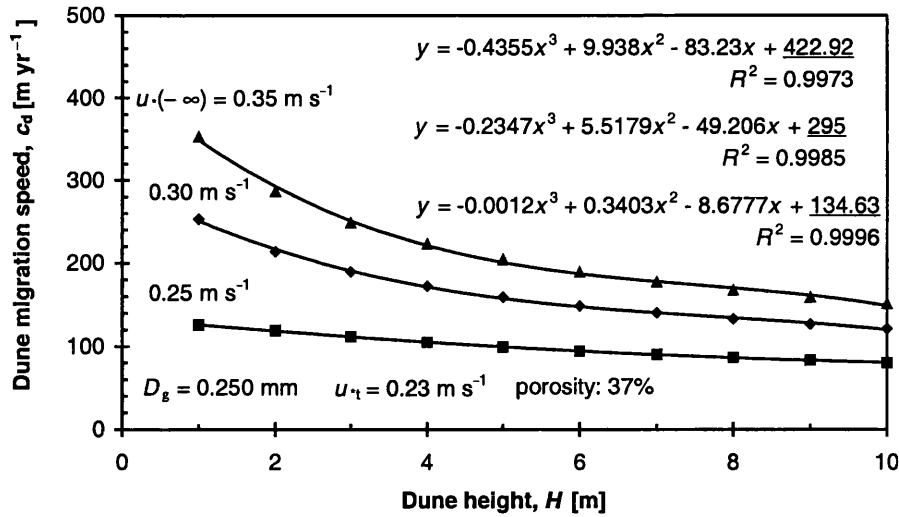


**Figure 4.18:** The calculated relation between dune migration speed ( $c_d$ ) and dune height ( $H$ ) for some shear velocities on a level surface ( $u_*(-\infty)$ ). Sand grain diameter ( $D_g$ ) is assumed to be 0.25 mm.

even for dunes higher than 150 m. From the assumption of equilibrium, where  $T_E = 0.0$ , there is no wind speedup, hence no dune migration. Although sand trapping efficiency ( $T_E$ ) depends on dune height,  $T_E$  is mainly determined by shear velocity on a level surface ( $u_*(-\infty)$ ), and rapidly decreases as  $u_*(-\infty)$  increases. For each dune height, dune migration speed first increases, and then decreases monotonically after reaching the maximum, as shear velocity on a level surface ( $u_*(-\infty)$ ) increases. The relation between shear velocity at the dune crest ( $u_*(0)$ ) and dune height has been estimated for a given shear velocity on a level surface ( $u_*(-\infty)$ ). Dune migration speed ( $c_d$ ) is not inversely proportional to dune height as was previously thought. For low dunes, small sand trapping efficiency ( $T_E$ ) suppresses  $c_d$ , whereas for high dunes, wind speedup and large  $T_E$  resist the decrease of  $c_d$ . Some field data show the same tendency (section 4.1.1). It has been suggested that the dune-to-plane-bed transition observed in subaqueous and Venusian bedforms could be associated with the decrease of sand trapping efficiency (section 4.1.2).

In section 4.2, the average windward slope angles of barchan dunes have been estimated with the Jackson-Hunt theory (1975). Wind flow over a dune was re-

placed by that over either a cosine hill or Gaussian hill. The model has succeeded in explaining the above relation between dune height and the windward slope, as a consequence of the balance between shear velocity increase over the windward surface and the sand trapping efficiency, since the dune is at equilibrium. Furthermore the calculations show the following. There is no significant difference between results estimated with the roughness length from the Owen formula and that of 1 mm (section 4.2.1). There is no significant difference between results estimated with a cosine hill and a Gaussian hill (section 4.2.1). As the surface shear velocity on a flat surface increases, the average windward slope of dunes decreases (section 4.2.1). By assuming a shear velocity on the level surface of  $0.22 \text{ m s}^{-1}$ , data for the windward slope angle and migration speed of dunes in southern Peru, where sand grain diameter is about 0.150 mm, fit the model (section 4.2.2). The model implies that the upper-limit in dune height may be higher in windier environments (section 4.2.2). With small shear velocities that are close to the threshold value, and small dune heights, dune migration speed increases with dune height. These positive relations may associate with zibar parabolic dunes (section 4.2.2). With sand grain diameter of 0.250 mm, which was chosen by considering table 2 in Long and Sharp (1964), windward slope angle and migration speed of dunes in California cannot be explained at the same time. Field data of windward slope angle can be approximated with good accuracy with a shear velocity on the level surface of  $0.55 \text{ m s}^{-1}$ , but this selection of shear velocity results in migration speed more than ten times larger than shown in field data (section 4.2.3). This has yet to be resolved.

In section 4.3, a short discussion was made on proto-dunes. Both the finite wind-directional length and migration speed of proto-dunes could be estimated with the model and are shown to be at the lower limit of barchan dunes. This implies that the present model, which was developed by assuming a slip face, may be a good predictor even for dunes without a slip face.

## CHAPTER 5

# Developing dune field model with discrete dynamics <sup>1</sup>

### 5.1 Introduction: modelling concepts for dune field dynamics

In this chapter, a model that simulates the morphology and dynamics of dune fields is developed. In order to present an accurate model, some important factors need to be considered: the wind pattern over a dune must be adequately determined; the induced sand transport must be precisely estimated; and many other physical factors must be incorporated. On the other hand, to achieve good results using modest computational time we must use simplified algorithms to monitor state space variations. In this chapter, following three pioneers (Nishimori and Ouchi, 1993; Nishimori *et al.*, 1998; de Castro, 1995; Werner, 1995), a dune field is modelled using discrete lattice dynamics (section 2.7.2). The model is built on the foundations of Werner's (1995) approach, which is thought to be superior to the other models in respect to its relation to real physical processes, specifically avalanche dynamics (see section 2.7.2, which also includes other problems in de Castro's (1995) model).

---

<sup>1</sup>Ricardo Carretero-González was involved in this and next chapters

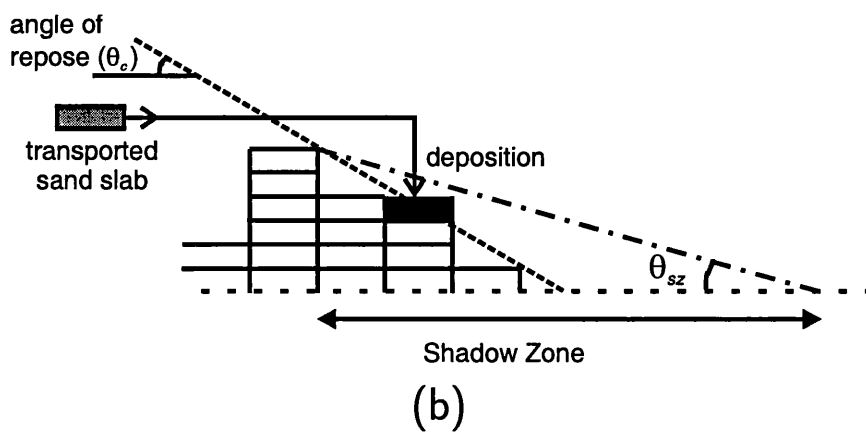
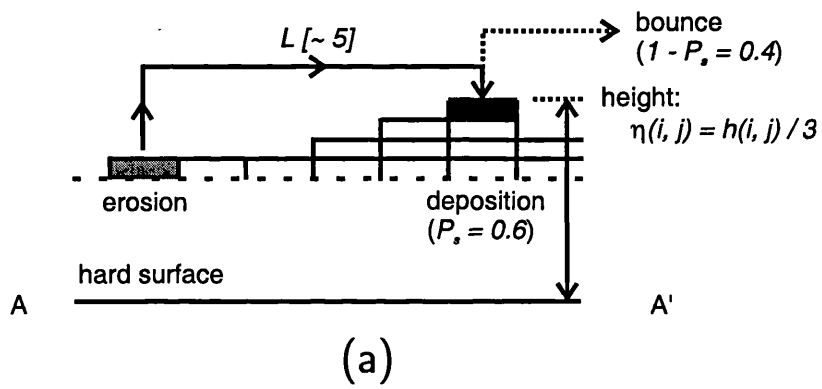
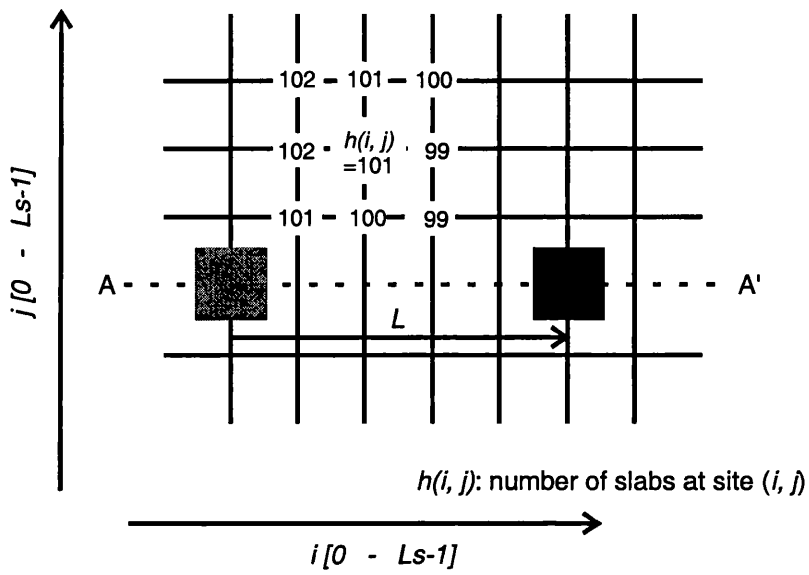
Although there have been obvious successes, problems remained in the initial Werner model. For example, the cross-sectional views of his modelled dunes are much more symmetric than in real dunes, as he noted in his paper (we will also see this problem later in this chapter (section 5.3)).

This chapter starts with modelling transverse dunes, appearing in infinitely deep sand fields under a uni-directional wind regime (section 2.3). Transverse dunes, which are the most two-dimensional in shape and configuration, are thought to be the simplest dunes (Figure 2.1). In chapters 3 and 4, wind speedup over a dune and sand trapping efficiency are emphasised as important factors when discussing equilibrium migration of transverse dunes. In the following, Werner's dune-field simulation model will first be analysed. Following this, two revisions to the Werner model will be introduced. The first revision incorporates wind structure over a dune, and the second considers the wind speedup over the windward surface of a dune (section 2.4.4). Then the modelling of sand availability and seasonally changing wind environment will be discussed (section 2.3).

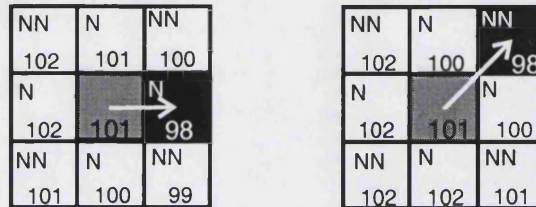
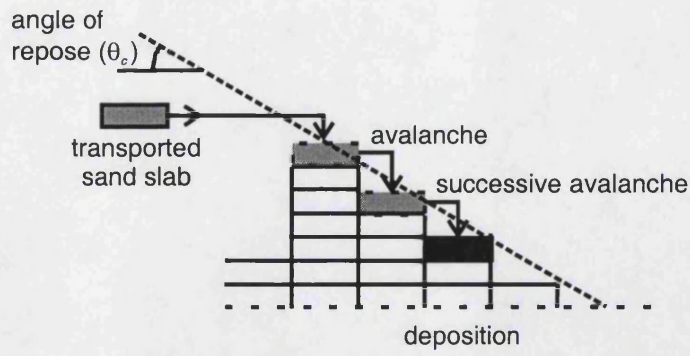
## 5.2 Werner's model and algorithm

Though some corrections and revisions are introduced in later sections, the basic model and concepts used here are predominantly the same as used by Werner (1995; briefly introduced in section 2.7.2). To model the formation and migration of free dunes we consider a model based on a discrete three-dimensional space. Consider a two-dimensional lattice labelled  $(i, j)$  (Figure 5.1(a)), where dune height is measured out of the page. This portion of space is assumed to be a typical section within a dune field.

Here we assume that the dune field consists of three-dimensionally discrete sand slabs (Figure 5.1(a)). Consequently the height ( $\eta(i, j)$ ) is discrete and propor-







N: Nearest neighbouring sites  
 NN: 2nd Nearest neighbouring sites

**in the steepest direction**

(c)

**Figure 5.1:** Lattice model configuration and algorithms: a) wind-directional sand transport, b) shadow zone and c) avalanching. In the shadow zone the deposition probability is 1.0.

tional to the number of sand slabs at each lattice site ( $h(i, j)$ ):

$$\eta(i, j) = \frac{h(i, j)}{3},$$

where 1/3 is slab aspect ratio. Periodic boundary conditions are adopted so that the small simulated area may be repeatedly copied to represent the whole dune field like a mosaic.

Initially we consider a horizontal wind to be active. The first step in the algorithm is to randomly choose a site  $(i, j)$ , from which a single slab is considered to be eroded and then transported downwind in the  $+i$  direction. The distance moved is a specific discrete number of lattice sites  $L(i, j)$ .  $L(i, j)$  can initially be considered as a constant integer ( $L_0$ ), but this is revised later (section 5.5). The transported slab is then deposited on top of the slab pile at the new site  $(i + L(i, j), j)$  with a probability ( $P_s$  or  $P_{ns}$ , see below). If the slab is not deposited at this site,

it is transported farther (*bouncing*) to the site  $(i + L(i, j) + L(i + L(i, j), j), j)$ , and is deposited again with a certain probability. This procedure continues until the slab is eventually deposited at a site. Based on Bagnold's observation that saltating sand grains are more likely to bounce on a stony surface than on a sandy surface (Bagnold, 1941, pp36–37), the deposition probability at sites with at least one slab is set higher ( $P_s = 0.6$ ) than the probability at sites without a slab ( $P_{ns} = 0.4$ ). Furthermore, the concept of a shadow or lee zone downwind of dunes is introduced (Figure 5.1(b)), in which the deposition probability is unity at any site within the lee zone, *i.e.*  $P_s = P_{ns} = 1.0$ . This shadow zone is taken as  $\theta_{sz} = 15^\circ$  from the dune crest, corresponding to the re-attachment point downwind which is roughly four times as long as the dune height from the dune (Figure 5.1(b); Frank and Kocurek, 1996a; section 2.4.4).

Together with this wind-directional transport, avalanching occurs at the place of the steepest descent if the number of slabs between any neighbouring sites differs by three (Figure 5.1(c)). The height of two slabs is equivalent to the angle of repose of  $33.7^\circ$  for the nearest neighbouring sites, and  $25.2^\circ$  for the second nearest due to  $\sqrt{2}$  times longer horizontal distance between the sites, respectively (section 2.4.5). An avalanche may occur both on erosional and depositional sites, and continue until no height difference between neighbouring sites exceeds three. The only slab movement not in the transport direction originates from this form of avalanching. All these simulation rules explained above in this section are the same as those in Werner's (1995) model, although angle of repose is set to  $30^\circ$  in his model and details in algorithm about the shadow zone may be different.

The initial morphology is generated by placing sand slabs, one by one, on the lattice at random locations<sup>2</sup>. In Werner's original paper, transverse dunes were simulated from the initial random morphology with 15 slabs per site on average. Here, because they appear in an infinitely deep sand field, 100 slabs are piled on

---

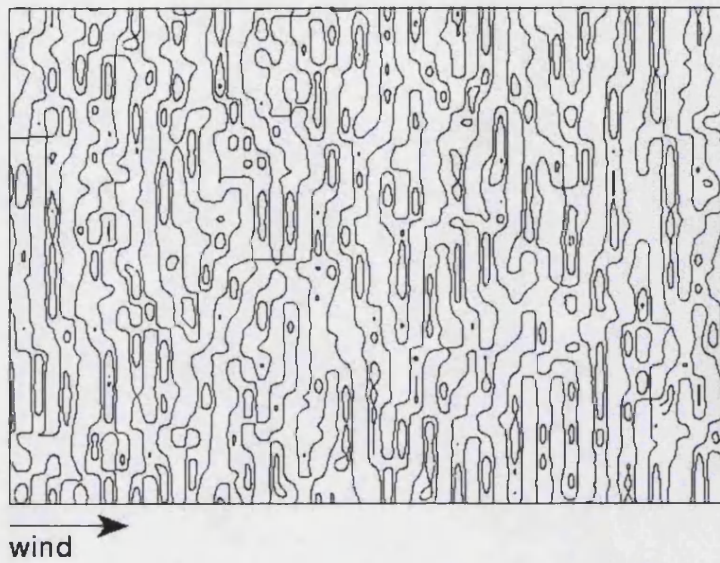
<sup>2</sup>In many simulations, an initial morphology was made in a slightly different manner. For a given average number of slabs ( $h_{avg}$ ), first,  $h_{avg} - 1$  number of slabs are piled up equally on every lattice site. Then the rest of slabs ( $h_{avg} \times L_s^2$ ; on a 1-dimensional lattice,  $h_{avg} \times L_s$ ) are placed randomly on top of the slab pile on each lattice site.

each site on average, which, as is shown in the next chapter, is enough as the underling sand-free surface does not appear. Alternatively, a dune is constructed on the level surface with a depth of 100 slabs, as the initial condition. The windward slope angle of the initial dune was set to  $10^\circ$ . In the simulation, time is denoted by  $t$ , being the number of lattice sites that have been polled for slab erosion divided by the number of surface lattice sites ( $L_s \times L_s$ ).

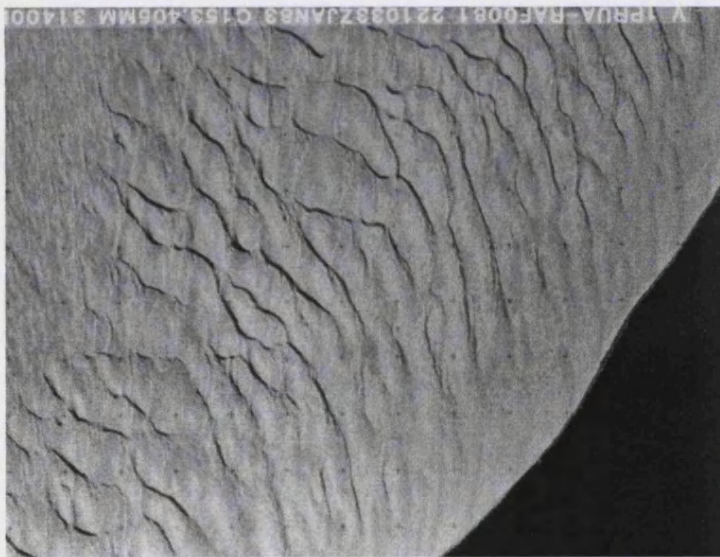
### 5.3 Simulated dune shape and dynamics with Werner's model

Figure 5.2(a) shows transverse dunes on a 2-dimensional  $1024 \times 1024$  lattice simulated after  $t = 500$ , from a random initial morphology without any distinctive pattern or orientation, whose minimum and maximum number of slabs are 95 and 104, respectively. Simulated transverse dunes are not distinct in shape (*cf.* figure 3A in Werner (1995)). The windward slope angles are almost the same as the angle of repose of  $33.7^\circ$ , which is much larger than those of real dunes (about  $10^\circ$ ). Consequently the resulting dunes have symmetrical cross sections, though as seen in Figure 5.2(b) transverse dunes in nature have asymmetrical cross sections with the gentler windward slopes. As seen in figure 3A in Werner's paper, the modelled transverse dunes also have symmetrical cross sections.

Using the same model, Figure 5.3 shows the cross-sectional views of an evolving isolated transverse dune on a level surface on a 2-dimensional lattice, whose initial number of slabs above the surface ( $h$ ) was 30. The simulation times ( $t$ ) are 0 to 500. The dune migrates downwind, during which time its windward slope steepens and its slip face in the lee becomes shallower. However at the same time, the previously level surface upwind and downwind of the dune, deform and the windward slope shows undulation. Meanwhile, downwind of the initial dune smaller accumulations form, which themselves grow as time evolves (*e.g.* close to  $i = 625$ ). Lower dunes migrate more quickly, but are ephemeral, and as time



(a)



(b)

**Figure 5.2:** Transverse dunes (a) in  $(i, j)$  space simulated with Werner's original model, from a random initial morphology, and (b) in nature (Wahiba Sands, Oman). The simulation time ( $t$ ) is 500. Contour lines are for 100, 105 and 110 slabs.

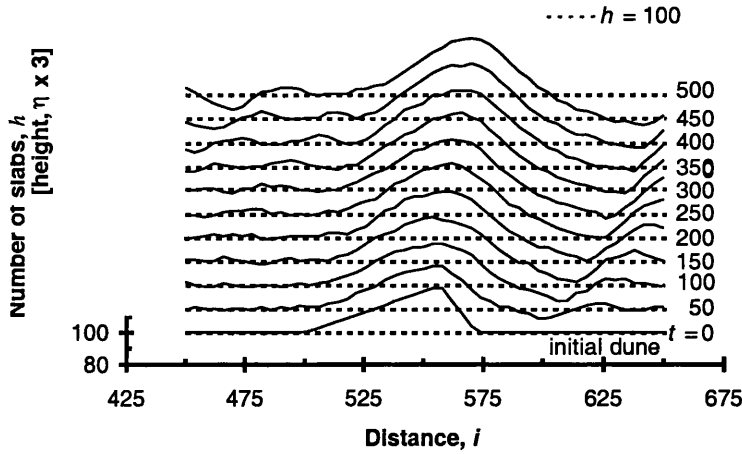


**Figure 5.3:** Evolution of an initially introduced, isolated transverse dune, simulated with Werner's original model. The dune's initial number of slabs above the surface shown by a dotted line is 30. The total simulation time ( $t$ ) is 500.

passes, dune patterns of longer wavelength consisting of larger dunes grow and dominate the dune field.

Shorter wavelengths are not sustained in the long term because of avalanching. The dune envelopes are shaped by sand accumulation and avalanching that suppresses short-wavelength undulations. With regard to avalanching, it can be shown that the wavelength limits the amplitude of undulation, so that only longer-wavelength undulations can grow higher, resulting in dunes with a distinct shape. Assuming that an undulation ( $f$ ) has a wavelength of  $\Lambda$  and a maximum height of  $\eta_\Lambda$ , the field may be approximated as a sinusoidal function:

$$f = (\eta_\Lambda - \eta_{avg}) \sin\left(\frac{2\pi}{\Lambda} x\right),$$

where  $x$  is a distance measure and  $\eta_{avg}$  is the average height. The local gradient ( $\partial f / \partial x$ ) is

$$\frac{\partial f}{\partial x} = (\eta_\Lambda - \eta_{avg}) \frac{2\pi}{\Lambda} \cos\left(\frac{2\pi}{\Lambda} x\right).$$

Since the gradient ( $\partial f / \partial x$ ) cannot exceed 2/3 which corresponds to the angle of

repose of  $33.7^\circ$  then

$$\eta_\Lambda - \eta_{\text{avg}} \leq \frac{\Lambda}{2\pi} \tan 33.7^\circ = \frac{\Lambda}{2\pi} \frac{2}{3} \simeq 0.11\Lambda.$$

Consequently, shorter-wavelength undulations can only achieve lower heights, and thus only longer-wavelength undulations can grow higher.

Next, it can be shown that sand accumulation is due to the existence of the shadow zones in the lee of dunes, where the deposition probability is unity. Without a shadow zone, the sand slab conservation equation can be described as

$$\begin{aligned} h_{t+1}(i, j) &= h_t(i, j) + (\text{transported-incoming sand slabs}) \\ &\quad - (\text{transported-outgoing (erosion) s.s.}) + \text{avalanche} \\ &= h_t(i, j) + \left( \sum_{i'=i-kL} (1 - P_s)^{k-1} P_s + \text{by-passing s.s.} \right) \\ &\quad - (1 + \text{by-passing s.s.}) + \text{avalanche}, \end{aligned} \quad (5.1)$$

where  $h_t(i, j)$  is the number of slabs at the site  $(i, j)$  at time  $t$ . Given that the system is infinitely large, the second term of the right-hand side of (5.1) is

$$\sum_{i'=i-kL} (1 - P_s)^{k-1} P_s \rightarrow P_s \sum_k (1 - P_s)^{k-1} = \frac{P_s}{1 - (1 - P_s)} = 1.$$

Because avalanching occurs equally at each site, equation (5.1) implies that on average, taken over all sites with a periodic boundary condition,

$$h_{t+1}(i, j) - h_t(i, j) = 0. \quad (5.2)$$

In the case of infinite sand depth, producing transverse dunes in Werner's model, dunes grow because incoming sand is accumulated once it has been deposited in the shadow zone, either directly or via avalanching. Without a shadow zone, from equations (5.1) and (5.2) the sand flux is found to be constant at every site.

## 5.4 No erosion in shadow zones

In the rest of this chapter, the Werner model (Werner, 1995) is revised. Each revision will be evaluated through computer simulations in chapter 6. In Werner's

original model the surface in the lee of a dune is eroded. In his model, shadow zones are applied only to sand slab deposition, and erosion still occurs in the shadow zones. A recent field study shows that the wind flow pattern in the lee of the dune is very complex, and that there is apparent sand transport even in the separation cell, which corresponds to the shadow zone in our model (Walker, 1999). However, it is thought to be a good first approximation that the wind speed within the separation cell is typically insufficient to cause significant sand movement (Frank and Kocurek, 1996a; see also section 2.4.4).

## 5.5 Introducing wind speedup

Wind speedup has been noted, both in the field and in the wind tunnel experiments (see for example Mulligan, 1988; Frank and Kocurek, 1996b; Lancaster *et al.*, 1996; Wiggs *et al.*, 1996; see also section 2.4.4). Mulligan found that the wind speed increases linearly over a transverse dune. The more important quantity here is wind shear velocity ( $u_*$ ), or equivalently the wind shear stress, that causes sand transport. Lancaster and co-workers found that the shear velocity increases linearly over a barchan dune, provided that the wind is strong enough such that the shear velocity significantly exceeds the threshold shear velocity (Lancaster *et al.*, figure 10). This wind speedup over a windward slope of a dune is necessary to sustain the shape of the windward slope (Bagnold, 1941; Zeman and Jensen, 1988; see also section 3.2.1).

In a revised model, Nishimori and co-workers attempted to introduce a more realistic slab transport rule compared to Werner's approach, based on the 1-dimensional wind flow calculation (2-dimensional wind flow pattern) over a well-developed dune, in which wind speedup is included (Nishimori *et al.*, 1998; section 2.7.2). In this section, a wind speedup effect is introduced into Werner's model with a kinematic rule.

### 5.5.1 Linear wind speedup: Kinematic formulation

If dunes migrate downwind at a constant speed ( $c_d$ ) without changing their shapes as is widely believed (Bagnold, 1941; section 2.4.6), then looking back to section 2.4.1 the following equation (2.2) holds (for derivation, see section 3.2.1):

$$\gamma c_d \frac{\partial \eta}{\partial x} = \frac{\partial q}{\partial x},$$

where  $\gamma$  is the sand bulk density in dunes,  $\eta(x, t)$  is the local height and  $q$  is the sand flux. Integrating (2.2) from  $x = -\infty$  to  $x = x$  leads to

$$q(x) - q(-\infty) = \gamma c_d \eta(x). \quad (5.3)$$

Let us assume that the sand flux ( $q(x)$ ) obeys Bagnold's sand transport formula (2.5):

$$q(x) = C_B \left(\frac{D_g}{D_r}\right)^{1/2} \left(\frac{\rho_a}{g}\right) (u_*(x))^3,$$

where  $C_B$  is a constant,  $D_g$  is sand grain diameter,  $D_r$  is reference diameter of 0.25 mm,  $\rho_a$  is air density and  $g$  is gravitational acceleration. Assuming that the shear velocity on a dune surface is  $\delta u_*(x)$  larger than that on a bare ground, due to the wind speedup over the dune, the corresponding increase of sand flux is written as

$$\begin{aligned} q(x) - q(-\infty) &= C_B \left(\frac{D_g}{D_r}\right)^{1/2} \left(\frac{\rho_a}{g}\right) [u_*(x)^3 - u_*(-\infty)^3] \\ &= C_B \left(\frac{D_g}{D_r}\right)^{1/2} \left(\frac{\rho_a}{g}\right) [(u_*(-\infty) + \delta u_*(x))^3 - u_*(-\infty)^3] \\ &= C_B \left(\frac{D_g}{D_r}\right)^{1/2} \left(\frac{\rho_a}{g}\right) u_*(-\infty)^3 \left[ \left(1 + \frac{\delta u_*(x)}{u_*(-\infty)}\right)^3 - 1 \right]. \end{aligned} \quad (5.4)$$

If the increase of shear velocity is small enough:

$$\delta u_*(x) \ll u_*(-\infty),$$

equation (5.4) becomes

$$\begin{aligned} q(x) - q(-\infty) &= C_B \left(\frac{D_g}{D_r}\right)^{1/2} \left(\frac{\rho_a}{g}\right) u_*(-\infty)^3 \left[ \left(1 + 3 \frac{\delta u_*(x)}{u_*(-\infty)}\right) - 1 \right] \\ &\approx 3 C_B \left(\frac{D_g}{D_r}\right)^{1/2} \left(\frac{\rho_a}{g}\right) u_*(-\infty)^2 \delta u_*(x). \end{aligned} \quad (5.5)$$



Combining (5.3) and (5.5)

$$\delta u_*(x) \approx \frac{\gamma c_d}{3 C_B \left(\frac{D_g}{D_r}\right)^{1/2} \left(\frac{\rho_a}{\rho_g}\right) u_*(-\infty)^2} \eta(x). \quad (5.6)$$

Though in Werner's model, both the transport length of sand slabs ( $L$ ) and the number of slabs to be removed ( $\delta h$ ) are constant (typically  $L = 5$  and  $\delta h = 1$ ),  $L$  is assumed here to be proportional to  $u_*(x)$ , so that from equation (5.6),

$$L(x) = L_0 + C_1 h(x), \quad (5.7)$$

where  $h(x)$  is the number of slabs at  $x$ . Given that the sand flux ( $q(x)$ ) can be approximated as

$$q(x) = L(x) \frac{\delta h(x)}{3},$$

where the coefficient  $1/3$  is the slab aspect ratio (Nishimori *et al.*, 1998), since

$$q(-\infty) = L_0 \frac{\delta h(x)}{3} \approx u_*(-\infty)^3,$$

and

$$\delta q(x) = \delta L(x) \frac{\delta h(x)}{3} \approx u_*(-\infty)^2 \delta u_*(x),$$

$\delta h(x)$  must be given by

$$\delta h(x) \approx u_*(-\infty)^2 = \text{const.} \quad (5.8)$$

Consequently from equations (5.7) and (5.8), the wind speedup over a dune can be introduced by letting the transport length of sand slab ( $L$ ) be

$$L(x) = L_0 + C_1 (h(x) - h_{\text{ref}}), \quad (5.9)$$

where  $x$  is the erosion/ongoing 'bounce' site,  $C_1$  is constant and  $h_{\text{ref}}$  is a reference number of slabs, which is slightly smaller than the average number of slabs ( $h_{\text{avg}}$ ). The exact definition of  $h_{\text{ref}}$  will be introduced in the next section (5.6). Equation (5.9) can be interpreted as the linear shear velocity increase observed by Lancaster *et al.* (1996, figure 10).

## 5.5.2 Non-linear wind speedup

In the previous subsection, by assuming that the increase of shear velocity is small enough ( $\delta u_*(x) \ll u_*(-\infty)$ ), linear slab transport was discussed. In the field, however, this condition is not always satisfied. A non-linear increase of shear velocity was observed by Frank and Kocurek (1996b, figure 3). More importantly, saltation length, which corresponds to the slab transport length ( $L$ ) in the model, non-linearly increases as shear velocity ( $u_*$ ) increases. From their microscale analysis of saltating sand grains, Anderson and Hallet established a set of equations describing saltation length ( $\lambda$ ) against shear velocity ( $u_*$ ) (Anderson and Hallet, 1986; Anderson, 1988). Figure 5.4 shows the relation between the saltation length ( $\lambda$ ) and the shear velocity ( $u_*$ ), calculated using their equations (2) to (5b) in the 1988 paper. Other parameters used here are sand grain diameter ( $D_g$ ) of 0.25 mm and lift-off angle of  $50^\circ$  (White and Schulz, 1977). Considering these two non-linear relations about shear velocity ( $u_*$ ), it seems to be reasonable that a non-linear shear-velocity-increase term ( $C_2$ ) may be introduced into slab transport length ( $L$ ) in the model, so that equation (5.9) can be revised as

$$\begin{aligned} L(i, j) &= L_0 + C_1 (h(i, j) - h_{\text{ref}}) + C_2 (h(i, j) - h_{\text{ref}})^2 & (h(i, j) \geq h_{\text{ref}}) \\ &= L_0 + C_1 (h(i, j) - h_{\text{ref}}) & (h(i, j) < h_{\text{ref}}), \end{aligned} \quad (5.10)$$

where  $L_0$ ,  $C_1$  and  $C_2$  are constants,  $(i, j)$  is the erosion/ongoing ‘bounce’ site and  $h_{\text{ref}}$  is the reference number of slabs defined in the next section.

## 5.6 Sand availability and reference number of slabs correction

To correctly model the effects of sand availability, which is thought to be the second most important control of dune type (see section 2.3), it is necessary to define the reference number of slabs ( $h_{\text{ref}}$ ) in equations (5.9) and (5.10) carefully. This is because the wind structure over a dune is determined not by the height

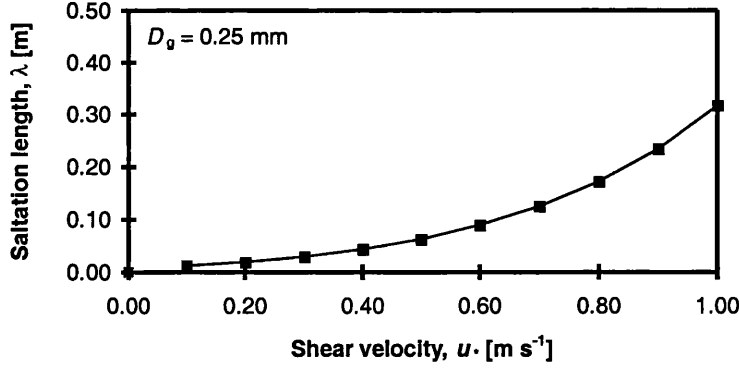


**Figure 5.4:** Relation between saltation length ( $\lambda$ ) and shear velocity ( $u_*$ ). Data are plotted following Anderson (1988). Other parameters, not specified in his paper but used here, are sand grain diameter ( $D_g$ ) of 0.25 mm and lift-off angle of  $50^\circ$  (White and Schulz, 1977).

measured from the hard ground beneath sand, but by the relative height measured from the level ground, on which dunes sit. Such a ground level falls as dunes grow with time. The reference number of slabs ( $h_{\text{ref}}$ ) is then defined here as

$$h_{\text{ref}}(t) = h_{\text{avg}} - \frac{1}{2 L_s^2} \sum_{(i,j)=(0,0)}^{(L_s-1,L_s-1)} |h(i, j; t) - h_{\text{avg}}|,$$

where  $L_s \times L_s$  is the lattice size. The second term of the right-hand side of this equation expresses how many slabs at a site on average incorporate dune construction both erosionally and depositionally.

## 5.7 Introducing wind directional change

As seen earlier in section 2.3, the primary factor that controls type and mobility of dunes is wind directional variability (how wind direction changes seasonally). Figure 5.5 shows how the lattice may be adjusted to model a dune field with bi- or multi-directional wind. When the wind is initially blowing parallel to the  $i$  axis, and then changes its direction with angle of  $\theta$  from  $i$  axis, the lattice may

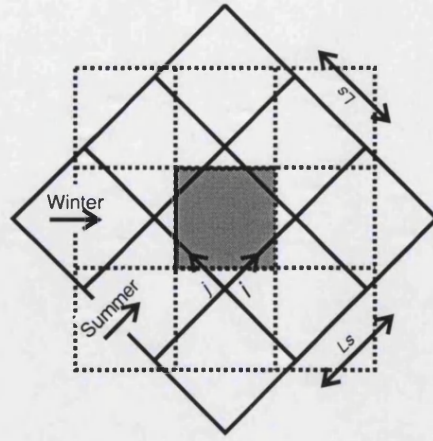


**Figure 5.5:** Modelling scheme for a dune field where the wind changes direction. The lattice is rotated in response to the wind directional change. After the rotation, neighbouring sites are checked to see if they break the angle-of-repose criterion.

be rotated by an angle  $\theta$  keeping the topography unchanged.

$$\begin{aligned}
 i &= \left(i_{\text{new}} - \frac{L_s}{2}\right) \cos \theta - \left(j_{\text{new}} - \frac{L_s}{2}\right) \sin \theta + \frac{L_s}{2} \\
 j &= \left(i_{\text{new}} - \frac{L_s}{2}\right) \sin \theta + \left(j_{\text{new}} - \frac{L_s}{2}\right) \cos \theta + \frac{L_s}{2} \\
 h(i_{\text{new}}, j_{\text{new}}) &= h(i, j).
 \end{aligned}$$

Consequently in the computations, the wind always blows parallel to the  $i$  axis. After the rotation, it is checked to see if any neighbouring sites break the angle-of-repose criterion. The drawback of this scheme is that the number of slabs is not conserved. If the average number of slabs ( $h_{\text{avg}}$ ) is small, the situation is worse. In the case of  $h_{\text{avg}} = 2.0$  the difference between the initial and the final numbers of slabs after  $t = 1500$  is about 10%. However, if we choose an optimal rotation (pivot) centre for each wind-direction change, which is usually different from  $(L_s/2, L_s/2)$ , such a difference in number of slabs can be reduced to the order of 0.1% with modest additional computational time. This is a practical remedy. An ideal solution is to use an infinitely large lattice (*i.e.*  $L_s \rightarrow +\infty$ ) to increase uniformity in spatial distribution of dunes.

## 5.8 Conclusions in this chapter

A simulation model for a transverse-dune field was developed based on Werner's model (1995). A portion of a large dune field is simulated on a two-dimensional square lattice, whose edges are connected with periodic boundary conditions. In the model, dunes are the accumulation of three-dimensionally discrete 'slabs', whose motion represents sand motion in nature. There are two types of slab motion: wind directional transport and avalanche. Furthermore, based on observational facts, a shadow zone in a lee of a dune and bouncing probability difference between bare and sandy surfaces were introduced (section 2.7.2; section 5.2).

Application to an infinitely deep sand field revealed that the original Werner model cannot correctly simulate transverse dunes with distinct shape, or with asymmetric wind-direction profile. Model analysis showed the importance of the shadow zone, without which dunes cannot grow (section 5.3). Two revisions were made by considering the wind structure over a dune. From consideration about the separation zone in the lee of the dune, a no-erosion criterion in shadow zones was introduced (section 5.4). Noting that the shear velocity increases over the windward surface of a dune, a wind speedup effect was introduced by adding a height-proportional increase term to the original slab transport length ( $L_0$ ) (section 5.5.1). Furthermore, by considering a non-linear dependence of shear velocity on the saltation length of a sand grain, a non-linear shear-velocity-increase term was introduced into the slab transport length (section 5.5.2). Sand availability and wind directional variability, the two most important controls of dune types, can now be studied with the introduction of reference number of slabs ( $h_{\text{ref}}$ ) (section 5.6) and lattice rotation (section 5.7), respectively.

## CHAPTER 6

# Comparisons with field studies

In chapter 5, after having examined the original Werner (1995) model, some revisions were made. In this chapter, each revision will be tested through computer simulations, and many aspects of morphology and dynamics of dune fields will be discussed. Table 6.1 shows the parameters used in the simulations that follow. For a historical reason, the concept of the reference number of slabs ( $h_{\text{ref}}$ ) in equations (5.9) and (5.10), which was defined in section 5.6, will be introduced from section 6.3. In sections 6.1 and 6.2, hence in Figures 6.1–6.8,  $h_{\text{ref}}$  is replaced with the average number of slabs ( $h_{\text{avg}}$ ).

### 6.1 No erosion in shadow zones

In section 5.4, by considering observational facts, a no-erosion criterion has been introduced in the shadow zones in the lee of dunes. Figure 6.1 shows cross-sectional views of transverse dunes simulated without erosion in shadow zones, on a 2-dimensional lattice from an initially isolated transverse dune with the number of slabs ( $h$ ) initially set at 30, built on a level surface (*cf.* Figure 5.3). The simulation times ( $t$ ) are 0 to 100. With no erosion in the shadow zones: a) the slip face in the lee is sustained; b) the dunes grow more quickly due to strong accumulation of sand slabs; and c) the dunes migrate downwind with constant

parameter	value
lattice size:	$L_s \times L_s = 1024 \times 1024$
slab aspect ratio	1/3
angle of repose	
to the nearest neighbour	$\tan^{-1}(2/3) = 33.7^\circ$
to the second nearest neighbour	$\tan^{-1}(2/3/\sqrt{2}) = 25.2^\circ$
shadow zone angle	$15^\circ$
transport length at the reference height	$L_0 = 5$ (unless specified in the text)
shear-velocity-increase:	
linear coefficient	$C_1 = 0.4$
non-linear coefficient	$C_2 = 0.002$
erosion probability:	
outside shadow zone	same at every site
in shadow zones	0.0
deposition probability:	
outside shadow zone:	
with at least a slab	$P_s = 0.6$
without a slab	$P_{ns} = 0.4$
in shadow zones	$P_s = P_{ns} = 1.0$

**Table 6.1:** Simulation parameters.

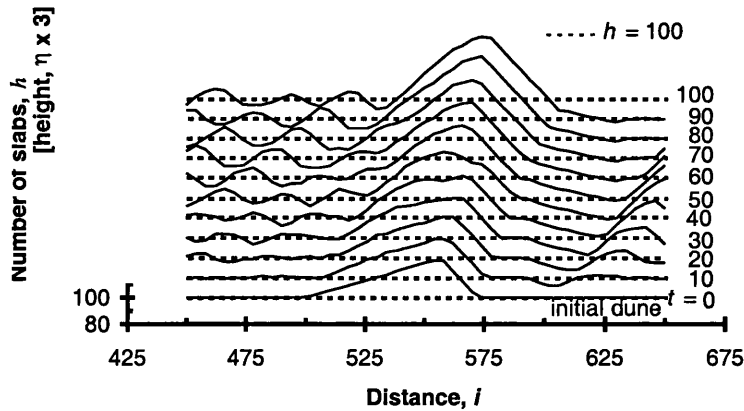


**Figure 6.1:** Evolution of an initially introduced, isolated transverse dune simulated without erosion in shadow zones. The dune's initial number of slabs above the surface is 30. The simulation time ( $t$ ) is 100.

speed during the period of a constant height. These features are similar to those of dunes in nature (section 2.4.6). Figure 6.2 shows transverse dunes simulated on a 2-dimensional lattice from an initially random morphology. Without erosion in the shadow zones, the dunes are higher than those shown in Figure 5.2(a), due to strong slab accumulation. In the remainder of this chapter we consider no erosion in shadow zones in all simulations.

## 6.2 The effects of wind speedup over a dune

In this section, the effects of wind speedup, which was introduced in section 5.5, are examined numerically. Wind speedup has been formulated by adding linear and non-linear height-dependent terms to the original constant slab transport length ( $L_0$ ) (see equation 5.10). To highlight the role of each term, in the first half of this chapter (section 6.2.1), the effects of linear wind speedup formulated in equation (5.9) in subsection 5.5.1 are examined. Subsequently in the next half (section 6.2.2), the effects of non-linear wind speedup formulated in equation (5.10) in section 5.5.2 are examined.



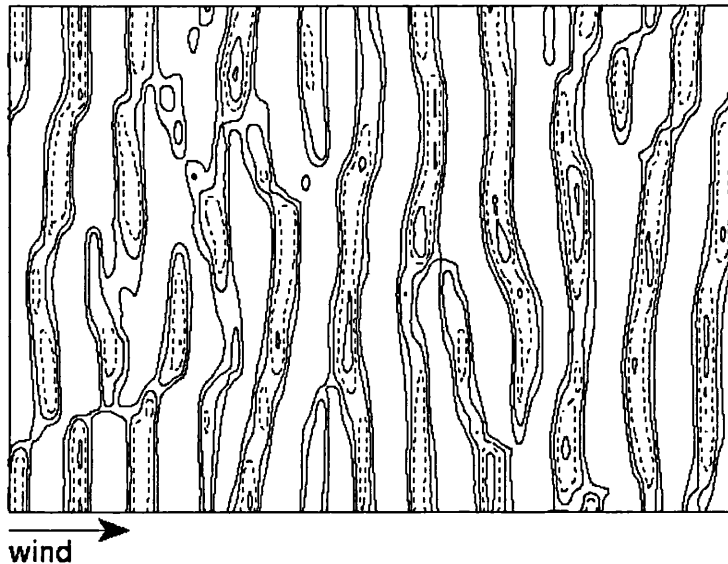


**Figure 6.2:** Transverse dunes simulated from an initially random morphology. The simulation time ( $t$ ) is 500. No erosion occurs in shadow zones. Contour lines are for 100, 110, 120, 130 and 140 slabs.

### 6.2.1 The effects of linear wind speedup

Simulations were carried out with and without a wind speedup term introduced in the form of equation (5.9). Figure 6.3 shows the simulation results started from the same initial transverse dune used in Figures 5.3 and 6.1, with various shear-velocity-increase coefficients ( $C_1$ ). Introducing wind speedup makes: a) dunes lower; b) dunes migrate more quickly; and c) dune windward slopes gentler, producing asymmetric dunes. For  $C_1 = 0.4$ , windward slopes with the angle of  $10^\circ$  are sustained. The dune did not vanish even with a higher shear-velocity-increase coefficient, say  $C_1 = 0.6$ , after  $t = 1,000,000$ . Figure 6.4 shows asymmetric transverse dunes formed on a 2-dimensional lattice from a random initial morphology by introducing wind speedup. The simulation time ( $t$ ) is 1,500, and the shear-velocity-increase coefficient ( $C_1$ ) is 0.4. The resulting transverse dunes are the most qualitatively similar to natural ones achieved yet.

Werner realised the problem of the symmetric cross-sectional views of dunes simulated with his original model (see Figure 5.2(a)), and thought “A possible remedy

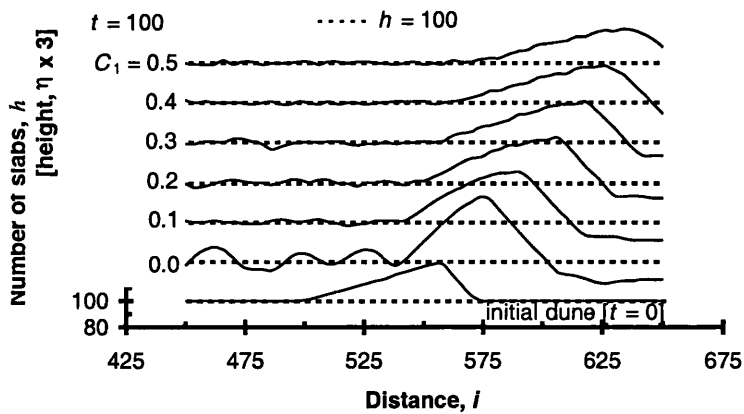


**Figure 6.3:** Evolution of an initially introduced, isolated transverse dune simulated with various shear-velocity-increase coefficients ( $C_1$ ). The dune's initial number of slabs above the surface is 30. The simulation time ( $t$ ) is 100.

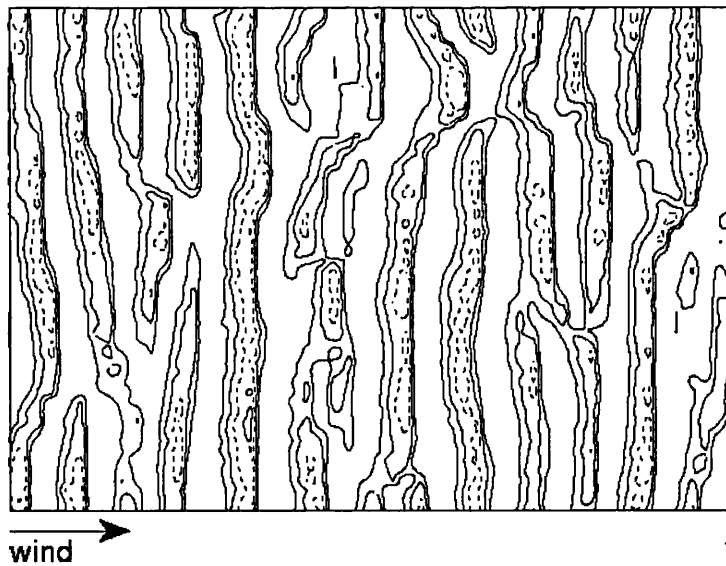


**Figure 6.4:** Asymmetric transverse dunes formed from a random initial morphology by introducing wind speedup. The simulation time ( $t$ ) is 1,500, and the shear-velocity-increase coefficient ( $C_1$ ) is 0.4. Contour lines are for 100, 105, 110 and 115 slabs.

is modifying the transport rules to account for the relationships among local morphology, wind profile, and transport flux in greater detail” (Werner, 1995). His prediction is now found to be partly correct. The asymmetry in the cross-sectional dune shape is indeed an outcome of the interaction between local morphology, wind profile, and transport flux, but can be formulated with a very simple rule as in equation (5.9).

The time evolution of a 1-dimensional dune field with the shear-velocity-increase coefficient ( $C_1$ ) of 0.4 is shown in Figure 6.5. The wavelength of the transverse dunes increases as time passes. For run times longer than that displayed in the figure, the equilibrium dune field seems to converge to only one isolated, asymmetric dune, which is surrounded by completely plane, bare ground. Consequently, the dune-to-dune spacing is equal to the lattice size,  $L_s = 1,024$ , meaning that the model is not adequate when the dune-to-dune spacing approaches the lattice size.

The reason for this equilibrium dune field configuration is thought to be related to sand trapping efficiency ( $T_E$ ), which is the proportion of moving sand trapped in the dune slip face in the lee (Wilson, 1972; Cooke *et al.*, 1993, pp346–347). At equilibrium, the sand flux coming to the dune must be the same as the outgoing flux (Zeman and Jensen, 1988; see also section 3.2.1). However, because the shadow zone extends more quickly than the slab transport length at the crest of dune ( $L$ ) increases as the dune grows higher, all the slabs crossing the dune crest will be captured in the dune, meaning the sand trapping efficiency ( $T_E$ ) is equal to 1.0, so that nothing regulates dune height. The wind speedup effect introduced with the form of equation (5.9), seems to regulate only the windward slope angle.

### **6.2.2 The effects of non-linear wind speedup and equilibrium dune field**

Figure 6.6 shows the time evolution of 1-dimensional dune field with non-linear increase of the transport length introduced in the form of equation (5.10). The

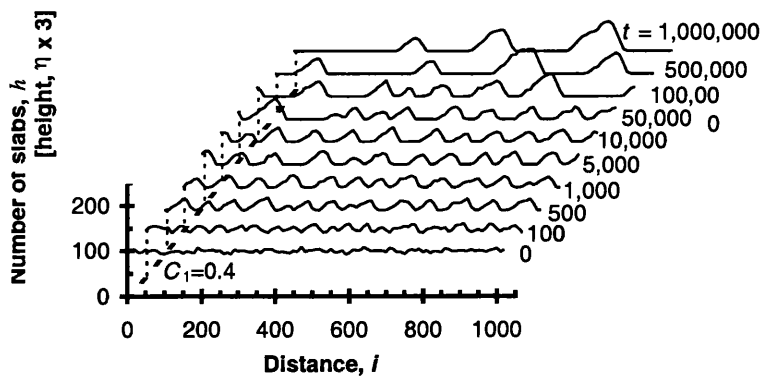


**Figure 6.5:** Time evolution of a 1-dimensional dune field, from a random initial morphology. The shear-velocity-increase coefficient ( $C_1$ ) is 0.4.

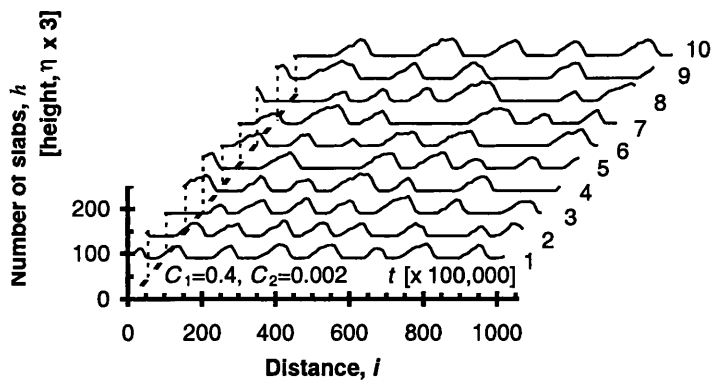


**Figure 6.6:** Time evolution of transverse dunes simulated on the 1-dimensional lattice with non-linear increase of the transport length, from a random initial morphology. Linear shear-velocity-increase coefficient ( $C_1$ ) is 0.4. Non-linear shear-velocity-increase coefficient ( $C_2$ ) is 0.002.

shear-velocity-increase coefficient ( $C_1$ ) is 0.4 and the non-linear shear-velocity-increase coefficient ( $C_2$ ) is taken as 0.002. The choice was made because preliminary trials showed that if  $C_2$  was 0.02 dunes with a distinct shape did not grow, whereas if  $C_2$  was 0.0001 no effect was observed. Comparing Figures 6.5 and 6.6, we find that introducing non-linear increase of the transport length a) makes dunes lower and b) increases the number of dunes.

In chapter 4, published field data are examined, and it was found that dune migration speed ( $c_d$ ) could be approximated as

$$c_d \simeq a_{c_d} + b_{c_d} \frac{1}{H}, \quad (6.1)$$

where  $a_{c_d}$  and  $b_{c_d}$  are positive constants and  $H$  is dune height (section 4.1.1). In chapters 3 and 4, it was discussed that equation (6.1) could theoretically be derived by assuming that the dunes were in equilibrium (section 3.2.1). If the dune is nearly at equilibrium but slowly growing, by considering the dimensionality, this near-equilibrium dune can be characterised as

$$\frac{\partial H}{\partial t} \ll c_d. \quad (6.2)$$

Combining equations (6.1) and (6.2) leads to

$$\frac{\partial H(t)}{\partial t} \ll \frac{b_{c_d}}{H(t)} < a_{c_d} + b_{c_d} \frac{1}{H(t)}. \quad (6.3)$$

Integrating equation (6.3) we obtain

$$H(t) \ll t^{1/2}.$$

Figure 6.7 shows the relations between maximum dune height and simulation time ( $t$ ) in the cases with and without non-linear increase of the transport length.  $C_1$  and  $C_2$  are the same as in Figure 6.6. In the case with non-linear increase of the transport length, the maximum dune height increases more slowly. The data are well correlated to the square root of time ( $t^{1/2}$ ), suggesting that the dune field is in near-equilibrium, and even at  $t = 1,000,000$ , the exact equilibrium state is not reached. The dune height far after  $t = 1,000,000$  is thought to be capped by the non-linear wind speedup effect, because some part of slab flux crossing at the

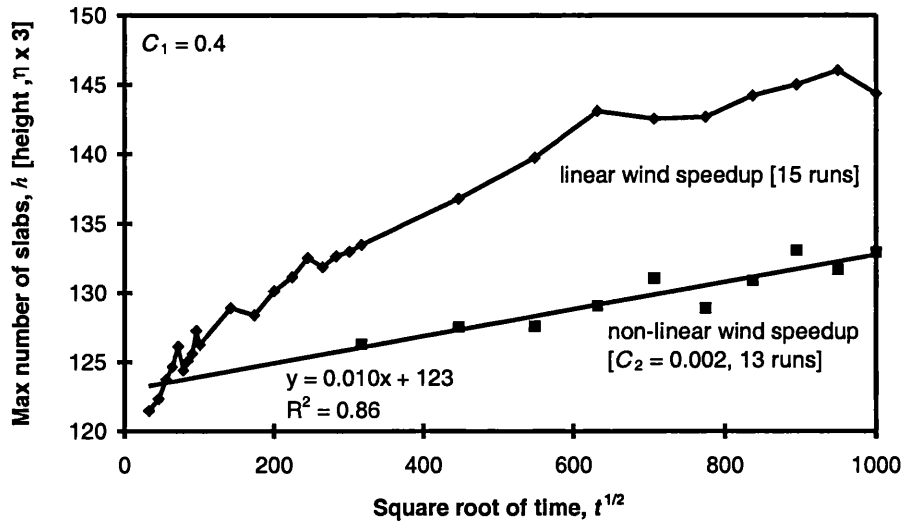


**Figure 6.7:** Relations between maximum dune height and simulation time ( $t$ ). The relations with and without the non-linear increase of the transport length are averaged from 13 and 15 runs on the 1-dimensional lattice, respectively. Linear shear-velocity-increase coefficient ( $C_1$ ) is 0.4. Non-linear shear-velocity-increase coefficient ( $C_2$ ) is 0.002.

crest of a dune goes outside the shadow zone, reducing sand trapping efficiency ( $T_E$ ) below 1.0, so that the incoming and outgoing slab fluxes balance. Lancaster reported that shear velocity reached  $0.6 \text{ m s}^{-1}$  at a site on the windward surface, whose horizontal distance is 35 m from the toe (windward bottom) of the dune (Lancaster, 1996; figure 10). The height of this dune was 5 m. According to Figure 4.1, a leakage of the sand flux is very likely to occur for this combination of shear velocity and dune height. To check if the dune height saturates, or not, more simulations are needed with longer time ( $t$ ). Figure 6.8 shows transverse dunes simulated on the 2-dimensional lattice, from a random initial morphology.  $C_1$  and  $C_2$  are 0.4 and 0.002, respectively, as in Figures 6.6 and 6.7. Simulation time ( $t$ ) is 1,500. Some dunes in Figure 6.8 are lower than corresponding dunes in Figure 6.4 because of the non-linear increase of the transport length.

As seen in Figures 6.5 and 6.6, after a long enough time, flat surfaces appear between dunes. However some transverse dune systems observed in nature do

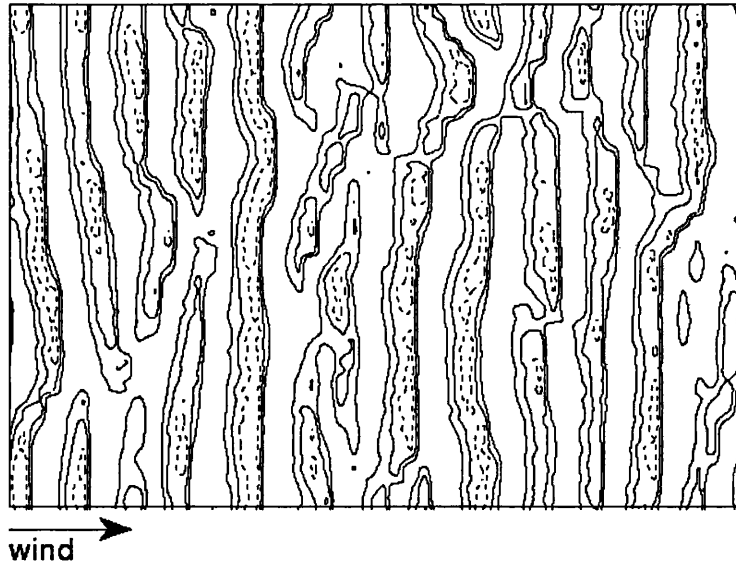


**Figure 6.8:** Transverse dunes simulated on the 2-dimensional lattice, from a random initial morphology. Linear shear-velocity-increase coefficient ( $C_1$ ) is 0.4. Non-linear shear-velocity-increase coefficient ( $C_2$ ) is 0.002. The simulation time ( $t$ ) is 1,500. Contour lines are for 100, 105 and 110 slabs.

not have distinct inter-dune flat surfaces. This discrepancy will be solved in the following section (6.3) by introducing the concept of reference number of slabs ( $h_{\text{ref}}$ ) in equation (5.10), which was defined in section 5.6.

Considering erosion in the shadow zone, the non-linear shear-velocity-increase coefficient ( $C_2$ ) may be overestimated. In Figure 6.7, dune heights after a long time period differ significantly in the cases with and without non-linear increase of the transport length.

## 6.3 The effects of sand availability and wind variability

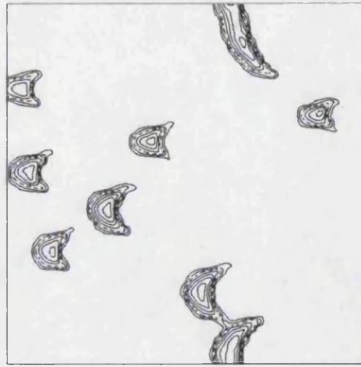
Wind variability and sand availability are thought to be the two most important controls of dune type (see section 2.3). In this section, the effects of these two controls are investigated. The first two subsections (6.3.1 and 6.3.2) discuss uni-directional wind regimes, and the last subsection (6.3.3) deals with bi-directional wind regimes. In the model, sand availability is defined as the average number of slabs per site ( $h_{\text{avg}}$ ) taken over all sites. The effects of sand availability are investigated with the concept of the reference number of slabs, which was introduced in section 5.6. Wind variability is simulated with the lattice rotation introduced in section 5.7.

### 6.3.1 Dune types in a uni-directional wind regime: pattern and sand availability

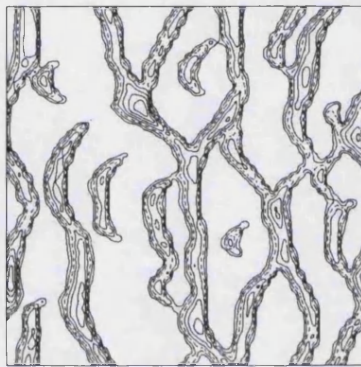
In Figure 6.9 we show the results of a simulation of  $t = 1500$  beginning with an almost flat surface. As  $h_{\text{avg}}$  increases, the dune field changes from no pattern ( $h_{\text{avg}} \leq 1.1$ ) to barchan dunes shown in Figure 6.9(a) for  $h_{\text{avg}} = 2.0$ , then to laterally connected barchan dunes (Figure 6.9(b),  $h_{\text{avg}} = 7.0$ ), and finally to transverse dunes (Figure 6.9(c),  $h_{\text{avg}} = 20.0$ ). The laterally connected barchan dunes are more sinuous than the transverse dunes formed in an infinitely deep sand field. The change from barchan dunes to transverse dunes in response to the increase of sand availability coincides with field observations (Livingstone and Warren, 1996, figure 5.22; reproduced in Figure 2.2).

Characteristics of each pattern can be extracted through the Fourier transform ( $h(i, j) \rightarrow \hat{h}(i, j)$ ). The Fourier components which are not thought to contribute to the pattern ( $\hat{h}(0, j)$  and  $\hat{h}(i, 0)$ ) are all excluded. As sand availability increases, the wavelength in the  $i$  direction decreases. For an infinitely deep sand field, the

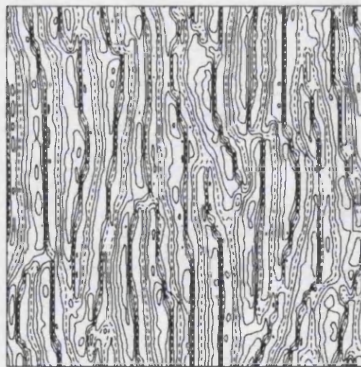




(a)



(b)



(c)

**Figure 6.9:** Different types of dune simulated with various sand availabilities ( $h_{avg}$ ); (a) 2.0, (b) 7.0 and (c) 20.0. All simulations started with an almost flat surface. The wind blows from left to right. The contour interval is  $h = 5$ .

first peak is 78.8, and the second is 102.4. Transverse dune systems formed in an infinitely deep sand field are more regular than one with inter-dune bare surfaces. The intensity ratio of the first peak to the second peak is higher when  $h_{\text{avg}} \geq 20.0$  than when  $h_{\text{avg}} = 10.0$ .

There is a sudden transition from no pattern to a pattern of isolated dunes without distinct asymmetry or slip face, namely dome dunes. This transition was checked by using 15 different sets of simulations. Table 6.2 shows the resulting maximum number of slabs ( $h_{\text{max}}$ ), for sand availability ( $h_{\text{avg}}$ ) values of 1.1 and 1.2. In all simulations with an average number of slabs per site ( $h_{\text{avg}}$ ) of 1.1, no pattern was formed, whereas for  $h_{\text{avg}}$  of 1.2, isolated dunes formed in all simulations. The threshold thus lies between  $h_{\text{avg}}$  of 1.1 and 1.2. As sand availability increases further to  $h_{\text{avg}} = 2.0$ , these dome dunes gradually change to barchan dunes.

If, rather than starting with an almost flat surface, we start with an initial surface consisting of barchan dunes, they remain as features even when the sand availability is less than the previously determined threshold.

In the following numerical experiments, the simulation time ( $t$ ) is 3000, the first half ( $t \leq 1500$ ) of this time being for the initial barchan dunes creation. At  $t = 1500$  half of the slabs at every site were removed, and then simulations were resumed. That is at  $t = 1500$  we reduced the barchan dunes to half their height, with a corresponding reduction in the steepness of the windward surfaces.

simulation	1	2	3	4	5	6	7	8	9	10
$h_{\text{max}}(h_{\text{avg}} = 1.1)$	5	5	5	4	5	5	4	5	5	4
$h_{\text{max}}(h_{\text{avg}} = 1.2)$	23	25	22	24	25	25	21	22	23	24
simulation	11	12	13	14	15					
$h_{\text{max}}(h_{\text{avg}} = 1.1)$	4	4	4	4	5					
$h_{\text{max}}(h_{\text{avg}} = 1.2)$	24	26	25	24	22					

**Table 6.2:** Maximum dune height when sand availabilities are below and above the threshold.

The initial sand availability ( $h_{\text{avg}}(t \leq 1500)$ ) was varied from 1.2 to 2.0. Table 6.3 shows the sand availabilities ( $h_{\text{avg}}$ ) for  $t \leq 1500$  and for  $t \geq 1500$ , the resulting maximum number of slabs ( $h_{\text{max}}$ ) and the patterns at  $t = 3000$ . ‘N’ and ‘D’ represent no pattern and the pattern with (barchan) dunes, respectively. Dunes did not disappear completely, even with the sand availability less than the threshold. However, many of these dunes are not strongly asymmetric in their wind-directional shape, and do not have distinct slip faces. In the region below the threshold, the system can be said to be bistable, *i.e.* both no pattern and the pattern with isolated (dome/barchan) dunes can exist, depending on the initial surface morphology. To check if there is another threshold in sand availability, below which initially placed barchan dunes disappear, more simulations are necessary.

### 6.3.2 Spatial and temporal scales in the model: quantitative comparison to nature

To estimate the scaling of length and time in our model we consider the downwind migration of barchan dunes. We fix the sand availability ( $h_{\text{avg}}$ ) at 2.0. Figure 6.10(a) shows a barchan dune field which appeared from an almost flat surface after  $t = 1500$ . Figure 6.10(b) shows the field with all other dunes removed except the one marked with a \* in Figure 6.10(a). To view migration of the complete dune field, in Figure 6.10(c) we plot the field  $t = 100$  later, *i.e.*  $t = 1600$ . In

$h_{\text{avg}}(t \leq 1500)$	1.2	1.3	1.4	1.5	1.6	1.7	1.8	1.9	2.0
$h_{\text{avg}}(t \geq 1500)$	0.43	0.59	0.65	0.70	0.75	0.79	0.82	0.75	0.95
$h_{\text{max}}$	3	19	21	23	23	25	27	24	27
pattern	N	D	D	D	D	D	D	D	D

**Table 6.3:** Conservation of the initial dune pattern below the threshold in sand availability. ‘N’ and ‘D’ represent no pattern and the pattern with (barchan) dunes, respectively.

Figure 6.10(d) we plot the corresponding migration of the isolated dune of Figure 6.10(b) after a further  $t = 100$ . From a) and c), the barchan dunes are found to be migrate downwind without changing their individual shapes or their alignment (section 2.4.6) (the two dunes at the bottom show a partially connected transient form). This is cooperative motion and, as seen in the migration from b) to d), without interaction with neighbouring dunes a barchan dune cannot maintain its shape during its downwind migration.

The dune labelled \* in Figure 6.10 is about 30 slabs (= 10 l.u.; lattice units) high, and migrates about 500 l.u. in a period of  $t = 100$ . Physically, a 10 m barchan dune is known to migrate typically 20 m annually (Cooke *et al.*, 1993, figure 23.24). Considering both these dynamics, temporal and spatial scales in the model can be estimated as follows:

$$\begin{aligned} 1 \text{ l.u.} &= 1 \text{ m} \\ 4 t &= 1 \text{ year.} \end{aligned} \tag{6.4}$$

Table 6.4 shows the relation between dune pattern and the slab transport length ( $L_0$ ) at the reference height. Sand availability ( $h_{\text{avg}}$ ) is 2.0. When the wind is too strong ( $L_0 = 50$ ), an almost flat surface appears. On the other hand, when the wind is weak ( $L_0 = 2$ ), the dunes are low. Both these results support earlier analyses (section 4.1; section 4.2). Sand flux ( $q$ ) on the level surface can be related to the slab transport length ( $L_0$ ) at the reference height as follows (Nishimori *et al.*, 1998; section 5.5.1):

$$q = \frac{[\frac{L_0^3}{3}] [\gamma] [L_0]}{[t]}, \tag{6.5}$$

where  $\gamma$  is the bulk sand density ( $1961 \text{ kg m}^{-3}$ ) for quartz sand with the lowest porosity in theory (0.26, see for example Pye and Tsoar 1990), which gives the highest estimation for the sand flux ( $q$ ). From equations (6.4) and (6.5), the sand flux ( $q$ ) for  $L_0 = 1$  is calculated as  $8.3 \times 10^{-5} \text{ kg m}^{-1} \text{ s}^{-1}$ , which is less than 10% of values observed for a reversing dune by Walker (1999). Table 6.4 predicts that if the sand flux is small enough, no dunes emerge, *i.e.* a threshold in sand flux exists. When  $L_0 = 3$  dune migration speed is about 60% of that when  $L_0 = 5$ .

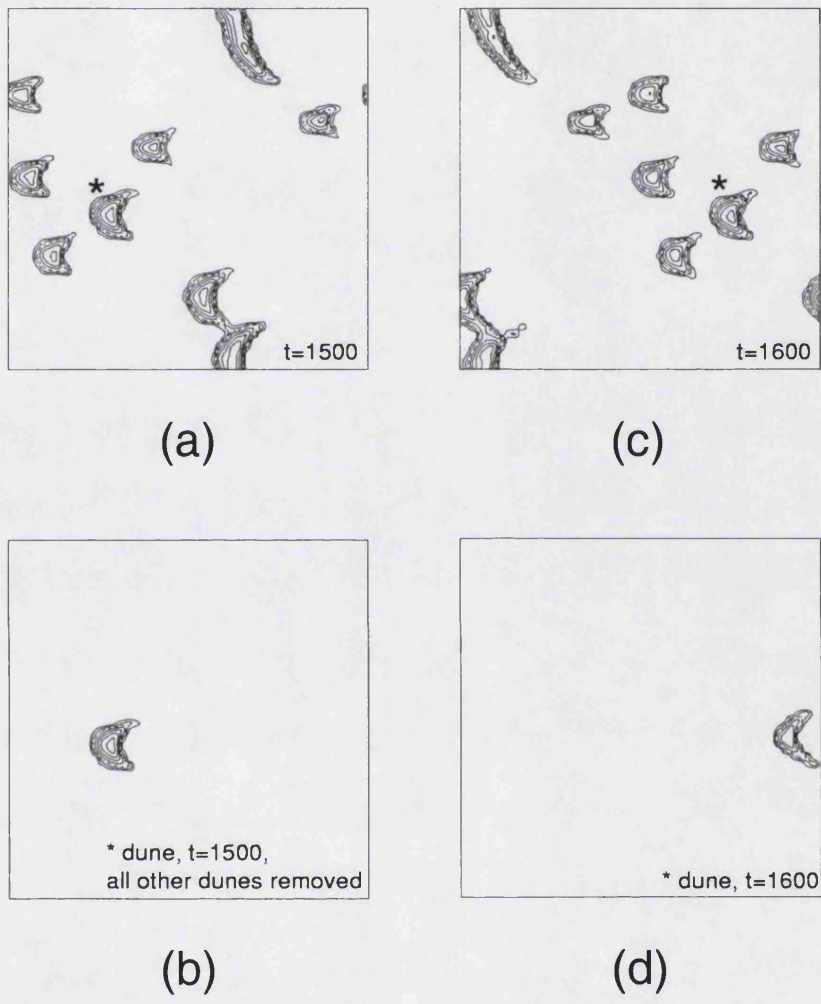


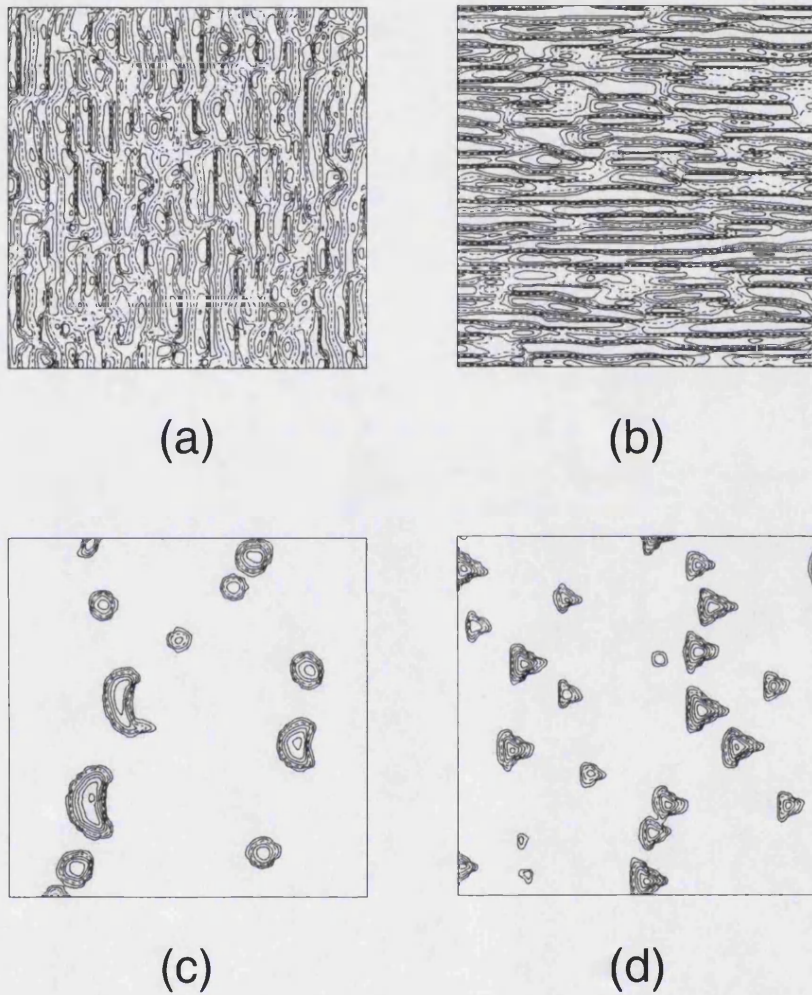
**Figure 6.10:** Downwind migration of barchan dunes. a) Barchan dune field appeared from a almost flat surface after  $t = 1500$ . b) A selected barchan dune from a). All others are removed. c) Barchan dune field of  $t = 100$  after a). d) The barchan dune of  $t = 100$  after b).

$L_0$	Dune pattern	$h_{\min}$	$h_{\max}$
0	No pattern	1	4
1	No pattern	1	5
2	Low transverse dunes	0	7
3	Barchan dunes	0	34
4	Barchan dunes	0	40
5	Barchan dunes	0	40
10	dome-like barchan dunes	0	31
25	A few dome dunes	0	15
50	No pattern	0	8

**Table 6.4:** Dune pattern and the slab transport length ( $L_0$ ) at the reference height.

### 6.3.3 Dune types in a bi-directional wind regime

Once we know the time scale in the model, we can simulate a dune field in which the wind direction changes seasonally, a common situation in nature. Figure 6.11 shows the relation between the dune type and the formative environment. The latter is comprised of an annual wind directional change and sand availability. Wind direction changes every half a year ( $t = 2$ ). Sand availability and the angle between the two directions of the wind ( $h_{\text{avg}}, \theta$ ) are a) (100, 60°), b) (100, 120°), c) (2, 60°) and d) (2, 120°). In a dune field with a limited amount of sand, different types of isolated dunes appear, depending on the angle between two wind directions ( $\theta$ ). When the angle is 60°, isolated dunes similar to dome or transverse dunes appear, whereas when the angle is 120°, star-dune-like isolated dunes with three crest lines appear. In a dune field with ample sand, the dune type changes significantly as the angle changes. When the angle is 60°, transverse dunes appear, whereas when the angle is 120°, linear dunes appear. The same transition between transverse dunes and linear dunes associated with wind directional change was also found in the modelling studies of Werner (1995) and Nishimori *et al.* (1998), and was theoretically predicted by Rubin and Hunter (1987).



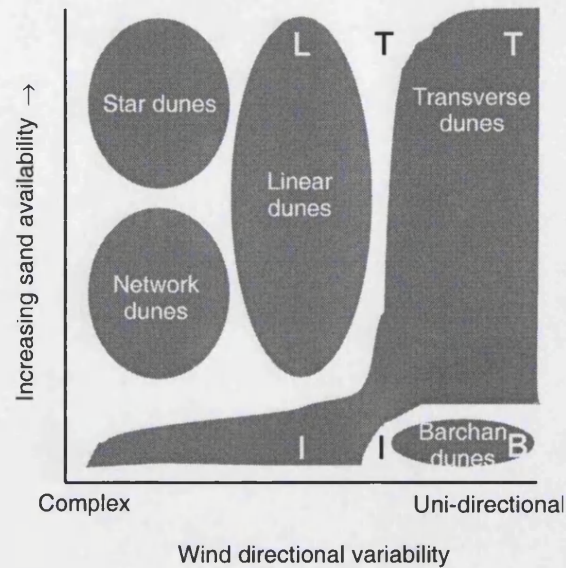
**Figure 6.11:** Dune types and wind directional change. Sand availability and angle between two directions of wind ( $h_{\text{avg}}, \theta$ ) are a) (100,  $60^\circ$ ), b) (100,  $120^\circ$ ), c) (2,  $60^\circ$ ) and d) (2,  $120^\circ$ ).

Figure 6.12 shows the summary of dune types against sand availability and wind directional change. Simulated results are embedded in the empirical diagram compiled by Livingstone and Warren (1996, figure 5.22). For an infinitely deep sand field, the model correctly matches nature. In a dune field with a limited amount of sand, the simulated results resemble the empirically compiled knowledge, yet more theoretical and field studies are called for especially for strongly bi-directional wind environments.

## 6.4 Conclusions in this chapter

In this chapter, the dune-field model developed in the previous chapter was numerically examined, and morphology and dynamics of dune fields were studied. Inconsistencies with the cross-sectional dune shape between Werner's (1995) model and nature can be solved by introducing no erosion in shadow zones (section 6.1). The asymmetric wind-directional profiles of transverse dunes and barchan dunes (which did not appear in Werner's model) can successfully be simulated with the inclusion of a wind speedup over a dune (section 6.2.1). The equilibrium height of transverse dunes may be achieved by introducing a non-linear increase of wind speedup (section 6.2.2), which may balance the decrease of sand trapping efficiency. In a uni-directional wind condition, the model shows the transition from barchan dunes to transverse dunes as sand availability increases (section 6.3.1). The model also predicts that there is a threshold in sand availability below which no pattern appears, if simulations begin with almost flat surfaces. If the simulation starts with barchan dunes, however, they remain even if the sand availability is less than the threshold (section 6.3.1). Fully developed dunes are shown to migrate downwind at a constant speed. By comparing migration speeds in simulation and in nature, spatial and temporal scales were specified (section 6.3.2). Dunes were found to grow when modest winds blow. When the wind is too weak or too strong, dunes cannot grow higher (section 6.3.2). This tendency is consistent with results of the single-dune model developed in chapters 3





**Figure 6.12:** Dune type diagram with regard to sand availability and wind direction variability (after Livingstone and Warren, 1996, figure 5.22). 'B', 'I', 'L' and 'T' denote respective barchan dunes, isolated dunes (see text), linear dunes and transverse dunes, which are simulated in this study.

and 4 (section 4.1.1; section 4.2.1). In a bi-directional wind condition with large amounts of sand, the model shows the transition from transverse dunes to linear dunes as wind angle increases. With limited amount of sand, isolated dunes similar to dome or transverse dunes and star-dune-like isolated dunes appear for acute and obtuse wind angles, respectively (section 6.3.3). The relation in simulations between type of dune and two main controls (wind variability and sand availability) resembles the corresponding empirical relation (Figure 6.12).

## CHAPTER 7

# Conclusions

This thesis has attempted to mathematically model the morphology and dynamics of desert sand dunes. In chapters 3 and 4, the shape and dynamics of single dunes were studied, the model being based on concrete physical processes. The outcome of these two chapters was then used in chapters 5 and 6, where dune fields were modelled on the basis of more abstract discrete (lattice) dynamics. Detailed conclusions were provided at the end of each chapter. Here only general conclusions are given, along with an attempt to address the more philosophical questions that were raised in the first chapter. Finally, there is a short discussion of future work.

### 7.1 General conclusions

In chapters 3 and 4, a semi-kinematic model was developed, which incorporated aerodynamic theory. The model describes the shape and migration speed of two-dimensional dunes at equilibrium. As far as the author is aware, it is the first model to link dune migration speed to wind speed at level ground. Such wind data are readily available at meteorological stations. It is also the first model to explain why the windward slopes of higher dunes are steeper. The model gives the framework for further theoretical study, and could influence future experimental

study.

During the construction of the model, particular attention was paid to self-consistency. The model shows that an equilibrium expression for dune migration speed must take into account sand trapping efficiency. The concept of sand trapping efficiency was introduced by Wilson (1972), but its importance has not generally been recognised. The model shows that sand trapping efficiency is strongly related to the wind speedup over the windward surface, and at equilibrium, estimating wind speedup is equivalent to estimating sand trapping efficiency. The model also shows that to correctly estimate sand trapping efficiency, it is important to use a grain-scale model rather than a continuum approximation. Further incorporation of wind-flow theory into the model led to the conclusion that a self-adjusting mechanism exists which maintains an equilibrium shape and migration speed, in spite of infringing the self-consistency of the model.

In chapters 5 and 6, dune field patterns were studied on the basis of lattice dynamics. The use of lattice dynamics for a dune-field study was initiated by three pioneers: Nishimori and co-workers (Nishimori and Ouchi, 1993; Nishimori *et al.*, 1998), Werner (1995) and de Castro (1995). The present model was built on Werner's approach, which was thought to be superior to other two models in respect to its relation to real physical processes. The present study shows that by incorporating physically-based rules into this prototype model we can mimic the morphology and dynamics of a dune field more correctly. The study also shows that by comparing simulated results and observed dynamic aspects of nature, more specifically dune migration, both spatial and temporal scales in the model can be specified, so that the model can have a quantitatively predictive power.

These two approaches are complimentary. Kinematic modelling has been shown to illuminate some aspects of the morphology and dynamics of dunes. The model is a bridge between the second-order, saltation-length scale and the year-order, dune-size scale. However, its success has so far been limited to two-dimensional cases because of the mathematical difficulties of three-dimensional modelling.

There is another problem. In terms of evolution, it is puzzling that dunes with different heights can be considered all at equilibrium. To address this question, we need a model which goes beyond the assumption of equilibrium, but this will soon encounter mathematical difficulties.

On the other hand, the model based on discrete dynamics allows the simulations of a dune field in three dimensions. Despite the obscure assumption that underlies the idea of a 'sand slab', the model has been shown to simulate a variety of dynamic patterns of dunes quickly, and these patterns are comparable to those in nature. During this part of the study, however, the lack of computational power has been found to be the major limitation. Relying only on computation, it is impossible to investigate states after an infinitely long period of time, some of which may be at equilibrium. It is also difficult to increase spatial resolution, which is necessary to mimic complex dune forms such as star dunes.

## **7.2 Assessment of models and methodology**

In the first chapter, the philosophy of modelling in geomorphology in general was discussed in addition to questions about how to model dunes and dune fields mathematically. The central question to be identified was whether models should be developed on a reductionist or on a universalist basis (section 1.2). In this section, the study in chapters 3–6 will be revisited first in the light of this issue. The two models developed in these chapters will then be evaluated in terms of Kirkby's (1996) four criteria for a good model, and in terms of engineering criteria, both of which were discussed in the first chapter (section 1.2). Finally, the present study will be evaluated in the light of the goal that was set at the beginning of the thesis (section 1.1).

### 7.2.1 Reductionism/universalism

Reductionists aim to explain macroscopic phenomena in terms of more microscopic dynamics. Through this practice, some phenomena and concepts, which may be seemingly independent, can be unified. In this thesis, the explanation of dune-scale morphology and dynamics in relation to saltation-scale dynamics linked wind speedup over the windward slope of the dune and sand trapping efficiency of the slip face in the lee. These two concepts have been discussed separately. For reductionist purposes, the system must be simple with good symmetries, hence the idealisation. Otherwise, the problems can hardly be dealt with mathematically. The first model examined a single two-dimensional dune, at equilibrium. Thanks also to the observational fact that the slip-face angle is invariant regardless of dune height (additional symmetry), it has been possible to discuss dune morphodynamics. This illustrates the severely limited applicability of reductionism. For some reversing dunes, for example, the slope of the leeward surface is not invariant to dune height (McKenna Neuman, 1997; Walker, 1999). For linear and star dunes, the two-dimensional approximation is no longer valid. Consequently, we are far from the goal of a systematic understanding of various types of dune, if we follow a reductionist path.

The dune field model was formulated by discrete (lattice) dynamics, this being a common tool in the study of non-linear dynamics, especially of pattern formation, as in the sand pile model that first demonstrated Self-Organised Criticality (SOC) (Bak *et al.*, 1987). This thesis, however, has not adopted a universalist standpoint. None of the discussion has assumed the presence of chaotic behaviour or SOC, or relied only on analogies to other non-linear phenomena. Yet, insights that stem from the study of non-linear dynamics are found to be beneficial. This is because if different systems can be described with the same equation, or more generally in the same mathematical formulation, the same behaviour can be expected in those systems. Indeed some behaviour such as exponential decay, oscillation and jump can frequently be seen in many different fields of study (*i.e.* those behaviours are universal). In the present study, for example, numerical

experiments to check whether different dune patterns can appear with the same parameters but from different initial conditions were motivated by the fact that many non-linear dynamical systems show bi-stability.<sup>1</sup> In the next subsection, the advantages and disadvantages of both models will be discussed in detail.

## 7.2.2 Four criteria for a good model (Kirkby, 1996)

The two models will be evaluated separately with Kirkby's four criteria: 1) physical basis, 2) simplicity, 3) generality and richness, and 4) potential for scaling up and down (Kirkby, 1996) (section 1.2).

### Model for a single dune (chapters 3 and 4)

1) Physical Basis: As there are no fundamental equations that describe the system comprised of interacting air and sand grains, models have usually been developed based on separate calculations of wind flow over topography and of sand flux as a function of wind shear velocity. The present model for these processes is comprised of the grain-scale sand deposition model (Anderson, 1988) and the aerodynamic theory derived from the fundamental airflow equation (Jackson and Hunt, 1975). The Anderson model was chosen because the conventional description based on sand flux formulae and the sediment conservation equation did not seem to be applicable at the dune crest, where the surface profile abruptly changes. Both the Anderson model (section 2.4.5) and the Jackson-Hunt theory (section 2.4.4; section 3.3.2) have been validated in the field. In the model, the observational fact that the slip-face angle is invariant regardless of dune height was introduced without discussing its origin, so that this is a phenomenological model. In addition, the assumption of equilibrium was introduced. Although there has been a discussion that the state of a slip face is far from equilibrium (Bak, 1987, 1996) (section 1.2), comparison between calculated results and field

---

<sup>1</sup>This was suggested by Steven R. Bishop, the joint supervisor of the author.

observations showed that the assumption of equilibrium appeared to be appropriate for dune-size and year-long scales.

2) **Simplicity:** This study presents the minimal, self-consistent model for dune migration speed, involving the sand flux balance at only three locations: the points upwind and downwind of the dune and dune crest. Although further introduction of the wind-flow theory enables the estimation of the windward surface profile, this introduction breaks the self-consistency rule of the model. In other words, the model is not closed. However, the wind-flow calculation is one-off, so that the model is much simpler in practice than conventional models which are based on iterative calculations of the interaction between topography and wind flow.

3) **Generality and Richness:** The modelling scheme is robust, and potentially applicable to subaqueous and other terrestrial bedforms, if there is an appropriate sand deposition model. A qualitative discussion has already been given about the dune-to-plane-bed transition observed in subaqueous and Venusian environments (section 4.1.2; section 4.2.1) (generality). The model can explain a variety of relations both in shape and in migration dynamics with only three input parameters; wind shear velocity, dune height and sand grain diameter (section 4.1.1; section 4.2.1) (richness). Strictly speaking, however, applicability is so far limited to two-dimensional bedforms with a slip face.

4) **Potential for Scaling Up and Down:** The model has already dealt with mega dunes (Wilson's draa) (section 4.1.1; section 4.2.1), though model validation is difficult in this case due to lack of field data (scaling up). It has also been seen that model results can be applied even to proto-dunes (section 4.3). However, the model may not be effective for ripples. Since the wavelength of ripples is comparable to saltation length, it is difficult to formulate ripple morphodynamics in terms of sand trapping efficiency (scaling down).

## Model for a dune field (chapters 5 and 6)

1) Physical Basis: The simulation rules were not derived from fundamental equations, but introduced phenomenologically, based on observations and aerodynamic considerations. For example, if wind blows in a desert, sand is transported in the wind direction. The stronger the wind, the greater distance sand is transported. These form the physical background of the slab transport in the model. Another example is that avalanching occurs in nature if the angle of a sandy slope exceeds the angle of repose of about  $32^\circ$ . In the model avalanching dynamics has been introduced in the same manner, without discussing its microscopic origin, hence the phenomenological basis of the model. Other dynamics such as wind speedup, slab bouncing and the shadow zone have also been introduced phenomenologically, though the origins of all these processes can be discussed in some detail.

2) Simplicity: The simulation rules are simple. This is evident when comparing to models with the Navier-Stokes equation, where interacting air pressure and three components of wind velocity are defined on a three-dimensional continuous space  $(x, y, z)$ . Consequently, the computational burden for such conventional models is very heavy. In the present model on the other hand, slab transport length ( $L$ ) is defined on a two-dimensional discrete space, and transport length is simply a function of local number of slabs at a location.

3) Generality and Richness: It has already been shown that a lattice model can be effective for vegetated dune fields (de Castro, 1995) (section 2.7.2). The present study has assumed a flat hard surface, on which slabs are piled up. By creating undulations on this hard surface, the effects of existing topography could be simulated. Simulations are expected to reproduce, for example, climbing and falling dunes (Lancaster, 1995, pp82–83) (generality). The model has been shown to mimic some of a variety of dune patterns (dome, barchan, transverse, linear and star-like dunes), and to enable systematic understanding of many different environments, according to wind environment (strength and directional complexity)



and sand availability (richness).

4) Potential for Scaling Up and Down: The model may apply to an inhomogeneous dune field by introducing regionally different parameters (*i.e.* a distributed model), if more computational capacity were to be available (scaling up). The use of discrete dynamics has already been recognised to be effective in the study of ripples (Nishimori and Ouchi, 1993; Anderson and Bunas, 1993; Landry and Werner, 1994) (section 2.7.2) (scaling down).

In short, both models are generally satisfactory in the light of these four criteria. Still, the first model suffers lack of richness, in that it cannot go beyond two-dimensional, equilibrium bedforms. The physical basis of the second model is still not secure. However, by simulating many other types of dune (*i.e.* collecting more circumstantial evidence), the model may become more convincing.

### 7.2.3 Engineering aspects

In respect of engineering, the most notable success is the estimation of dune migration speed. Civil engineers will benefit from the first model when exploiting deserts with roads or pipelines for oil and gas. The ability to predict responses in shape and migration speed to environmental change is important. More specifically, it is important to investigate the dynamics of dunes under rare high winds. Engineers are thought to be interested in how dunes that have been developed in modest wind conditions change in shape and in migration speed during a storm, which is a short-term event of a day or a few days. In such conditions, the assumption of equilibrium is clearly inappropriate, and the dune field model may be able to take over the predictive role from the kinematic model. In the dune field model, as both spatial and temporal scales can be estimated, a storm event of a certain duration can easily be simulated. In the 'storm', the slab transport length is increased for a certain period of time such that sand flux in the model conforms to the natural behaviour at a considered wind speed (section 6.3.2).

Also using the dune field model, effects of pre-existing topography such as rocks on dune dynamics can be investigated.

## 7.2.4 Contributions to geomorphology in general and to other disciplines

Finally in this section, the present study is assessed in respect to the goal that was set at the beginning of this thesis (section 1.1): to provide geomorphology and other disciplines with novel concepts and methodologies, as well as to give new interpretations to long-debated issues in geomorphology.

This study has provided no novel concept or methodology, comparable to Self-Organised Criticality (SOC) or Coupled Map Lattice (CML) (section 1.2). If restricting the discussion only to geomorphology and its closely related disciplines, however, this study *has* provided a new modelling method for a single dune (Figure 3.5) and new interpretations to some concepts.

In the idealised condition that dunes are at equilibrium, estimating shear-velocity increase (wind speedup) between an upwind point and the dune crest was found to be equivalent to estimating how much of the sand flux at the crest is trapped by the slip face in the lee (sand trapping efficiency). These two concepts, wind speedup and sand trapping efficiency, have been discussed separately. The latter has indeed not previously attracted much attention.

Through two models, the present study has revealed that some aspects of the shape and migration speed of dunes can be explained with the idealisation (assumption) of equilibrium, and that such an equilibrium state is associated with non-linearity in the dynamical system that describes a dune or a dune field.

As well as some distinct patterns in the simulated results, the dune field model shows strong non-linearity: possible saturation in height (section 6.2.2), thresh-

olds in sand flux and in sand availability (section 6.3.1), and the presence of different patterns depending on initial configurations (bi-stability) (section 6.3.1). Further investigations may reveal new phenomena and be used as a prototype for studies of discrete nonlinear systems. Such phenomena were indeed recently discovered in the experiments of subaqueous ripples (Lundbek Hansen *et al.*, 2001)(section 7.3.2), as will be discussed in the next section.

## 7.3 Future work

Many of the results of both of the models that have been summarised above are encouraging, and suggest further study. Some future topics have already been mentioned briefly when each model was assessed with Kirkby's (1996) four criteria (section 7.2.2). In this section, future topics are discussed in more detail.

### 7.3.1 Single dune model

For more precise estimation of dune migration speed, a better estimation of sand trapping efficiency is necessary, for which wake and turbulence effects on sand-grain trajectories need to be incorporated into the model (section 2.4.2). It is also important to bear in mind that wind structure in the lee of a dune fluctuates significantly (section 2.4.4).

It is suggested that the wind-directional profile of a barchan dune can be explained in terms of the self-adjusting mechanism such that a dune is at equilibrium. With the same assumption of equilibrium it may also be possible to explain why the cross-sectional shape that is perpendicular to the wind is independent of dune height. To check this, the model should be extended into three dimensions. A possible modelling scheme would be to consider a barchan dune as part of a sinuous transverse dune whose linguoid height is zero (section 4.4).

When a dune is far from equilibrium, it is probably difficult to investigate the windward surface profile from the estimation of sand trapping efficiency. In such a situation, we may need to rely on the iterative calculation models illustrated in Figures 2.3 and 3.2.

### 7.3.2 Dune field model

This thesis has discussed barchan, transverse, dome and linear dunes in particular relation to their formative environments. However some other types of free dune, such as star, network and zibar parabolic dunes, have yet to be simulated (section 2.2). A natural extension of the present study might be to simulate parabolic dunes, which occur where vegetation is present (Lancaster, 1995, pp76–77). Others may be simulations of climbing and falling dunes, in which existing topography should be incorporated into the model (Lancaster, 1995, pp82–83). Ultimately, the model will aim at a dune field where many types of dunes co-exist (Figure 7.1). Such a model will be hierarchical and distributed, by assigning regionally different parameters for each subset of the whole simulated area (lattice). The study of coastal dune systems is an example of areas that require a distributed model. In de Castro's (1995) coastal dune-field model, as the simplest approximation, parameters are constant throughout the simulated area, but different boundary conditions are enforced on the upwind and downwind edges, each representing sea and inland respectively.

The study of transitions between types of dune may be an intriguing topic that could be investigated with the model, especially in respect to pattern formation in a non-linear system. We have already seen, for example, two types of transition when increasing sand availability in a uni-directional wind environment (section 6.3.1). There was an acute transition from no pattern to a pattern of isolated (dome) dunes, where the system also shows bi-stability depending on initial conditions. Gradual transitions from dome to barchan, from barchan to transverse dunes have been modelled. A detailed and comprehensive study in a parameter

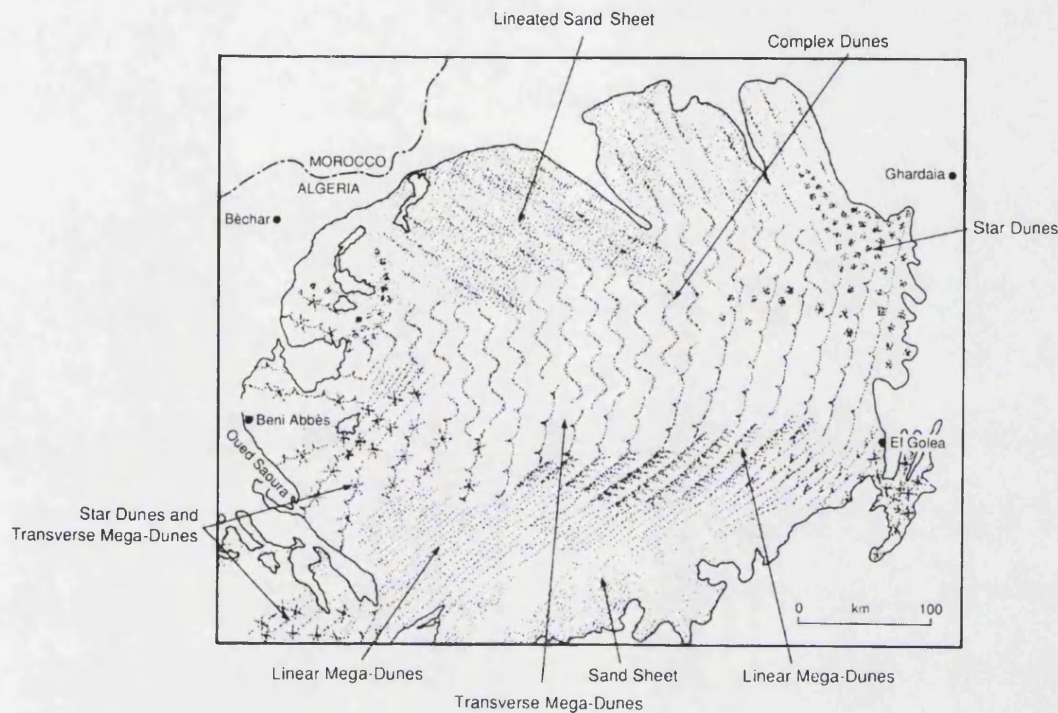


**Figure 7.1:** Various types of dune in the Great Western Sand Sea in Algeria (transferred from Cooke *et al.*, 1993, figure 28.5; the original is in Breed *et al.*, 1979).

space, for example in sand-availability-wind-complexity space, is important (*cf.* an example of such an investigation can be seen in the study of Duffing's equation which describes a periodically forced oscillator (Ueda, 1980 referred to in Thompson and Stewart, 1985, figure 1.10).

Because the simulation rules are introduced phenomenologically, continuous comparison between simulated results and observations of natural bedforms is vital to the improvement of the models. Unlike the study of aeolian bedforms, the study of subaqueous bedforms can use the detailed and quantitative data that are readily available. For example recent flume experiments show how ripples grow: the initial flat surface is destabilised and a two-dimensional transverse pattern appears; as it grows, the ripples change their form in a more three-dimensional manner (Baas, 1999; Figure 7.2). This secondary instability, which is the breaking of the symmetry in the direction at right angles to the current (*i.e.* the origin of sinu-

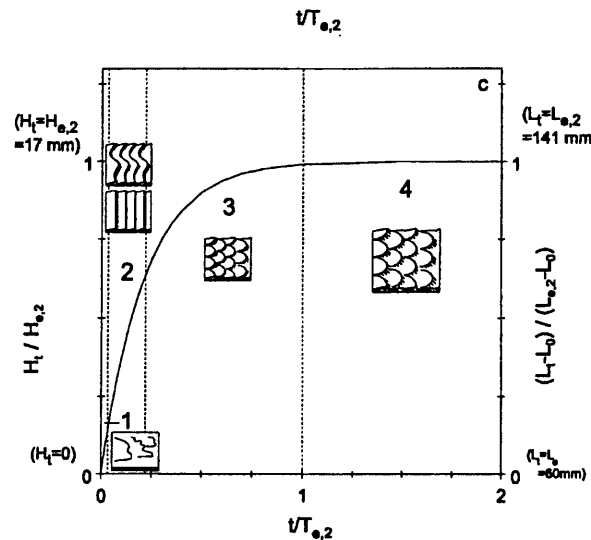


**Figure 7.2:** Current ripples development observed in a flume (transferred from Baas, 1999).

osity), has also been observed in bedforms under oscillatory currents (Lundbek Hansen *et al.*, 2001). The study of subaqueous bedforms is interesting not only for geomorphology or sedimentology. It provides topics that are intriguing for the study of pattern formation in non-linear and non-equilibrium systems. For example, in addition to the above secondary instability, Lundbek Hansen *et al.*, (2001) also showed how the wavelength of ripples changed, depending on parameters (amplitude and frequency of the oscillation). For these bedforms, well defined experiments are available. Parameters are easily controllable and recurrent results are available at time scales of only minutes to days. These experiments may have the potential to be prototypes in the study of non-linear dynamics, alongside, or even taking over from, conventional experiments such as those of Bénard convection and in studies of electrically-driven liquid crystal convection (Cross and Hohenberg, 1993).

### 7.3.3 Collaboration

The mathematical modelling of dunes and dune fields is at the boundary where many fields of study, such as geomorphology, geology, meteorology, physics and

mathematics, meet. Collaboration amongst people from these fields of study is essential for improved modelling. We have already seen in the previous section that insights based on non-linear dynamics can play a significant role (section 7.2.1) in the investigation of dune-field morphodynamics. Another successful example of collaboration was in the attempt to model a single dune. The author was familiar with the idea of self-consistent modelling, through the knowledge of phase transition and magnetic recording. The suggestion that model results might be applicable to dune-to-plane-bed transition in subaqueous bedforms was made by Andrew Warren<sup>2</sup>, who had a wide range of knowledge of dunes. To revise each model further, fluid dynamic, meteorological, climatological and geological knowledge will be necessary.

---

<sup>2</sup>the primary supervisor of the author

# References

- Al-Hinai, K.G. and Moore, J.M. 1987. 'Monitoring of sand migration in eastern Arabia by remote sensing', *20th International Symposium on Remote Sensing of Environment, Proceedings*, Environment Research Institute of Michigan, Ann Arbor, Michigan, 10 pp.
- Allen, J.R.L. 1968. *Current Ripples: Their Relation to Patterns of Water and Sediment Motion*, North Holland, Amsterdam, 433 pp.
- Allen, J.R.L. 1970. *Physical Processes of Sedimentation: An Introduction*, George Allen and Unwin, London, 248 pp [revised readings, 1977].
- Anderson R.S. 1987a. 'A theoretical model for aeolian impact ripples', *Sedimentology*, **34**, 943–956.
- Anderson R.S. 1987b. 'Eolian sediment transport as a stochastic process: the effects of a fluctuating wind on particle trajectories', *Journal of Geology*, **95**, 497–512.
- Anderson, R.S. 1988. 'The pattern of grainfall deposition in the lee of aeolian dunes', *Sedimentology*, **35**, 175–188.
- Anderson, R.S. and Hallet, B. 1986. 'Sediment transport by wind: toward a general model', *Geological Society of America Bulletin*, **97**, 523–535.
- Anderson, R.S. and Bunas, K.L. 1993. 'Grain size segregation and stratigraphy in aeolian ripples modelled with a cellular automaton', *Nature*, **365**, 740–743.



- Baas, J.H. 1999. 'An empirical model for the development and equilibrium morphology of current ripples in fine sand', *Sedimentology*, **46**, 123–138.
- Bagnold, R.A. 1941. *The Physics of Blown Sand and Desert Dunes*, Methuen & Company, London, 265 pp [reprint, 1954].
- Bak, P. 1996. *How Nature Works: The Science of Self-organised Criticality*, Springer-Verlag, New York, 212 pp.
- Bak, P., Tang, C. and Wiesenfeld, K. 1987. 'Self-organised criticality. An explanation of  $1/f$  noise', *Physical Review Letters*, **59**, 381–384.
- Bassett, K. 1994. 'Comments on Richards: the problems of 'real' geomorphology', *Earth Surface Processes and Landforms*, **19**, 273–276.
- Belcher, S.E. and Hunt, J.C.R. 1998. 'Turbulent flow over hills and waves', *Annual Review of Fluid Mechanics*, **30**, 507–538.
- Bennett, S.J., Bridge, J.S. and Best, J.L. 1998. 'Fluid and sediment dynamics of upper stage plane beds', *Journal of Geophysical Research*, **103**(C1), 1239–1274.
- Bougan, S. and Greeley, R. 1985. 'Microdunes and other aeolian bedforms in high-density atmospheres', in Bandorff-Nielsen, O.E., Møller, J.T., Rasmussen, K.R., and Willetts, B.B., editors. *Proceedings of international workshop on the physics of blown sand*, University of Aarhus, Aarhus, Denmark, 369–376.
- Breed, C.S., Fryberger, S.G., Andrews, S., McCauley, C., Lennartz, F. Gebel, D. and Horstman, K. 1979. 'Regional Studies of sand seas using Landsat (ERTS) imagery', in McKee, E.D., editor. *A Study of Global Sand Seas. United States Geological Survey Professional Paper*, **1052**, United States Government Printing Office, Washington, 305–397.
- Bristow, C.S., Bailey, S.D. and Lancaster, N. 2000. 'The sediment structure of linear sand dunes', *Nature*, **406**, 56–59.

- Brookfield, M.E. 1977. 'The origin of bounding surfaces in ancient aeolian sandstones', *Sedimentology*, **24**, 303–332. *Sedimentology*, **31**, 413–431.
- Burkinshaw, J.R., Illenberger, W.K. and Rust, I.C. 'Wind-speed profiles over a reversing transverse dune', in Pye, K., editor. *The Dynamics and Environmental Context of Aeolian Sedimentary Systems*, The Geological Society, London, 25–36.
- Butterfield, G.R. 1991. 'Grain transport rates in steady and unsteady turbulent airflows', *Acta Mechanica*, **Supplement 1**, 97–122.
- Cooke, R.U., Warren, A. and Goudie, A.S. 1993. *Desert Geomorphology*, UCL Press, London, 526 pp.
- Coursin, A. 1964 'Observations et expériences faites en avril et mai 1956 sur les barkhanes du Souhel el Abiodh (région est de Port-Étienne)' *Institut Française de l'Afrique Noire, Bulletin, Série A* **26**, 989–1022.
- Cross, M.C. and Hohenberg, P.C. 1993. 'Pattern formation outside of equilibrium', *Reviews of Modern Physics*, **65**, 851–1112.
- de Castro, F. 1995. 'Computer simulation of the dynamics of a dune system', *Ecological Modelling*, **78**, 205–217.
- Edgett, K.S. and Malin, M.C. 2000. 'New views of Mars eolian activity, materials, and surface properties: three vignettes from the Mars Global Surveyor Mars orbital camera', *Journal of Geophysical Research*, **105**, 1623–1650.
- Engelund, F. and Fredsøe, J. 1974. 'Transition from dunes to plane bed in alluvial channels' Lyngby, Technical University of Denmark, *Institute of Hydrodynamics and Hydraulic Engineering Series Paper*, **4**.
- Finkel, H.J. 1959. 'The barchans of southern Peru', *Journal of Geology*, **67**, 614–647.
- Frank, A and Kocurek, G 1996a. 'Toward a model for airflow on the lee side of aeolian dunes', *Sedimentology*, **43**, 451–458.

- Frank, A.J. and Kocurek, G. 1996b. 'Airflow up the stoss slope of sand dunes: limitations of current understanding', *Geomorphology*, **17**, 47–54.
- Fredsøe, J. 1982. 'Shape and dimensions of stationary dunes in rivers', *Journal of the Hydraulics Division, Proceedings. American Society of Civil Engineers*, **108** (HY8), 932–947.
- Fryberger, S.G. 1979. 'Dune forms and wind regime', in McKee, E.D., editor. *A Study of Global Sand Seas. United States Geological Survey Professional Paper*, **1052**, United States Government Printing Office, Washington, 137–169.
- Fryberger, S.G., Al-Sari, A.M., Clisham, T.J., Rizvi, S.A.R. and Al-Hinai, K.G. 1984. 'Wind sedimentation in the Jafurah sand sea, Saudi Arabia', *Sedimentology*, **31**, 413–431.
- Gillette, D.A. 1999. 'Physics of aeolian movement emphasising changing of the aerodynamic roughness height by saltating grains (the Owen effect)', in Goudie, A.S., Livingstone, I. and Stokes, S., editors. *Aeolian Environments, Sediments and Landforms*, John Wiley & Sons, Chichester, U.K., 129–142.
- Goudie, A.S. 1999. 'The history of desert dune studies over the last 100 years', in Goudie, A.S., Livingstone, I. and Stokes, S., editors. *Aeolian Environments, Sediments and Landforms*, John Wiley & Sons, Chichester, U.K., 1–13.
- Goudie, A.S., Livingstone, I. and Stokes, S. (Eds) 1999. *Aeolian Environments, Sediments, and Landforms*, John Wiley & Sons, Chichester, U.K., 325 pp.
- Greeley, R., Arvidson, R.E., Elachi, C., Geriger, M.A., Plaut, J.J., Saunders, R.S., Schubert, G., Stofan, E.R., Thouvenot, E.J.P., Wall, S.D. and Weitz, C.M. 1992. 'Aeolian features on Venus: preliminary Magellan results', *Journal of Geophysical Research*, **97**, 13319–13345.
- Greeley, R. and Iversen, J.D. 1985. *Wind as A Geological Process on Earth, Mars, Venus and Titan*, Cambridge University Press, Cambridge, 333 pp.

- Hallet, B. 1990. 'Spatial self-organisation in geomorphology: from periodic bedforms and patterned ground to scale-invariant topography', *Earth-Science Reviews*, **29**, 57–75.
- Hardisty, J. and Whitehouse, R.J.S. 1988a. 'Evidence for a new sand transport process from experiments on Saharan dunes', *Nature*, **332**, 532–534.
- Hardisty, J. and Whitehouse, R.J.S. 1988b. 'Effect of bedslope on desert sand transport', *Nature*, **334**, 302.
- Hastenrath, S.L. 1967. 'The barchans of the Arequipa region, southern Peru', *Zeitschrift für Geomorphologie*, **11**, 300–311.
- Hesp, P.A. and Hastings, K. 1998. 'Width, height and slope relationships and aerodynamic maintenance of barchans', *Geomorphology*, **22**, 193–204.
- Howard, A.D. 1977. 'Effect of slope on the threshold of motion and its application to orientation of wind ripples', *Geological Society of America Bulletin*, **88**, 853–856.
- Howard, A.D., Morton, J.B., Gad-el-Hak, M. and Pierce, D.B. 1978. 'Sand transport model of barchan dune equilibrium', *Sedimentology*, **25**, 307–338.
- Howard, A.D. and Walmsley, J.L. 1985. 'Simulation model of isolated dune sculpture by wind', in Bendorff-Nielsen, O.E., Møller, J.T., Rasmussen, K.R., and Willetts, B.B., editors. *Proceedings of international workshop on the physics of blown sand*, University of Aarhus, Aarhus, Denmark, 377–391.
- Huang, H.Q. and Nanson, G.C. 'Hydraulic geometry and maximum flow efficiency as products of the principle of least action', *Earth Surface Processes and Landforms*, **25**, 1–16.
- Hungr, O. 2000. 'Analysis of debris flow surges using the theory of uniformly progressive flow', *Earth Surface Processes and Landforms*, **25**, 483–495.
- Hunt, J.C.R., Leibovich, S. and Richards, K.J. 1988. 'Turbulent shear flow over hills', *Quarterly Journal of the Royal Meteorological Society*, **114**, 1435–1470.

- Hunt, J.C.R. and Nalpanis, P. 1985. 'Saltating and suspended particles over flat and sloping surfaces. I. Modelling concepts', in Bandorff-Nielsen, O.E., Møller, J.T., Rasmussen, K.R., and Willetts, B.B., editors. *Proceedings of international workshop on the physics of blown sand*, University of Aarhus, Aarhus, Denmark, 9–36.
- Hunter, R.E. 1977a. 'Basic types of stratification in small eolian dunes', *Sedimentology*, **24**, 361–387.
- Hunter, R.E. 1977b. 'Terminology of cross-stratified sedimentary layers and climbing-ripple structures', *Journal of Sedimentary Petrology*, **47**, 697–706.
- Hunter, R.E. 1985. 'A kinematic model for the structure of lee-side deposits', *Sedimentology*, **32**, 409–422.
- Iversen, J.D. and Rasmussen, K.R. 1994. 'The effect of surface slope on saltation threshold', *Sedimentology*, **41**, 721–728.
- Jackson, P.S. and Hunt, J.C.R. 1975. 'Turbulent wind flow over a low hill', *Quarterly Journal of the Royal Meteorological Society*, **101**, 929–955.
- Jimenez JA, Maia LP, Serra J, Morais J. 1999. 'Aeolian dune migration along the Ceará coast, north-eastern Brazil', *Sedimentology* **46**, 689–701.
- Kaneko, K. (Ed.) 1993. *Theory and Applications of Coupled Map Lattices*, John Wiley & Sons, Chichester, U.K., 192 pp.
- Kawamura, R. 1951. 'Study on sand movement by wind' (in Japanese), *Report*, **5(3/4)**, Institute of Science and Technology, Tokyo, 95–112. Translated as *Report*, **HEL-2-8** (1964), Hydraulics Engineering Laboratory, University of California, Berkeley, CA, 38 pp.
- Kennedy, J.F. 1963. 'The mechanics of dunes and antidunes in erodible-bed channels', *J. Fluid Mech.*, **16**, 521–544.
- Kirkby, M.J. 1996. 'A role for theoretical models in geomorphology?' in Rhoads, B.L. and Thorn, C.E., editors. *The Scientific Nature of Geomorphology*:

*Proceedings of the 27th Binghamton Symposium in Geomorphology, held 27–29 September, 1996*, John Wiley & Sons, Chichester, U.K., 257–272.

- Knott, P. 1979. *The structure and pattern of dune-forming winds*. PhD dissertation, University of London [2 volumes].
- Kocurek, G., Townsley, M., Yew, E., Havholm, K. and Sweet, M.L. 1992. 'Dune and dune-field development on Padre Island, Texas, with implications for interdune deposition and water-table-controlled accumulation', *Journal of Sedimentary Petrology*, **62**, 622–635.
- Kocurek, G. and Lancaster, N. 1999. 'Aeolian system sediment state; theory and Mojave Desert Kelso dune field example', *Sedimentology*, **46**, 505–515.
- Lancaster, N. 1985. 'Variations in wind velocity and sand transport on the windward flanks of desert sand dunes', *Sedimentology*, **32**, 581–593.
- Lancaster, N. 1988. 'Controls of eolian dune size and spacing', *Geology*, **16**, 972–975.
- Lancaster, N. 1989. 'The dynamics of star dunes: an example from the Gran Desierto, Mexico', *Sedimentology*, **36**, 273–289.
- Lancaster, N. 1991. 'The orientation of dunes with respect to sand-transporting winds: a test of Rubin and Hunter's gross bedform-normal rule', *Acta Mechanica*, **Supplement 2**, 89–102.
- Lancaster, N. 1995. *Geomorphology of Desert Dunes*, Routledge, London, pp 290.
- Lancaster, N. 1996. 'Field studies of sand patch initiation processes on the northern margin of the Namib Sand Sea', *Earth Surface Processes and Landforms*, **21**, 947–954.
- Lancaster, N., Nickling, W.G., McKenna Neuman, C.K. and Wyatt, V.E. 1996. 'Sediment flux and airflow on the stoss slope of a barchan dune', *Geomorphology*, **17**, 55–62.

- Landry, W. and Werner, B.T. 1994. 'Computer simulations of self-organised wind ripple patterns', *Physica D*, **77**, 238–260.
- Leopold, L.B. and Langbein, W.B. 1962. 'The concept of entropy in landscape evolution', *United States Geological Survey Professional Paper*, **500-A**, United States Government Printing Office, Washington, 20 pp.
- Lettau, K. and Lettau, H.H. 1978. 'Experimental and micrometeorological field studies of dune migration', in Lettau, H.H. and Lettau, K., editors. *Exploring the World's Driest Climates, Institute of Environmental Science Report*, **101**, Center for Climatic Research, University of Wisconsin, Madison, 110–147.
- Livingstone, I. and Warren, A. 1996. *Aeolian Geomorphology*. Addison Wesley Longman, Harlow, United Kingdom, 211 pp.
- Long, J.T. and Sharp, R.P. 1964. 'Barchan-dune movement in Imperial Valley, California', *Geological Society of America Bulletin*, **75**, 149–156.
- Lundbek Hansen, J., van Hecke, M., Haaning, A., Ellegaard, C., Andersen, K.H., Bohr, T. and Sans, T. 2001. 'Instabilities in sand ripples', *Nature*, **410**, 324.
- Mandelbrot, B.B. 1982. *The Fractal Geometry of Nature*, W.H. Freeman, San Francisco, U.S.A., 468 pp.
- Mason, P.J. and Sykes, R.I. 1979. 'Flow over an isolated hill of moderate slope', *Quarterly Journal of the Royal Meteorological Society*, **105**, 383–395.
- McDonald, R.R. and Anderson, R.S. 1995. 'Experimental verification of aeolian saltation and lee side deposition models', *Sedimentology*, **42**, 39–56.
- McKee, E.D. (Ed.) 1979a. *A Study of Global Sand Seas. United States Geological Survey Professional Paper*, **1052**, United States Government Printing Office, Washington, 429 pp.

- McKee, E.D. 1979b. 'Introduction to a study of global sand seas', in McKee, E.D., editor. *A Study of Global Sand Seas. United States Geological Survey Professional Paper, 1052*, United States Government Printing Office, Washington, 1–19.
- McKenna Neuman, C., Lancaster, N. and Nickling, W.G. 1997. 'Relations between dune morphology, air flow, and sediment flux on reversing dunes, Silver Peak, Nevada', *Sedimentology*, **44**, 1103–1113.
- McLean, S.R. 1990. 'The stability of ripples and dunes', *Earth-Science Reviews*, **29**, 131–144.
- Melton, F.A. 1940. 'A tentative classification of sand dunes-its application to dune history in the southern high plains', *Journal of Geology*, **48**, 113–174.
- Mitha, S., Tran, M.Q., Werner, B.T. and Haff, P.K. 1986. 'The grain-bed impact process in aeolian saltation', *Acta Mechanica*, **63**, 267–278.
- Mulligan, K.R. 1988. 'Velocity profiles measured on the windward slope of a transverse dune', *Earth Surface Processes and Landforms*, **13**, 573–582.
- Murray, A.B. and Paola, C. 1994. 'A cellular model of braided rivers', *Nature*, **371**, 54–57.
- Namikas S. and Sherman D.J. 1997. 'Predicting aeolian sand transport: revisiting the White model', *Earth Surface Processes and Landforms* **22**, 601–604.
- Nickling, W.G. and McKenna Neuman, C. 1999. 'Recent investigations of airflow and sediment transport over desert dunes', in Goudie, A.S., Livingstone, I. and Stokes, S., editors. *Aeolian Environments, Sediments and Landforms*, John Wiley & Sons, Chichester, U.K., 15–47.
- Nishimori, H. and Ouchi, N. 1993. 'Formation of ripple patterns and dunes by wind-blown sand', *Physical Review Letters*, **71**, 197–200.
- Nishimori, H., Yamasaki, M. and Andersen, K.H. 1998. 'A simple model for the various pattern dynamics of dunes', *International Journal of Modern Physics B*, **12**, 257–272.



- Oulehri, T. 1992. *Etude géodynamique des migrations de sables éoliens dans la région de Laâyoune (Nord du Sahara marocain)*. PhD dissertation, l'Université Paris 6, Paris. no. 92-12
- Owen, P.R. 1964. 'Saltation of uniform sand grains in air', *Journal of Fluid Mechanics*, **20**, 225–242.
- Phillips, J.D. 1996. 'Deterministic complexity, explanation, and predictability in geomorphic systems' in Rhoads, B.L. and Thorn, C.E., editors. *The Scientific Nature of Geomorphology: Proceedings of the 27th Binghamton Symposium in Geomorphology, held 27–29 September, 1996*, John Wiley & Sons, Chichester, U.K., 315–335.
- Prigozhin, L. 1999. 'Nonlinear dynamics of aeolian sand ripples', *Physical Review E*, **60**, 729–733.
- Pye, K. and Tsoar, H. 1990. *Aeolian sand and sand dunes*, Unwin Hyman, London, 396 pp.
- Raupach, M.R. 1991. 'Saltation layers, vegetation canopies and roughness lengths', *Acta Mechanica*, **Supplement 1**, 83–96.
- Rhoads, B.L. 1994. 'On being a 'real' geomorphologist', *Earth Surface Processes and Landforms*, **19**, 269–272.
- Rhoads, B.L. and Thorn, C.E. (Eds) 1996. *The Scientific Nature of Geomorphology: Proceedings of the 27th Binghamton Symposium in Geomorphology, held 27–29 September, 1996*, John Wiley & Sons, Chichester, U.K., 481 pp.
- Rice, M.A., Willetts, B.B. and McEwan, I.K. 1995. 'An experimental study of multiple grain-size ejecta produced by collisions of saltating grains with a flat bed', *Sedimentology*, **42**, 695–706.
- Rice, M.A., Willetts, B.B. and McEwan, I.K. 1996. 'Observations of collisions of saltating grains with a granular bed from high-speed cine-film', *Sedimentology*, **43**, 21–31.

- Richards, K. 1990. 'Real' geomorphology', *Earth Surface Processes and Landforms*, **15**, 195–197.
- Richards, K. 1994. 'Real' geomorphology revisited', *Earth Surface Processes and Landforms*, **19**, 277–281.
- Richards, K. 1996. 'Samples and cases: generalisation and explanation in geomorphology' in Rhoads, B.L. and Thorn, C.E., editors. *The Scientific Nature of Geomorphology: Proceedings of the 27th Binghamton Symposium in Geomorphology, held 27–29 September, 1996*, John Wiley & Sons, Chichester, U.K., 171–190.
- Rubin, D.M. and Hunter, R.E. 1982. 'Bedform climbing in theory and nature', *Sedimentology*, **29**, 121–138.
- Rubin, D.M. and Hunter, R.E. 1987. 'Bedform alignment in directionally varying flows', *Science*, **237**, 276–278.
- Rubin, D.M. and Ikeda, H. 1990. 'Flume experiments on the alignment of transverse, oblique, and longitudinal dunes in directionally varying flows', *Sedimentology*, **37**, 673–684.
- Ruelle, D. 1991. *Chance and Chaos*, Princeton University Press, Chichester, U.K., 195 pp.
- Sauermann, G., Rognon, P., Poliakov, A. and Herrmann, H.J. 2000. 'The shape of the barchan dunes of southern Morocco', *Geomorphology*, **36**, 47–62.
- Schuster, H.G. 1988. *Deterministic Chaos: An Introduction* [Second Revised Edition], VCH Verlagsgesellschaft mbH, Weinheim, Germany, 270 pp.
- Sherman, D.J., Jackson, D.W.T., Namikas, S.L. and Wang, J. 1998. 'Wind-blown sand on beaches: an evaluation of models', *Geomorphology*, **22**, 113–133.
- Singhvi, A.K. and Wintle, A.G. 1999. 'Luminescence dating of aeolian and coastal sand and silt deposits: applications and implications', in Goudie,

- A.S., Livingstone, I. and Stokes, S., editors. *Aeolian Environments, Sediments and Landforms*, John Wiley & Sons, Chichester, U.K., 293–317.
- Stam, J.M.T. 1996. 'Migration and growth of aeolian bedforms', *Mathematical Geology*, **28**, 519–536.
- Stam, J.M.T. 1997. 'On the modelling of two-dimensional aeolian dunes', *Sedimentology*, **44**, 127–141.
- Takayasu, H. 1990. *Fractals in the Physical Sciences*, Manchester University Press, Manchester, 170 pp.
- Taylor, P.A., Mason, P.J. and Bradley, E.F. 1987. 'Boundary-layer flow over low hills (a review)', *Boundary-Layer Meteorology*, **39**, 107–132.
- Thompson, J.M.T. and Stewart, H.B. 1986. *Nonlinear Dynamics and Chaos: Geometrical Methods for Engineers and Scientists*, John Wiley & Sons, Chichester, U.K., 376 pp.
- Tsoar, H. 1983. 'Dynamic processes acting on a longitudinal (seif) dune', *Sedimentology*, **30**, 567–578.
- Ueda, Y. 1980. 'Steady motions exhibited by Duffing's equation: a picture book of regular and chaotic motions', in Holmes, P.J., editor. *New Approaches to Nonlinear Problems in Dynamics*, SIAM, Philadelphia, 311–322.
- Van Boxel, J.H., Arens, S.M. and Van Dijk, P.M. 1999. 'Aeolian processes across transverse dunes. I: modelling the air flow', *Earth Surface Processes and Landforms*, **24**, 255–270.
- Valance, A. and Rioual, F. 1999. 'A nonlinear model for aeolian sand ripples', *European Physical Journal B*, **10**, 543–548.
- Van Dijk, P.M., Arens, S.M. and Van Boxel, J.H. 1999. 'Aeolian processes across transverse dunes. II: modelling the sediment transport and profile development', *Earth Surface Processes and Landforms*, **24**, 319–333.

- Walker, I.J. 1999. 'Secondary airflow and sediment transport in the lee of a reversing dune', *Earth Surface Processes and Landforms*, **24**, 437–448.
- Walmsley, J.L. and Howard, A.D. 1985. 'Application of a boundary-layer model to flow over an eolian dune', *Journal of Geophysical Research*, **90**, 10631–10640.
- Warren, A. 1988. 'The dynamics of dune networks in the Wahiba Sands: a progress report', in Dutton, R., editor. *Scientific results of the Royal Geographical Society's Oman Wahiba Sands project 1985-1987*, *Journal of Oman Studies, Special Report*, **3**, 169–181.
- Warren, A. and Allison, D. 1998. 'The palaeoenvironmental significance of dune size hierarchies', *Palaeo*, **137**, 289–303.
- Wasson, R.J. and Hyde, R. 1983. 'Factors determining desert dune type', *Nature*, **304**, 337–339
- Weng, W.S., Hunt, J.C.R., Carruthers, D.J., Warren, A., Wiggs, G.F.S., Livingstone, I. and Castro, I. 1991. 'Air flow and sand transport over sand dunes', *Acta Mechanica, Supplement 2*, 1–22.
- Werner, B.T. 1995. 'Eolian dunes: computer simulations and attractor interpretation', *Geology*, **23**, 1107–1110.
- Werner, B.T. 1999. 'Complexity in natural landform patterns', *Science*, **284**, 102–104.
- Werner, B.T. and Fink, T.M. 1993. 'Beach cusps as self-organized patterns', *Science*, **260**, 986–971.
- Werner, B.T. and Kocurek, G. 1997. 'Bed-form dynamics: Does the tail wag the dog?', *Geology*, **25**, 771–774.
- Werner, B.T. and Kocurek, G. 1999. 'Bedform spacing from defect dynamics', *Geology*, **27**, 727–730.

- White, B.R. and Schulz, J.C. 1977. 'Magnus effect in saltation', *Journal of Fluid Mechanics*, **81**, 497–512.
- Wiggs, G.F.S., Livingstone, I. and Warren, A. 1996. 'The role of streamline curvature in sand dune dynamics: evidence from field and wind tunnel measurements', *Geomorphology*, **17**, 29–46.
- Willetts, B.B. and Rice, M.A. 1989. 'Collisions of quartz grains with a sand bed: the influence of incident angle', *Earth Surface Processes and Landforms*, **14**, 719–730.
- Wilson, I.G. 1970. *The external morphology of wind-laid sand deposits*. PhD dissertation, University of Reading.
- Wilson, I.G. 1972. 'Aeolian bedforms—their development and origins', *Sedimentology*, **19**, 173–210.
- Wippermann, F.K. and Gross, G. 1985. 'The wind-induced shaping and migration of an isolated dune: a numerical experiment', *Boundary-Layer Meteorology*, **36**, 319–334.
- Wolfram, S. (Ed.) 1986. *Theory and Applications of Cellular Automata*, World Scientific, Singapore, 560 pp.
- Yalin, M.S. 1977. *Mechanics of Sediment Transport* [Second Edition], Pergamon Press, Oxford, U.K., 298 pp.
- Zeman, O. and Jensen, N.O. 1987. 'Modification of turbulence characteristics in flow over hills', *Quarterly Journal of the Royal Meteorological Society*, **113**, 55–80.
- Zeman, O. and Jensen, N.O. 1988. 'Progress report on modeling permanent form sand dunes', Risø National Laboratory Report, **RISØ-M-2738**, Roskilde, Denmark, 27 pp.